

## Nature-inspired superlyophobic surfaces

**Citation for published version (APA):**

Wu, D. (2007). *Nature-inspired superlyophobic surfaces*. [Phd Thesis 1 (Research TU/e / Graduation TU/e), Chemical Engineering and Chemistry]. Technische Universiteit Eindhoven. <https://doi.org/10.6100/IR630116>

**DOI:**

[10.6100/IR630116](https://doi.org/10.6100/IR630116)

**Document status and date:**

Published: 01/01/2007

**Document Version:**

Publisher's PDF, also known as Version of Record (includes final page, issue and volume numbers)

**Please check the document version of this publication:**

- A submitted manuscript is the version of the article upon submission and before peer-review. There can be important differences between the submitted version and the official published version of record. People interested in the research are advised to contact the author for the final version of the publication, or visit the DOI to the publisher's website.
- The final author version and the galley proof are versions of the publication after peer review.
- The final published version features the final layout of the paper including the volume, issue and page numbers.

[Link to publication](#)

**General rights**

Copyright and moral rights for the publications made accessible in the public portal are retained by the authors and/or other copyright owners and it is a condition of accessing publications that users recognise and abide by the legal requirements associated with these rights.

- Users may download and print one copy of any publication from the public portal for the purpose of private study or research.
- You may not further distribute the material or use it for any profit-making activity or commercial gain
- You may freely distribute the URL identifying the publication in the public portal.

If the publication is distributed under the terms of Article 25fa of the Dutch Copyright Act, indicated by the "Taverne" license above, please follow below link for the End User Agreement:

[www.tue.nl/taverne](http://www.tue.nl/taverne)

**Take down policy**

If you believe that this document breaches copyright please contact us at:

[openaccess@tue.nl](mailto:openaccess@tue.nl)

providing details and we will investigate your claim.

# **Nature-Inspired Superlyophobic Surfaces**

PROEFSCHRIF

ter verkrijging van de graad van doctor aan de  
Technische Universiteit Eindhoven, op gezag van de  
Rector Magnificus, prof.dr.ir. C.J. van Duijn, voor een  
Commissie aangewezen door het College voor  
Promoties in het openbaar te verdedigen  
op maandag 8 oktober 2007 om 16.00 uur

door

Di Wu

geboren te Tianjin, China

Dit proefschrift is goedgekeurd door de promotoren:

prof.dr. G. de With

en

prof.dr. R.A.T.M. van Benthem

Copromotor:

dr. W. Ming

Wu, Di

Nature-inspired superhydrophobic surfaces / by Di Wu

A catalogue record is available from the Eindhoven University of Technology Library

ISBN: 978-90-386-1126-6

Copyright © 2007 by Di Wu

Front cover page: the atomic force microscopy 3D-image of a superhydrophobic surface and lotus leaves.

Back cover page: a water droplet sits on a superhydrophobic surface.

Cover Design: Chunling Xu

An electronic copy of this thesis is available at the website of the Eindhoven University Library in PDF format ([www.tue.nl/en/services/library](http://www.tue.nl/en/services/library)).

Printed by Eindhoven University Press

## Table of Contents

<b>1</b>	<b>Introduction</b>	<b>1</b>
1.1	General introduction	2
1.2	Natural superhydrophobic surfaces	2
1.3	Theoretical background	5
1.3.1	Young's equation	5
1.3.2	Wenzel's equation	5
1.3.3	Cassie's equation	6
1.3.4	Contact angle hysteresis	7
1.4	Recent attempts to develop superhydrophobic surfaces	8
1.5	Applications	10
1.6	Objectives and the scope of this thesis	11
<b>2</b>	<b>Superhydrophobic coatings based on fluorinated polyurethanes</b>	<b>15</b>
2.1	Introduction	16
2.2	Experimental	17
2.2.1	Materials	17
2.2.2	Synthesis of fluorinated IMCI	18
2.2.3	Preparation of partially fluorinated PU films	18
2.2.4	Preparation of roughened, fluorinated PU films	19
2.2.5	Characterization techniques	19
2.3	Results and Discussion	20
2.3.1	Synthesis of F <sub>n</sub> -IMCI	20
2.3.2	Reaction between SLO and F <sub>8</sub> -IMCI	23
2.3.3	Wettability of smooth polymeric films	24
2.3.4	Wettability of rough polymeric films	27
2.4	Rough coatings with PDMS-covered nanoparticles	29
2.5	Conclusions	31



<b>3. Superhydrophobic coatings based on raspberry-like particles</b>	<b>35</b>
3.1. Introduction	36
3.2. Experimental	38
3.2.1 Materials	38
3.2.2 Raspberry-like particles from epoxy-amine chemistry	38
3.2.2.1 Preparation of amino-functionalized silica nanoparticles	38
3.2.2.2 Preparation of epoxy-functionalized silica microparticles	39
3.2.2.3 Epoxy-amino approach to synthesize raspberry-like silica particles	39
3.2.3 Raspberry-like particles from aldehyde-amine chemistry	40
3.2.3.1 Preparation of amino-functionalized silica microparticles	40
3.2.3.2 Preparation of aldehyde-functionalized silica microparticles	40
3.2.3.3 Aldehyde-amine approach to synthesize raspberry-like silica particles	41
3.2.4 Preparation of epoxy-amine films with dual-size surface roughness	41
3.2.5 Preparation of superhydrophobic films with PDMS	41
3.2.6 Characterization techniques	42
3.3 Results and discussion	43
3.3.1 Two-step synthesis of modified silica particles	43
3.3.2 One-step synthesis of amino-functionalized silica particles	45
3.3.3 Synthesis of raspberry-like particles	46
3.3.4 Preparation of superhydrophobic coatings	48
3.3.5 Superhydrophobic coatings containing raspberry-like particles with different size ratio	53
3.4 Modeling study for superhydrophobicity	54
3.5 Conclusions	58
<b>4 Superhydrophobic surfaces by a layer-by-layer approach</b>	<b>61</b>
4.1 Introduction	62
4.2 Experimental	63
4.2.1 Materials	63
4.2.2 Preparation of partially cured epoxy coatings	64
4.2.3 Preparation of epoxy coatings with silica microparticles	64

4.2.4 Preparation of superhydrophobic surfaces	64
4.2.4.1 Preparation of superhydrophobic surfaces with PDMS	64
4.2.4.2 Superhydrophobic surfaces with perfluorodecyltrichlorosilane modification	65
4.2.5 Characterization techniques	65
4.3 Results and discussion	66
4.3.1 Preparation of partly cured epoxy coatings	66
4.3.2 Characterization of epoxy coatings with silica microparticles	68
4.3.3 Surface wettability on single-sized structured surfaces	69
4.3.4 Adhesion between particles and polymer matrix	71
4.3.5 Superhydrophobic coatings from layer-by-layer approach	73
4.3.6 SiCl <sub>4</sub> -strengthened superhydrophobic coatings	75
4.4 Conclusions	77
<b>5 Lipophobicity on superhydrophobic surfaces</b>	<b>79</b>
5.1 Introduction	80
5.2 Experimental	81
5.2.1 Materials	81
5.2.2 Preparation of surface-fluorinated superhydrophobic films	81
5.2.3 Probe liquids with different surface tensions	82
5.2.4 Contact angle measurements	82
5.3 Results and discussion	82
5.4 A modeling approach toward superlipophobicity	86
5.5 Conclusions	87
<b>6 Superhydrophobic and superlipophobic textiles</b>	<b>89</b>
6.1 Introduction	90
6.2 Experimental	91
6.2.1 Materials	91
6.2.2 <i>In-situ</i> 1-step formation of amine-functional silica particles on cotton fibers	92

6.2.3 Two-step formation of amine-functional silica particles	92
6.2.4 Surface modification by PDMS	92
6.2.5 Surface modification by 1 <i>H</i> ,1 <i>H</i> ,2 <i>H</i> ,2 <i>H</i> -perfluorodecyltrichlorosilane	93
6.2.6 Characterization	93
6.3 Results and discussion	93
6.3.1 Chemical modification of cotton textiles	93
6.3.2 Surface wettability and topology of PDMS-modified textiles	96
6.3.3 Lipophobicity of fluorinated, particle-coated textiles	102
6.4 Conclusions	103
<b>7 Conclusions and recommendations</b>	<b>105</b>
7.1 Conclusions	105
7.2 Recommendations	107
<b>Summary</b>	<b>109</b>
<b>Acknowledgements</b>	<b>117</b>
<b>Curriculum vitae</b>	<b>119</b>

# Chapter 1

## Introduction

**Abstract:** Super water- and oil repellent surfaces have attracted much interest for both fundamental research and practical applications. Up to now, many methods have been developed to produce superhydrophobic surfaces, but less attention on superlipophobic surfaces has been paid. The objective of this thesis is to develop a simple method to prepare robust superhydrophobic coatings and, possibly, superlipophobic coatings. After first introducing the natural superhydrophobic surfaces, the theoretical background of the wetting behavior is then given in this chapter. Subsequently, some recent attempts to develop superhydrophobic surfaces and their applications are described. Finally, the objectives and the scope of this thesis are given.

## 1.1 General introduction

Wettability is one of the most important properties of a solid surface and the contact angle has been commonly used to characterize the surface wettability. A surface with water contact angle large than  $150^\circ$  and a low sliding angle (the critical angle where a water droplet with a certain weight begins to slide down the inclined plate) is usually called a superhydrophobic surface. Superhydrophobic surfaces have attracted much interest because of their potential practical applications such as anti-sticking<sup>1,2</sup>, anti-contamination<sup>3,4</sup>, and self-cleaning coating<sup>5,6</sup>. Attracted by their potential industrial applications, numerous attempts to preparing artificial superhydrophobic surfaces have been done by mimicking the lotus leaf structure<sup>7-9</sup>. Porous structures<sup>10-12</sup>, nano fibers<sup>13,14</sup> and carbon nanotubes<sup>15</sup> have also been used to develop superhydrophobic surfaces. Techniques involved in developing such surfaces include plasma treatment, chemical etching, chemical vapor deposition, lithography, and so forth.

However, most of the methods are expensive and substrate limited, require the use of harsh chemical treatment, or are vulnerable to environment attacks. Therefore, real applications of such superhydrophobic surfaces have been very limited so far.

Currently, many researches are focusing on superhydrophobic surfaces. However, oil repellency is also a very important property for the superhydrophobic surface to maintain its self-cleaning property. If a self-cleaning surface is not oil repellent, when it is in a dirty environment, oily materials can accumulate on the surface, eventually fill the textures, leading to the loss of the superhydrophobic and self-cleaning properties.

The objective of this thesis is to develop a simple method to prepare robust superlyophobic (both superhydrophobic and superlipophobic) coatings.

## 1.2 Natural superhydrophobic surfaces

Superhydrophobic and self-cleaning surfaces exist widely in nature. Butterfly wings, legs of a water strider and leaves of some plants are good examples. Insects and plants use this property to keep them dry or protect them against diseases. Among them, the most famous one is the lotus leaf, as shown in Figure 1.1, which is the symbol of purity in several Asian religions, and is considered sacred by Buddhists. Despite growing in muddy water, the leaves remain clean. When rain hits the leaves of the lotus plant,

rainwater droplets roll off the surface, wash off any contaminations and dust. The self-cleaning property of the lotus plant has intrigued researchers for decades. Thanks to the innovation of scanning electron microscopy, today, scientists know the plant's ability to repel water and dirt results from the superhydrophobicity, due to the combination of micrometer-scale hills and valleys and nanometer-scale waxy bumps, in combination with the reduced adhesion between surfaces and particles<sup>3</sup>.

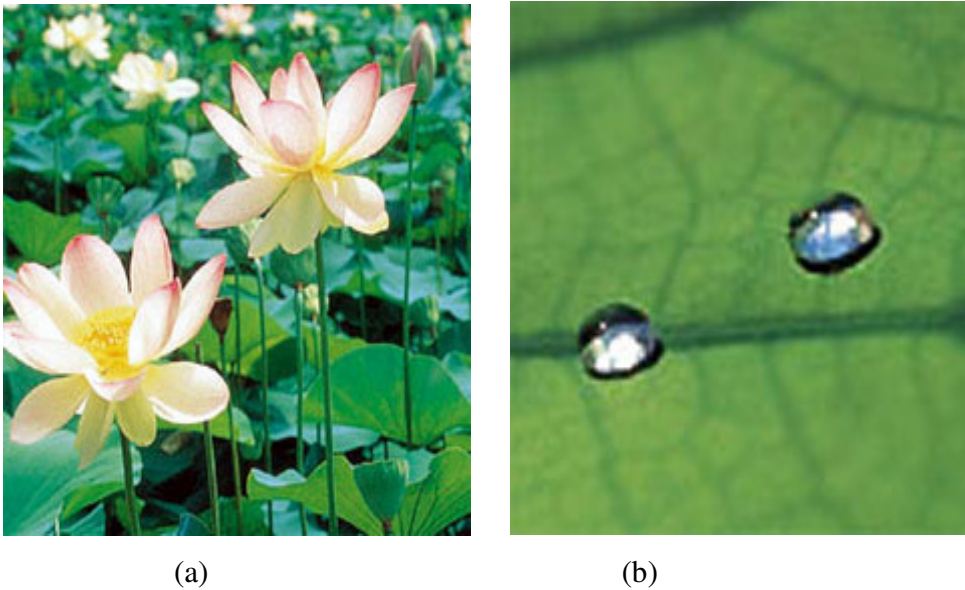


**Figure 1.1** (a) *Lotus flower*, and (b) *lotus leaf with water droplets on top*.

The leaves of a lotus have epidermal cells on their rough surface covered with wax crystals (Figure 1.2a)<sup>3</sup>. The wax crystals provide a hydrophobic layer and the double-size structure gives the surface high roughness. Therefore, water droplets on the surface are in the Cassie state (details will be described in 1.3.3)<sup>16</sup>, which means the water will form a spherical droplet, and can roll over easily on the surface. On the other hand, contaminations on the surface are usually larger than the cellular structure of the leaves, leaving the particle resting on the tips of the surface structure. As a result, the contact area and thus the interfacial interactions are minimized. When a water droplet rolls over the contamination, dirt particles are adsorbed to the water droplet, and moved away from the surface as demonstrated in Figure 1.2b.

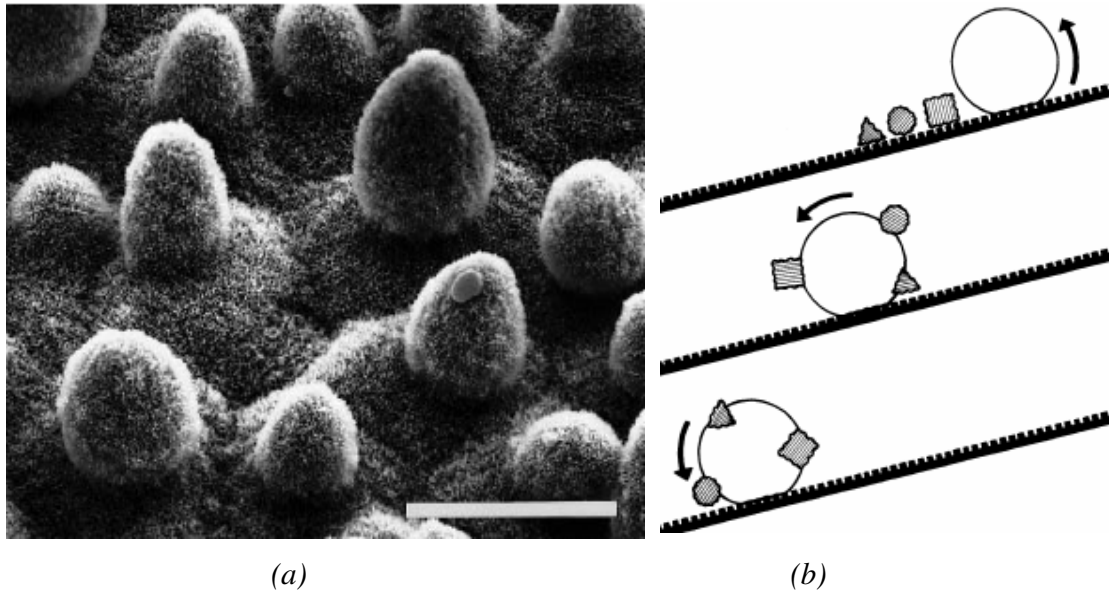


**Figure 1.2.** (a) SEM image of lotus leaf. Epidermal cells are covered with nano wax crystals (bar: 20  $\mu\text{m}$ ), and (b) diagram showing the self-cleaning process on a rough surface<sup>3</sup>.

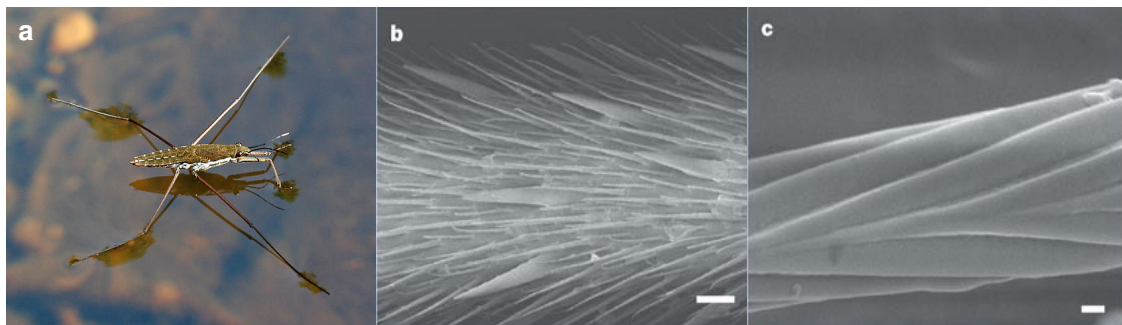


**Figure 1.3.** (a) A water strider rests on water surface, and SEM images of a water strider's leg (b) showing numerous oriented spindly microsetae (scale bar: 20  $\mu\text{m}$ ), and (c) the fine nanoscale grooved structure on a seta (scale bar: 200 nm)<sup>17</sup>.

Another example is the water strider. This insect propels itself over the still water surface of lakes and rivers (Figure 1.3a). Their capability of standing and walking freely on surface of water comes from their special legs. Reported by Jiang *et al.*<sup>17</sup>, a water strider's leg contains hierarchical micro- and nanostructures. There are numerous needle-shaped setae on the legs. Moreover, there are many nanoscale grooves on each micrometer sized seta (Figure 1.3b&c). This unique hierarchical structure gives water strider's leg the super water repellency. These hydrophobic legs make it possible to support the weight of the water strider on a water surface.

## 1.3 Theoretical Background

### 1.3.1 Young's equation

When a drop is deposited onto a solid surface, it forms a so-called contact angle ( $\theta$ ). The contact angle of a liquid on a perfectly smooth and chemically homogeneous solid surface is given by Young's equation<sup>18</sup>:

$$\cos \theta = \frac{\gamma_{SV} - \gamma_{SL}}{\gamma_{LV}} \quad (1.1)$$

where  $\gamma_{SV}$ ,  $\gamma_{SL}$ , and  $\gamma_{LV}$  are the interfacial tensions of the solid-vapor, solid-liquid and the liquid-vapor interface, respectively (Figure 1.4).

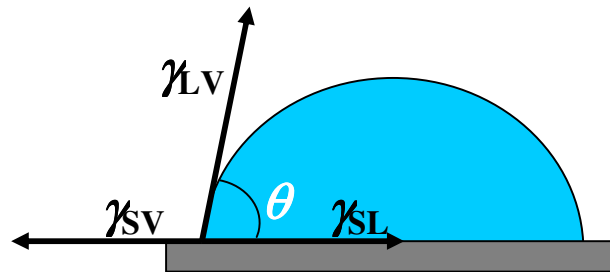


**Figure 1.4.** A water droplet on a smooth surface.

Wetting of realistic surfaces which are rough and chemically heterogeneous is more complex. The earliest work on the effect of surface roughness on contact angle was done by Wenzel<sup>19</sup> and Cassie & Baxter<sup>16</sup> many years ago.

### 1.3.2 Wenzel's equation

Wenzel developed a model where the liquid may completely penetrate into the roughness grooves (Figure 1.5a), and the contact angle on rough surfaces is given by the following equation<sup>19</sup>:

$$\cos \theta_w = r \cos \theta \quad (1.2)$$

In this equation,  $\theta_w$  is the contact angle on a rough surface,  $\theta$  is the Young's contact angle on a similar smooth surface, and  $r$  is the surface roughness factor, defined as the ratio between the actual and projected surface area ( $r = 1$  for a perfectly smooth surface, and  $r > 1$  for a rough one). The Wenzel equation predicts that wetting is enhanced by



roughness, when  $\theta$  is  $< 90^\circ$ ; and the wetting is lessened by roughness, when  $\theta$  is  $> 90^\circ$  (Figure 1.5b).

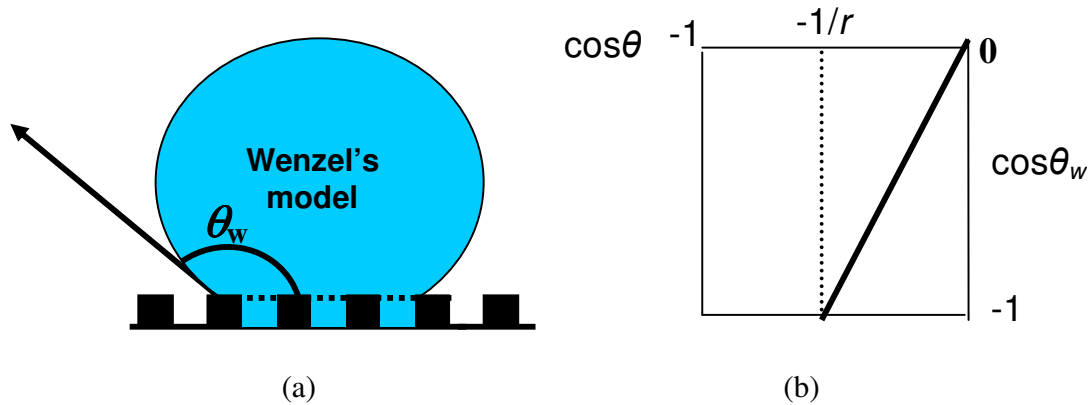


**Figure 1.5.** (a) A drop of liquid in the Wenzel state, and (b) the apparent contact angle as predicted by the Wenzel equation.

However, when  $\theta > 90^\circ$ , under some roughness condition, air bubbles may be trapped in the rough grooves. In this case, the drop is actually situated on a composite surface, and the wetting behavior is described by Cassie & Baxter<sup>16</sup>.

### 1.3.3 Cassie's equation

The Cassie-Baxter state<sup>16</sup>, also known as the composite or heterogeneous state, is a wetting state where, different from the Wenzel's state, it is considered that the grooves under the droplet are filled with vapor instead of liquid, as schematically shown in Figure 1.6.

This state is first described by Cassie and Baxter. In this case, the liquid-surface interface is actually an interface consisting of two phases, namely a liquid-solid interface and a liquid-vapor interface. And the apparent contact angle is the sum of all the contributions of the different phases as described below:

$$\cos \theta_c = f_1 \cos \theta_1 + f_2 \cos \theta_2 \quad (1.3)$$

where  $\theta_c$  is the apparent contact angle,  $f_1$  and  $f_2$  are the surface fractions of phase 1 and phase 2, respectively;  $\theta_1$  and  $\theta_2$  are the contact angles on phase 1 and phase 2, respectively. This equation is the general form, which also applies when there is no roughness. When one of these surfaces is the air-liquid interface,  $f$  is the solid fraction, defined as the fraction of the solid surface that is wetted by the liquid. Then the air

fraction is  $(1-f)$ . With  $\theta = 180^\circ$  for air, the resulting contact angle can be calculated by the following equation:

$$\cos \theta_c = f \cos \theta + (1-f) \cos 180^\circ = f \cos \theta + f - 1 \quad (1.4)$$

The parameter  $f$  ranges from 0 to 1, where at  $f = 0$  the droplet does not touch the surface at all and at  $f = 1$  the surface is completely wetted, the same as the behavior of a flat surface.

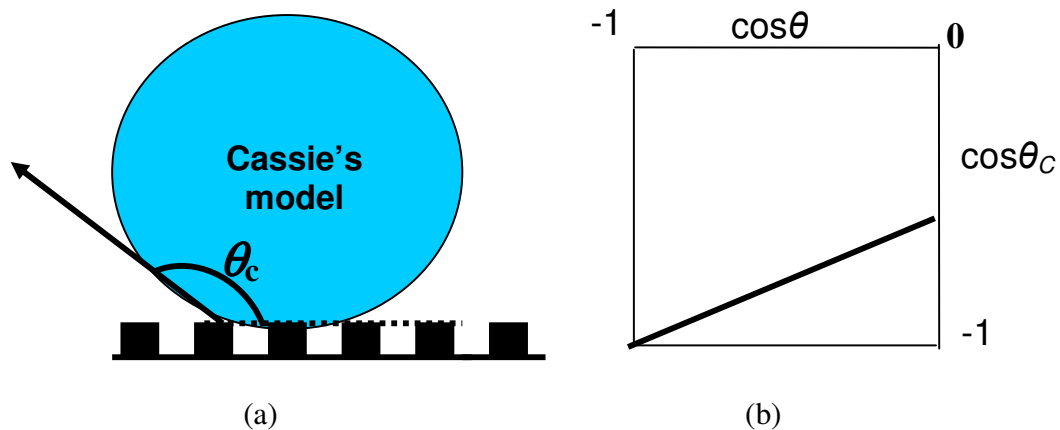


**Figure 1.6.** (a) A drop of liquid in Cassie state, and (b) the apparent contact angle as predicted by Cassie equation.

When a droplet is in the Cassie state, the small contact area between the droplet and solid surface allows the droplet to roll easily over the surface.

### 1.3.4 Contact angle hysteresis

The contact angle we mentioned above is the static contact angle, which defines the energetically most favorable state of a droplet on a solid surface. However, different contact angles can coexist along the contact line due to either chemical heterogeneity, surface roughness or surface reorganization upon its contact with a probe liquid<sup>20</sup>. A small droplet of water can remain immobile on a tilted surface; the water contact angle at the back of the droplet is smaller than that at the front of the droplet, as shown in Figure 1.7a. The two different contact angles can also be observed when more water is added to and withdrawn from the droplet. When water is added into a water droplet, the contact angle will increase until the contact line starts to move forward; this contact angle is

called advancing contact angle. On the other hand, when water is withdrawn from a water droplet, the contact angle will decrease until the contact line starts to recede; this contact angle is called receding contact angle (Figure 1.7b). The difference between advancing and receding contact angles is defined as the contact angle hysteresis. The contact angle hysteresis is a measure for how well a drop of liquid sticks to the surface. It is therefore important that a self-cleaning surface has a low contact angle hysteresis.

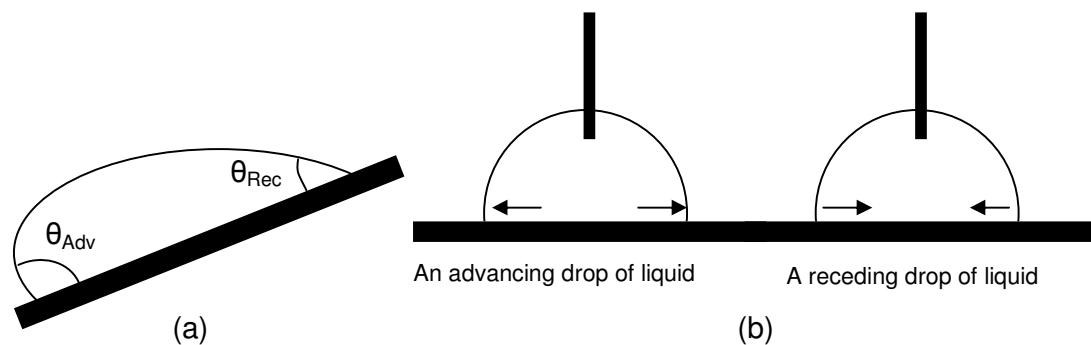


**Figure 1.7.** (a) Contact angle hysteresis on a tilted surface, and (b) schematic illustration of advancing and receding contact angles on a flat surface via increasing and decreasing the volume of droplet, respectively.

#### 1.4 Recent attempts to develop superhydrophobic surfaces

Currently, there are two main approaches to develop superhydrophobic surfaces. One is to introduce roughness onto a hydrophobic surface. For example, using a nanocasting technique, Sun *et al.*<sup>21</sup> prepared a superhydrophobic PDMS surface by directly copying the surface of a lotus leaf. They first made a negative PDMS template using lotus leaf as an original template. After that, they used the negative template to make a positive PDMS template which mimics the surface of lotus leaf (Figure 1.8a). Han *et al.*<sup>22</sup> developed a one-step method for fabricating superhydrophobic polyethylene (PE) film from in-situ ethylene polymerization via a direct catalytic route (Figure 1.8b). The advancing water contact angle on the film is  $164^\circ$  and sliding angle of a  $10\text{-}\mu\text{L}$  water droplet is  $3^\circ$ . The key feature of this PE film is its dual-size surface structure which offers air pockets between the water droplets and the surface. These air pockets help the water droplet resting on the film remain in the Cassie regime.

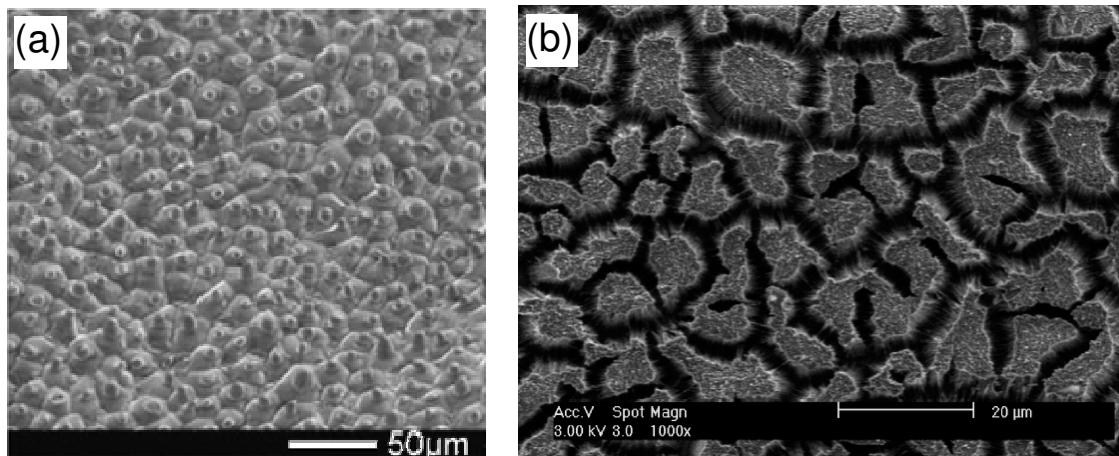


**Figure 1.8.** (a) Lotus leaf-like PDMS surface<sup>21</sup>, and (b) PE film with double-size roughness<sup>22</sup>.

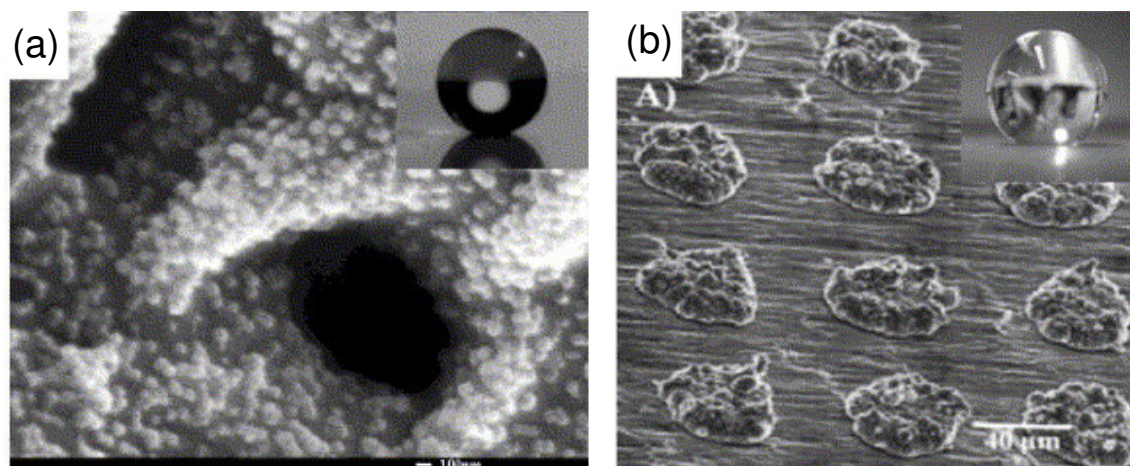


**Figure 1.9.** (a) Double-roughened superhydrophobic surfaces made by layer-by-layer assembly<sup>12</sup>, and (b) copper surface with dual-scale roughness<sup>7</sup>.

The other approach is to modify a rough surface with a material of low surface energy. For example, Zhai *et al.*<sup>12</sup> used a layer-by-layer approach to create a honeycomb-like polyelectrolyte multilayer surface covered with silica nanoparticles. Superhydrophobicity was then achieved by coating this rough surface with a semifluorinated silane (Figure 1.9a). Shirtcliffe *et al.*<sup>7</sup> prepared a double-roughened copper surface which mimics the lotus leaf by electrodeposition and patterning technique. Further hydrophobization yielded a superhydrophobic surface with a water contact angle of 160° (Figure 1.9b).

Recently, there have been a growing number of reports on developing superhydrophobic surfaces by layer-by-layer assembling silica particles of various sizes on solid surfaces. For example, Zhang *et al.*<sup>23</sup> developed a superhydrophobic surface by layer-by-layer deposition of poly(diallyldimethylammonium chloride)/sodium silica multilayer films on silica-sphere-coated substrate followed with a fluorination treatment. SiCl<sub>4</sub> was used in this process as a cross-linker to increase the mechanical robustness of the film. Bravo *et al.*<sup>24</sup> created a transparent superhydrophobic film by applying dual-size silica nanoparticles (20 nm, 50 nm) on a glass substrate. Subsequently, the film was treated with 1*H*,1*H*,2*H*,2*H*-perfluorooctyltrichlorosilane to obtain superhydrophobicity.

## 1.5 Applications

Superhydrophobic and self-cleaning coatings have numerous potential applications. Self-cleaning coatings on the satellite dishes, solar energy panels, exterior architectural glass and green houses can be cleaned by an occasional rain shower. The low friction between superhydrophobic surfaces and liquid offers potential applications on microfluidics, piping and boat hulls<sup>25</sup>. The superhydrophobic surfaces also show their applications on antifouling on boats<sup>26,27</sup> and antisticking of snow for antennas and windows<sup>1,2</sup>.

However, very few products with superhydrophobic surfaces have been developed for the real applications in our daily life. There are many problems to be solved. The first one is the wear resistance. The natural superhydrophobic surfaces such as lotus leaves can be easily repaired, for example, epicuticular wax is secreted by the leaf continuously. However, for most artificial superhydrophobic surfaces, the nano- and microtextures on them are fragile, and are easily destroyed by impacts, or even by simply rubbing them with a tissue paper. The second problem is contamination. Oily substances can accumulate on the superhydrophobic surfaces even those surfaces are supposed to be self-cleaning. These oils can eventually fill the textures, leading to an irreversible loss of the superhydrophobic properties. Therefore, the oil repellency is also important on self-cleaning surfaces.

Other problems which include durability, transparency, ease of mass production and so on, are also to be solved before the superhydrophobic coatings can be applied widely in our daily life.

## **1.6 Objectives and the scope of this thesis**

The objectives of this thesis are: (1) to develop superhydrophobic surfaces by mimicking the lotus leaf structure, (2) to improve the mechanical robustness of the superhydrophobic surfaces, and (3) to develop superlipophobic surface with an aim of preventing oil contamination. That is why in the title the term “superlyophobic” is used to include both “superhydrophobicity” and “superlipophobicity”.

Chapter 2 demonstrates that polymeric films with very low surface energy can be prepared by thermally curing a mixture of solventless liquid oligoesters and partially fluorinated polyisocyanates through the self-stratification process. In order to create a superhydrophobic film, silica microparticles and nanoparticles are used to generate surface roughness. The possible reasons for the high water contact angle hysteresis on such a surface will be discussed in this chapter.

Chapter 3 describes a novel way of developing superhydrophobic films with dual-size hierarchical structure by depositing well-defined silica-based raspberry-like particles on an epoxy-based polymer matrix, followed by the surface modification with PDMS. The surface mimics the lotus leaf. The effect of the size ratio of raspberry particles on the wettability of the film will be studied in this chapter.

Chapter 4 introduces a layer-by-layer (LbL) approach to prepare superhydrophobic surface, with the aim of improving the mechanical robustness of the film. The particles are partly embedded into the polymer matrix which increases the adhesion force between the particles and the polymer matrix. Nanoparticles are grafted on the microparticle surface by amine-epoxy reaction. The adhesion between nano- and microparticles is enhanced by using  $\text{SiCl}_4$  as a cross-linker.

Chapter 5 studies the lipophobicity on superhydrophobic surfaces. We examine the possibility to obtain lipophobicity on the fluorinated surface with a dual-size structure. The surface is treated with *1H,1H,2H,2H*-perfluorodecyltrichlorosilane through a self-assembling process. The contact angles of probe liquids with different surface tensions on

the superhydrophobic surface will be examined. And the wettabilities of several hydrophobic liquids (hexadecane, oleic acid and sunflower oil) on this surface will be studied.

In Chapter 6, a biomimetic procedure to prepare superhydrophobic cotton textiles will be introduced. By in-situ introducing silica particles to cotton fibers to create a dual-size surface roughness, followed by hydrophobization with PDMS, normally hydrophilic cotton has been turned superhydrophobic. Moreover, a superlipophobic textile is prepared by modifying the microparticles covered cotton textile with perfluoroalkylsilane.

Finally, some conclusions and recommendations will be given in Chapter 7.

## References

1. Saito, H.; Takai, K.; Takazawa, H.; Yamauchi, G. *Mater. Sci. Res. Int.* **1997**, *3*, 216.
2. Kako, T.; Nakajima, A.; Irie, H.; Kato, Z.; Uematsu, K.; Watanabe, T.; Hashimoto, K. *J. Mater. Sci.* **2004**, *39*, 547.
3. Barthlott, W.; Neinhuis, C. *Planta* **1997**, *202*, 1.
4. Lafuma, A.; Quere, D. *Nat. Mater.* **2003**, *2*, 457.
5. Furstner, R.; Barthlott, W.; Neinhuis, C.; Walzel, P. *Langmuir* **2005**, *21*, 956.
6. Otten, A.; Herminghaus, S. *Langmuir* **2004**, *20*, 2405.
7. Shirtcliffe, N. J.; McHale, G.; Newton, M. I.; Chabrol, G.; Perry, C. C. *Adv. Mater.* **2004**, *16*, 1929.
8. Jiang, L.; Zhao, Y.; Zhai, J. *Angew. Chem. Int. Ed.* **2004**, *43*, 4338.
9. Zhao, N.; Xu, J.; Xie, Q. D.; Weng, L. H.; Guo, X. L.; Zhang, X. L. *et al.*, *Macromol. Rapid Commun.* **2005**, *26*, 1075.
10. Yabu, H.; Shimomura, M. *Chem. Mater.* **2005**, *17*, 5231.
11. Xu, L.; Chen, W.; Mulchandani, A.; Yan, Y. *Angew. Chem. Int. Ed.* **2005**, *44*, 6009.
12. Zhai, L.; Cebeci, F.C.; Cohen, R.E.; Rubner, M.F. *Nano Lett.* **2004**, *4*, 1349.
13. Ma, M.; Hill, R.M.; Lowery, J.L.; Fridrikh, S.V.; Rutledge, G.C. *Langmuir* **2005**, *21*, 5549.
14. Ma, M.; Mao, Y.; Gupta, M.; Gleason, K.K.; Rutledge, G.C. *Macromolecules* **2005**, *38*, 9742.

15. Huang, L.; Lau, S.P.; Yang, H.Y.; Leong, E.S.P.; Yu, S.F.; Prawer, S. *J. Phys. Chem. B* **2005**, *109*, 7746.
16. Cassie, A. B. D.; Baxter, S. *Trans. Faraday Soc.* **1944**, *40*, 546.
17. Gao, X. F.; Jiang, L. *Nature* **2004**, *432*, 36.
18. Young, T. *Philos. Trans. R. Soc. London* **1805**, *95*, 65.
19. Wenzel, R. N. *Ind. Eng. Chem.* **1936**, *28*, 988; *J. Phys. Colloid Chem.* **1949**, *53*, 1466.
20. Johnston, E.; Bullock, S.; Uilk, J.; Gatenholm, P.; Wynne, K. J. *Macromolecules* **1999**, *32*, 8173.
21. Sun, M.H.; Luo, C.X.; Xu, L.P.; Ji, H.; Qi, O.Y.; Yu, D. P. *et al.*, *Langmuir* **2005**, *21*, 8978.
22. Han, W.; Wu, D.; Ming, W.; Niemantsverdriet, J.W.; Thuene, P. C. *Langmuir* **2006**, *22*, 7956.
23. Zhang, L.B.; Chen, H.; Sun, J.Q.; Shen, J. C. *Chem. Mater.* **2007**, *19*, 948.
24. Bravo, J.; Zhai, L.; Wu, Z. Z.; Cohen, R. E.; Rubner, M. F. *Langmuir* **2007**, *23*, 7293.
25. Fukuda, K.; Tokunaga, J.; Nobunaga, T.; Iwasaki, T.; Kunitake Y. *J. Soci. Naval Architects Japan* **1999**, *186*, 73.
26. Scardino, A.; De Nys, R.; Ison, O.; O'Connor, W.; Steinberg, P. *Biofouling* **2003**, *19*, 221.
27. Schultz, M. P.; Kavanagh, C. J.; Swain, G. W. *Biofouling* **1999**, *13*, 323.





## Chapter 2

# Superhydrophobic coatings based on fluorinated polyurethanes\*

**Abstract:** In this chapter, smooth polymeric films with a water contact angle about  $110^\circ$  were obtained from a mixture of well-defined fluorinated isocyanates and hydroxyl-end-capped solventless liquid oligoesters. Subsequently, microsized silica particles were embedded in the polymeric film to roughen the surface. The advancing water contact angle is above  $150^\circ$  on this roughed polyurethane film with a fluorine-rich top layer. The cause of the high water contact angle hysteresis is discussed in this chapter.

---

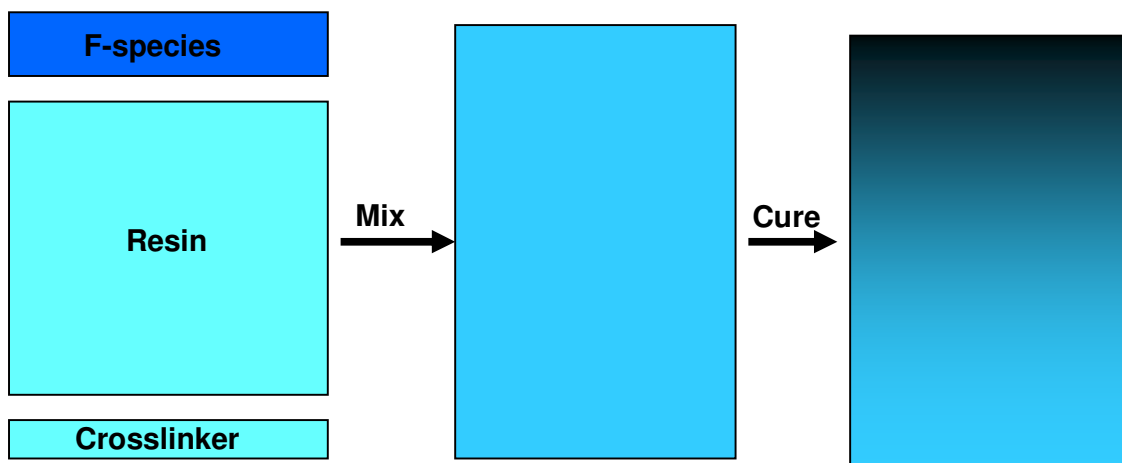
\* Part of this Chapter has been submitted for publication: Wu, D.; Ming, W.; van Benthem, R.A.T.M.; de With, G. Superhydrophobic fluorinated polyurethane films, submitted to *J. Adhesion Sci. Technol.*, 2007.

## 2.1 Introduction

Generally, superhydrophobic surfaces are created through the combination of surface roughening and lowering of the surface energy<sup>1-19</sup>. It is well known that a fluorinated polymer has a low wettability due to its low surface energy<sup>20-33</sup>. Therefore, it is an ideal building block to develop a superhydrophobic coating. On the other hand, the low wettability is basically a surface property, so it is unnecessary to have fluorine in the bulk. Surface segregation provides an excellent strategy to create a coating with a fluorine-rich surface. In such an approach, due to its low surface energy, the fluorinated species would migrate toward the air/film interface to minimize the interfacial energy<sup>22,23,34,35</sup>. Thus, only a very small quantity of fluorinated species is needed to provide a surface with low surface energy. The surface segregation process is demonstrated in Scheme 2.1.

In our previous studies<sup>36</sup>, low surface energy polymeric films were developed from a mixture of a hydroxyl-end-capped solventless liquid oligoester (SLO), a partially fluorinated isocyanate and a polyisocyanate. In this approach, a novel fluorinated isocyanate ( $F_n$ -IMCI) was used for its well-defined structure<sup>37</sup> which provides an easy and accurate adjustment of the fluorine content in the polymeric films. In order to generate surface roughness, microsized silica particles were added to the polymeric film.

This Chapter describes our attempts of developing a superhydrophobic coating by using a self-stratification approach. The first part of this Chapter will focus on the synthesis of a well-defined fluorinated isocyanate. The second part will deal with developing a film with a fluorine-rich top layer. Finally, the approach of developing superhydrophobic coatings was attempted by combining low surface energy and proper surface roughness. The surface properties were examined by water contact angle measurement, atomic force microscopy (AFM) and X-ray photoelectron spectroscopy (XPS).

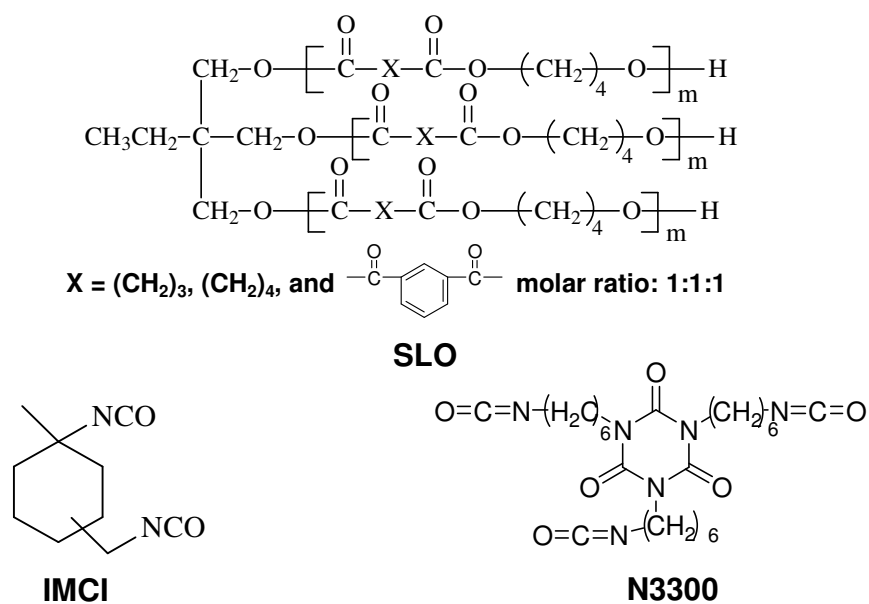


**Scheme 2.1.** Surface segregation of perfluoroalkyl chains in a polymeric network<sup>36</sup>.

## 2.2 Experimental

### 2.2.1 Materials

The solventless liquid oligoester (SLO, Scheme 2.2) was synthesized in our group<sup>36,39</sup>. Two different perfluoroalkyl alcohols,  $C_nF_{2n+1}-CH_2CH_2OH$  ( $n = 6$  and  $8$ , denoted as  $F_6-OH$  and  $F_8-OH$ , respectively), were kindly supplied by Clariant GmbH (with trademarks of Fluowet EA 600 and EA 800, respectively). 3/4-isocyanatomethyl-1-methylcyclohexylisocyanate (IMCI, Scheme 2.2) was generously supplied by DSM. Zirconium(IV) butoxide was purchased from Fluka. A polyisocyanate cross-linker, under the trademark Desmodur N3300 was obtained from Bayer AG. Vinyl-terminated poly(dimethylsiloxane) and the tetrakis(dimethylsiloxy)silane (a 4-functional cross-linker) were obtained from ABCR, the catalyst *cis*-dichlorobis(diethyl sulfide)platinum(II) was obtained from Strem Chemicals. Aluminum panels were purchased from Q-Panel Co. Silica particles ( $\sim 0.9 \mu m$ , with trademarks of NYASIL 6200) were from NYACOL Nano Technologies Inc.



**Scheme 2.2.** Molecular structure of SLO, IMCI and N3300.

### 2.2.2 Synthesis of fluorinated IMCI

The well-defined fluorinated IMCI was synthesized via a one-step reaction between IMCI and a perfluoroalkyl alcohol (F<sub>6</sub>-OH and F<sub>8</sub>-OH), the overall OH/NCO molar ratio was maintained at 0.8/2 or 1/2 under a dry N<sub>2</sub> atmosphere at 60 °C for 1 h and catalyzed by zirconium(IV) butoxide.

### 2.2.3 Preparation of partially fluorinated PU films

The fluorinated isocyanate (F<sub>6</sub>-IMCI or F<sub>8</sub>-IMCI) was mixed with an appropriate amount of SLO and N3300 (cross-linker) in butyl acetate. The overall OH/NCO molar ratio was maintained at about 1. Film 2A was prepared from a mixture of 0.065 g F<sub>8</sub>-IMCI (0.1 mmol NCO), 0.636 g N3300 (2.5 mmol NCO) and 0.78 g SLO (2.6 mmol OH). After a homogeneous mixture was formed, a coating was applied on a clean aluminum panel by spin coating. The coating was then cured at 80 °C for 2 h. The reaction between SLO and F<sub>8</sub>-IMCI was monitored by a real-time ATR-FTIR. Using a similar process, film 2B was prepared from a mixture of F<sub>6</sub>-IMCI, SLO and N3300.

Because of the steric hindrance, the remaining isocyanate group in F<sub>8</sub>-IMCI was much less reactive than the isocyanate groups in cross-linker N3300. So, alternatively, F<sub>n</sub>-

IMCI was first reacted with SLO at an NCO/OH ratio of 1/20, before adding cross-linker to the reaction mixture. Otherwise, NCO groups in N3300 may consume all the OH groups in the SLO before F<sub>n</sub>-IMCI can have a chance to be grafted onto the SLO.

#### **2.2.4 Preparation of roughened, fluorinated PU films**

First, F<sub>8</sub>-IMCI was mixed with SLO, the overall NCO/OH molar ratio was 1:20 to make sure there were enough OH groups remaining on SLO after all the NCO groups were consumed. The product mixture was dissolved in butyl acetate. Next, cross-linker N3300 was added to SiO<sub>2</sub> particles (0.9 μm) butyl acetate suspension. Finally, the solution of F<sub>8</sub>-IMCI, SLO and the suspension of SiO<sub>2</sub> were mixed together and keep the OH/NCO molar ratio was about 1.1. The SiO<sub>2</sub> particle concentration for the mixture was 60 wt %. Films were applied on clean aluminum panels by an automatic film applicator (Coatmaster 509 MC, Erichsen) and then cured at 80 °C for 1 h. The calculated thickness of the dry film was about 6 μm.

#### **2.2.5 Characterization techniques**

##### **<sup>1</sup>H-NMR**

<sup>1</sup>H-NMR analyses were performed using a Varian Mercury-VX 400 MHz spectrometer at room temperature. Samples were dissolved in CDCl<sub>3</sub> (5% wt).

##### **ATR-FTIR measurements**

Real-time infrared spectra were recorded on a BioRad Excalibur spectrophotometer equipped with a deuterated tri-glycine sulfate (DTGS) detector, a MKII Goden Gate heated diamond 45° ATR top plate (Specac Ltd., Kent, England), and a 3000 series high stability temperature controller (Specac). After the reaction mixture was deposited on the diamond unit, infrared spectra (two scans per spectrum) were collected every 5-30 s at a resolution of 16 cm<sup>-1</sup>.

##### **XPS measurements**

X-ray photoelectron spectroscopy measurements were performed with a VG Escalab 200 using a standard aluminum anode (Al-Kα 1486.6 eV) operating at 240 W. Spectra were taken at takeoff angles of 30° and 90°, corresponding to the probe depths of about 5

nm and 10 nm, respectively. The measurement was operated with a background pressure of  $2 \times 10^{-9}$  mbar.

### **MALDI-TOF-MS**

MALDI-TOF-MS measurements were carried out on a Voyager-DE-STR (Applied Biosystems) equipped with a 337 nm nitrogen laser. *Trans*-2-[3-(4-*tert*-butylphenyl)-2-methyl-2-propenylidene]malononitrile was used as the matrix. The matrix was dissolved in THF at a concentration of approximately 40 mg/mL. Sodium trifluoroacetate (Aldrich, 98%) was used as the cationization agent and was added to THF at a concentration of 5 mg/mL. The sample was dissolved in THF at a concentration of 2 mg/mL. In a typical measurement, the matrix, cationization agent and sample solution were premixed in a 5:1:1 ratio. Approximately 0.5  $\mu$ L of the mixture obtained was hand spotted on the target plate and left to dry. Mass spectra were recorded in the reflector mode. For each spectrum, 1000 laser shots were accumulated.

### **Contact angle measurements**

Contact angles were measured with deionized water using a Dataphysics OCA 30 instrument at room temperature. All the contact angles were determined by averaging values measured at three different points on each sample surface. Dynamic advancing and receding angles were recorded while the probe fluid was added to and withdrawn from the drop, respectively.

### **Atomic force microscopy (AFM)**

Atomic force microscopy measurements were performed on a Veeco Multimode SPM Nanoscope III (Santa Barbara, CA) instrument. The cantilever of choice was no-contact gold-coated NSG 11 (NT-MDT, Russia).

## **2.3 Results and Discussion**

### **2.3.1 Synthesis of F<sub>n</sub>-IMCI**

IMCI consists of two isocyanate groups, one is directly bonded to a carbon atom in the cyclohexane ring, resulting in considerable steric hindrance, while the other (primary) isocyanate group is separated from the ring by a methylene spacer and is therefore more accessible. When zirconium(IV) butoxide is used as the catalyst for the reaction between alcohol and IMCI, the selectivity of the reaction between the alcohol and the primary

isocyanate group is as high as 99%<sup>37</sup>. Therefore, by controlling the OH/NCO molar ratio at 1:2, a perfluoroalkyl chain could be selectively grafted on IMCI, leaving the other isocyanate group for further reaction.

Both IMCI and fluorinated IMCI were characterized by <sup>1</sup>H NMR on a Varian 400 MHz instrument with CDCl<sub>3</sub> as the solvent, as shown in Figure 2.1. The following peaks were identified. For IMCI,  $\delta = 3.30$  (m, 2H, -CH<sub>2</sub>-NCO); and for F<sub>8</sub>-IMCI,  $\delta = 2.45$  (m, 2H, -CH<sub>2</sub>CH<sub>2</sub>CF<sub>2</sub>-), 3.10 (m, 2H, -CH<sub>2</sub>-NHC(O)-O-), 4.40 (t, 2H, -O-CH<sub>2</sub>CH<sub>2</sub>CF<sub>2</sub>-), 4.90 (m, 1H, -CH<sub>2</sub>-NHC(O)-O-). F<sub>6</sub>-IMCI has the same spectrum as F<sub>8</sub>-IMCI.

After the fluorination, the peak at 3.30 ppm in IMCI disappeared completely, indicating that the primary NCO was reacted completely.

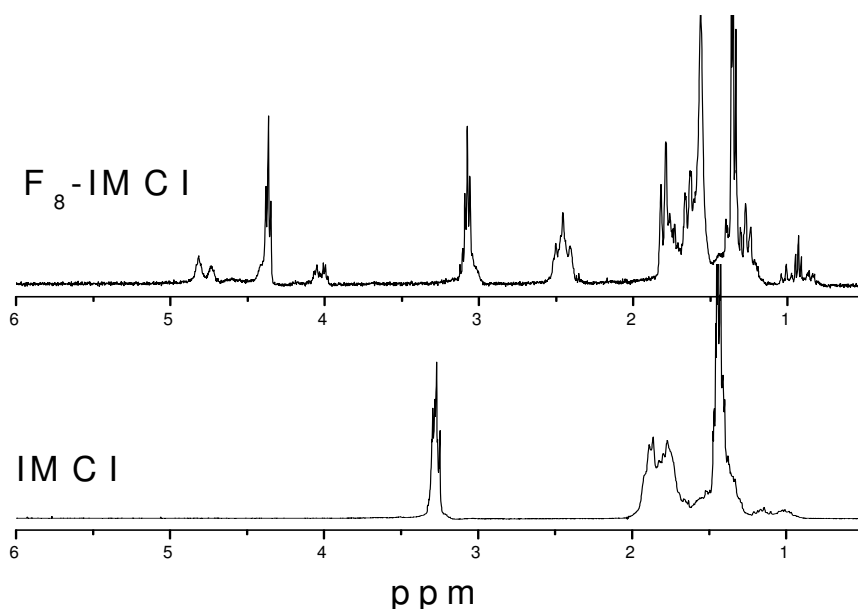


**Figure 2.1.** Proton NMR spectra of IMCI and F<sub>8</sub>-IMCI.

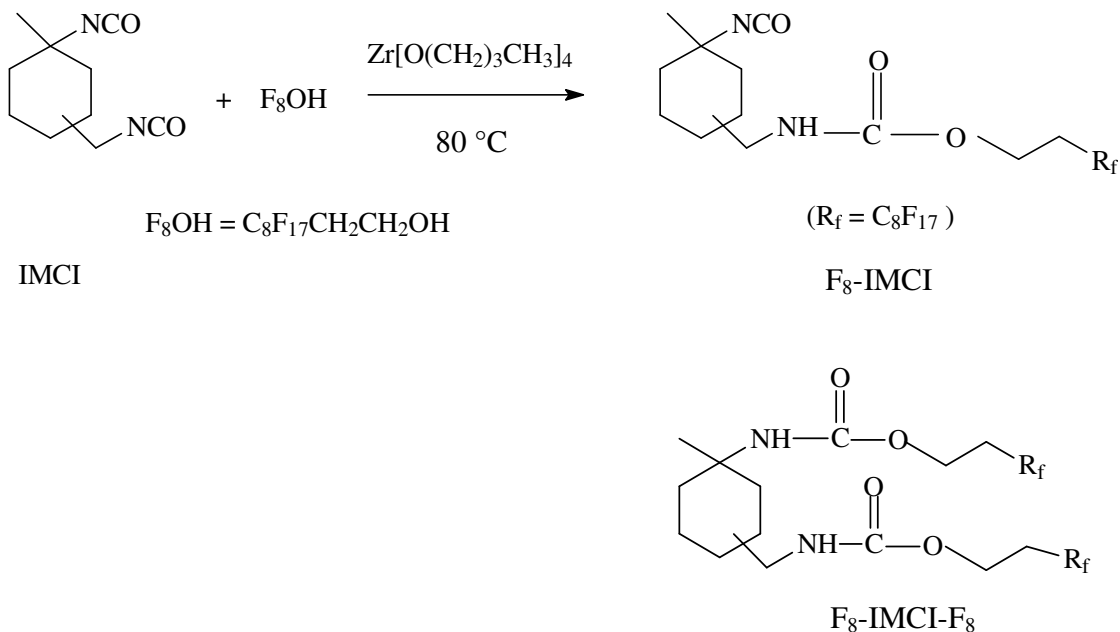
The well-defined structure of the F<sub>n</sub>-IMCI enables an easy and accurate adjustment of the fluorine content in the polymeric film created by cross-linking F<sub>n</sub>-IMCI, SLO and N3300.

According to the reaction formula of IMCI and F<sub>8</sub>-OH, the OH/NCO molar ratio should be 1/2. When the film was developed by F<sub>8</sub>-IMCI, and the water contact angles on the film were checked, different results were obtained before and after the samples were



rinsed with acetone. Before rinsing with acetone, the advancing CA on a smooth film based on SLO, F<sub>8</sub>-IMCI and N3300 is 120°, with CA hysteresis about 60°. In contrast, after the same film surface was rinsed with acetone and dried in air at 80 °C for 15 min, the advancing CA is 97°, and the receding CA is 55°. The advancing CA decreases by 23°. To find out the reason, the fluorine concentration on the sample surface before and after rinsing with acetone was checked with XPS at takeoff angle of 30° and 90°, respectively. Before washing with acetone, the overall F/C atomic ratio in the film at takeoff angle of 30° and 90° was 0.57 and 0.46, respectively; after rinsing, the overall F/C atomic ratio reduced to 0.19 and 0.13, respectively. These results indicate that there is a fluorine-rich layer on the surface that can be easily rinsed away. The possible reason is that some fluorinated species are not chemically bonded to the bulk of the film. So we checked the product of our first synthetic step with MALDI-TOF MS.

In MALDI-TOF mass spectra, two peaks were found at 681 m/z and 1145 m/z which correspond to molecules [F<sub>8</sub>-IMCI + Na]<sup>+</sup> and [F<sub>8</sub>-IMCI-F<sub>8</sub> + Na]<sup>+</sup>, respectively, which indicated that a side reaction happened as shown in Scheme 2.3.



**Scheme 2.3.** *IMCI reaction.*

The by-product  $F_8$ -IMCI- $F_8$  has no NCO group available to react further with SLO, so it cannot be cross-linked to the bulk of the film. On the other hand, because of its relatively low molecular weight and high fluorine concentration,  $F_8$ -IMCI- $F_8$  will migrate to the surface of the film very easily, and can be washed away. Therefore, the fluorine concentration on the film surface decreases dramatically after rinsing with acetone.

To eliminate the by-product  $F_8$ -IMCI- $F_8$ , the molar ratio between OH and NCO was reduced from 1/2 to 0.8/2 and the reaction temperature was decreased from 80 °C to 60 °C. Under this condition, there will be a very small amount of unreacted IMCI existing at the end of reaction. Since the primary NCO is much more reactive than the tertiary NCO in the presence of the catalyst we used (the selectivity is above 99%)<sup>37</sup>, there should be no  $F_8$ -IMCI- $F_8$  present in the final product. The remaining IMCI can work as a chain extender in the following film formation. The new product was checked with MALDI-TOF MS again. In the MALDI-TOF mass spectrum, the peak at 1145 m/z completely disappeared which indicates that there is no  $F_8$ -IMCI- $F_8$  left in the new product.

### 2.3.2 Reaction between SLO and $F_8$ -IMCI

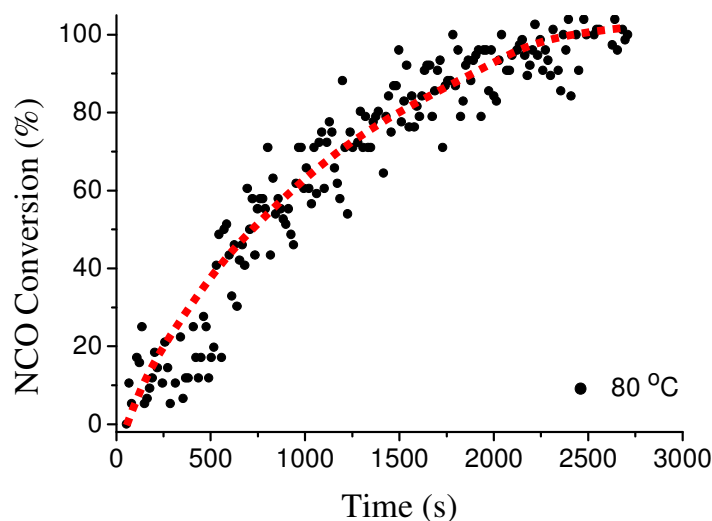


**Figure 2.2.** Conversion of NCO during reaction between  $F_8$ -IMCI and SLO at 80 °C.

The reaction between SLO and  $F_n$ -IMCI was monitored by a real-time ATR-FTIR at 80 °C. The peak at 2261  $cm^{-1}$ , corresponding to the NCO group, decreased steadily as

reaction proceeded. On the other hand, the CH<sub>2</sub> stretch (2948 cm<sup>-1</sup>) remained the same throughout the reaction, which can be taken as an internal standard. The NCO conversion for the reaction between F<sub>8</sub>-IMCI and SLO as a function of reaction time is shown in Figure 2.2. The complete consumption of the NCO was reached in a period of about 30 min.

### 2.3.3 Wettability of smooth polymeric films

The wettability of a film is reflected by the contact angle (CA) of water on the surface. The advancing and receding water CA on smooth films based on SLO, F<sub>n</sub>-IMCI (F<sub>8</sub>-IMCI and F<sub>6</sub>-IMCI) and N3300 were measured after those films were rinsed with acetone. Table 2.1 contains water contact angle data. Without fluorine present in the films, the advancing water CA on the film surface is about 87°. After adding a small amount of fluorinated species, the advancing water CA increased from 87° to 110° in the case of F<sub>8</sub>-IMCI. It is interesting to notice that film 2A is more hydrophobic than film 2B even the latter has slighter higher bulk fluorine concentration. A similar result has been obtained in our previous study<sup>36</sup>. The reason is that the driving force for the surface enrichment of the fluorinated species is stronger for F<sub>8</sub>-IMCI than for F<sub>6</sub>-IMCI, due to the longer perfluoroalkyl chains in the former.

**Table 2.1.** Water CA on the polymer films from SLO, F<sub>n</sub>-IMCI and N3300.

Films	Film composition	F content (wt%)*	Water contact angle $\theta_A$ (°)	Water contact angle $\theta_R$ (°)
Film 0	N3300,SLO	0	86.7 ± 0.8	41.1 ± 1.1
Film 2A	F <sub>8</sub> -IMCI, N3300, SLO	2.1	110.4 ± 1.7	63.1 ± 1.6
Film 2B	F <sub>6</sub> -IMCI, N3300, SLO	3.8	99.3 ± 1.2	56.2 ± 0.5

\* wt% was calculated from the film composition, assuming all the added fluorinated species are chemically bonded to the network.

Table 2.1 also indicates that large water contact angle hysteresis is present on these films. It is well known that contact angle hysteresis arises from three sources<sup>38</sup>: surface roughness, chemical heterogeneity and surface reorganization. To find out what causes

the high water CA hysteresis on these films, the topology of the films was first checked by AFM on several spots of the films. The film surface roughness in the  $0.5\mu\text{m} \times 0.5\mu\text{m}$  is within 5 nm (Figure 2.3a), so it is not likely to be the source for the high contact angle hysteresis. On the other hand, the AFM phase image shown on Figure 2.3b clearly shows that there is no phase contrast on the film which indicates the distribution of the fluorinated species is quite homogeneous even at the nanometer scale on the surface on this film; therefore, the chemical heterogeneity is not expected to contribute significantly to the CA hysteresis.

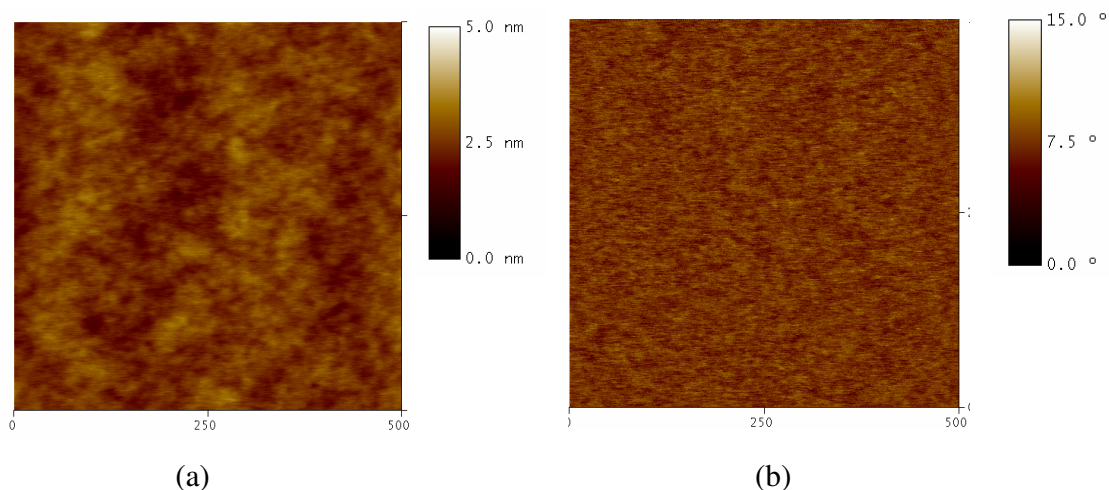


**Figure 2.3.** AFM non-contact mode images ( $500\text{ nm} \times 500\text{ nm}$ ) of the surface of Film 2A: (a) height image; (b) phase image.

In our previous work<sup>39</sup>, low surface energy cross-linked films on the basis of partially fluorinated hydroxyl-end-capped solventless liquid oligesters have been developed. Low energy ion scattering (LEIS), a unique technique that only analyzes the composition of the outermost atomic layer<sup>40</sup>, was used to determine the fluorine content in the first atomic layer of the film (Figure 2.4). Sample 1 is a PU film without any fluorine, two peaks can be found at 1100 eV and 1450 eV, which correspond to carbon and oxygen atoms, respectively. Samples 2 to 5 are PU films with different fluorine contents. Only C, F (1600 eV) signals were detected for samples 2-5, where the overall F content in sample 2 was only 0.18 wt%. N and O atoms were completely shielded, indicating that the film was covered by perfluoroalkyl side chains completely. However, a large water contact

angle hysteresis (above 30°) still exists. Therefore, the high CA hysteresis is likely due to the surface reorganization during the CA measurements.

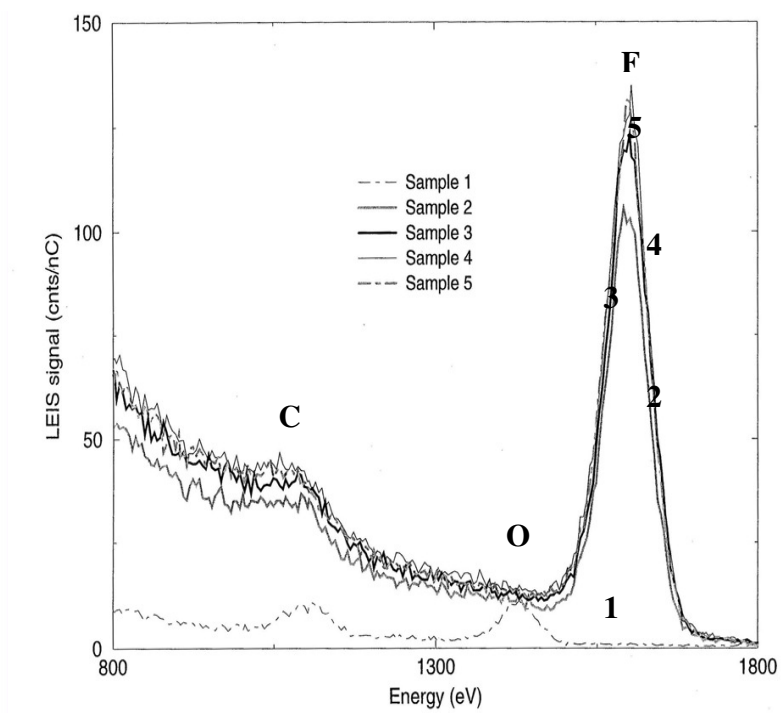


**Figure 2.4.** LEIS spectra of the PU films cured at 80 °C from a mixture of normal and fluorinated oligesters and a cross-linker N3300<sup>39</sup>.

After a surface is wetted by water molecules during the contact angle measurement, polar groups may be exposed to the film surface due to the surface reorganization, and the interaction between the polar groups and water would decrease the water receding contact angle, thus increasing the water contact angle hysteresis.

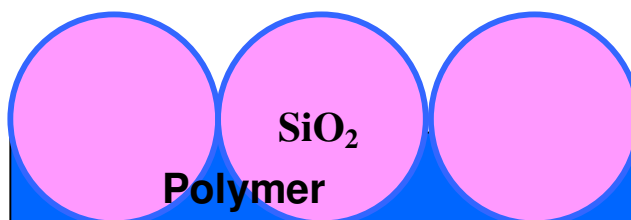
The PU film we prepared is a cross-linked film with low  $T_g$  (about 15 °C), so the network and the perfluoroalkyl side chains have some degree of mobility. On the unwetted surface, the perfluoroalkyl side chains are oriented preferentially towards the coating-air interface, resulting in a low surface energy and high advancing water contact angle. However, for the surface already wetted by water, water may penetrate into deeper layers and “drag out” some polar groups (e.g. urethane), leading to a relatively low water receding contact angle<sup>41</sup>.

Therefore, it is very likely that the low receding water contact angle is the consequence of the surface reorganization induced by water. A large water contact angle hysteresis may always exist even when the surface is covered with perfluoroalkyl side chains because of the reorganization of the film surface upon contact with water.

#### 2.3.4 Wettability of rough polymeric films

It is well known that surface roughness amplifies the wetting or de-wetting behavior of the surface. Since the advancing CA on the smooth based film 2A is  $110^\circ$  ( $> 90^\circ$ ), creating roughness on the film surface will increase the CA.

In Scheme 2.4, we depict a rough structure by dispersing microsized  $\text{SiO}_2$  particles in a polymer matrix. As we know the surface energy of silica particles is much larger than that of polyurethane. Therefore, the polymer solution is able to wet the silica particle surface easily. In this model, we assume that a very thin layer of polymer completely covers the silica particle surface. According to this model, the volume ratio between  $\text{SiO}_2$  and polymer resin was about 2.2:1, thus the  $\text{SiO}_2$  concentration in the solid film should be about 90 wt%. However, a film with 90 wt%  $\text{SiO}_2$  concentration had a very poor mechanical property; the film was brittle and can be easily destroyed by simple scratching, so we had to decrease the  $\text{SiO}_2$  concentration. As the  $\text{SiO}_2$  concentration decreased, the robustness of the film improved, on the other hand, the roughness of the film surface decreased. We found that the film with 60 wt%  $\text{SiO}_2$  particles had both proper roughness and proper mechanical strength. When the  $\text{SiO}_2$  concentration was below 30 wt%, a smooth film was formed.



**Scheme 2.4.** Schematic illustration of a rough surface prepared by dispersing  $\text{SiO}_2$  particles in polymer matrix.

Surface topology of the film containing 60 wt% silica particles was examined by AFM (Figure 2.5). The peak-valley distance is about 900 nm.

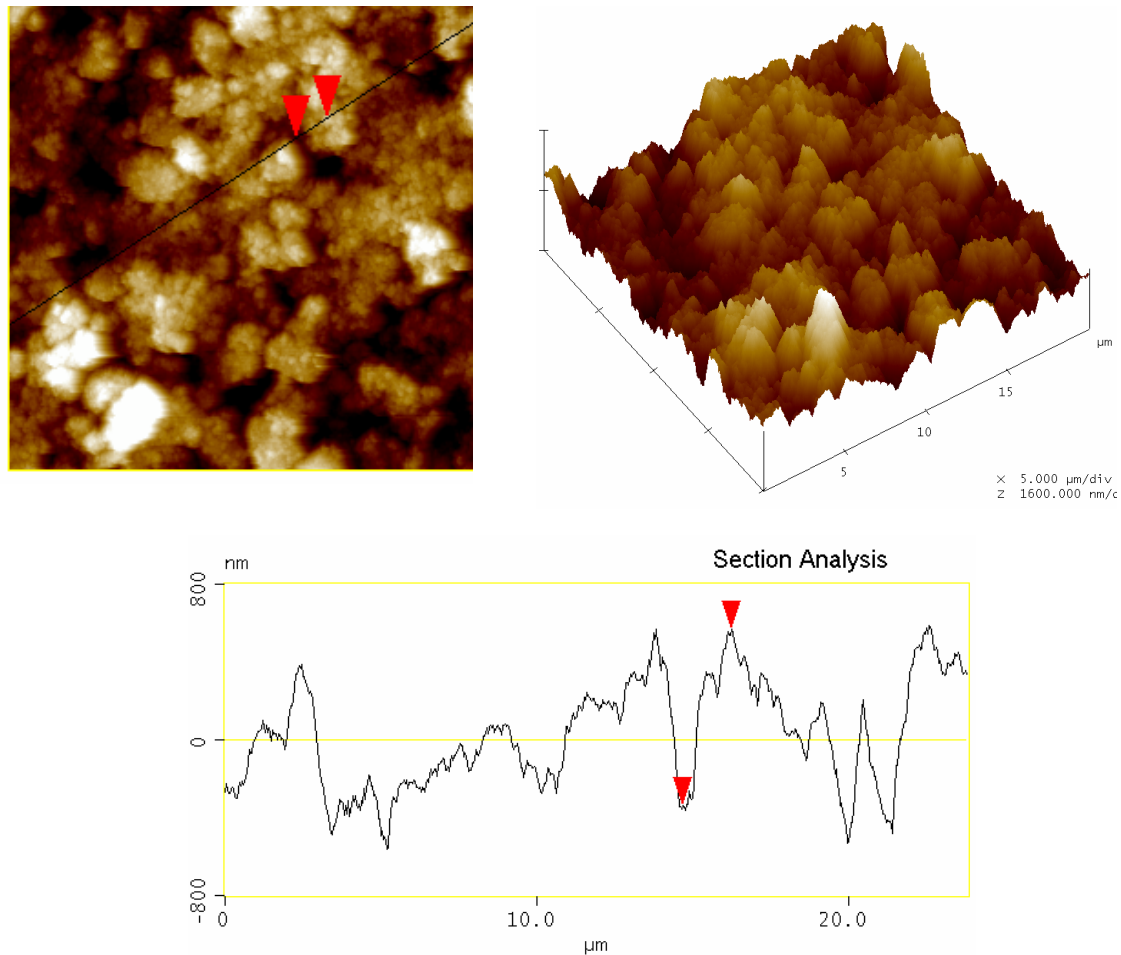


**Figure 2.5.** AFM non-contact mode images of a rough surface prepared by dispersing  $\text{SiO}_2$  particles in polymeric film. (Upper left image:  $20 \mu\text{m} \times 20 \mu\text{m}$ )

The water advancing CA on the rough polymeric film is  $150.2 \pm 1.2^\circ$  with a CA hysteresis of about  $68^\circ$ . We believe there are three possible reasons for this large hysteresis. One is the surface reorganization of the polyurethane film with perfluoroalkyl side chains as we mentioned above. The second reason is the coverage of polymer film on the particles surface. In the model we described above, theoretically, the low surface tension polymer should completely cover the high surface tension silica particles, but, practically, there may be still some particle surfaces which are not covered by polymer.

This chemical inhomogeneity can raise the CA hysteresis significantly. The last reason may be that the surface roughness is insufficient to enter the Cassie state.

As we mentioned in Chapter 1, when a water droplet is deposited on a solid surface, two distinct wetting behaviors have been observed depending on the surface roughness. There are the Wenzel state<sup>42</sup> and the Cassie state<sup>43</sup>. In the roughness regime where Wenzel's mode is dominant, both the advancing contact angle and contact angle hysteresis increase as the surface roughness increases. When the roughness factor exceeds a critical level, the wetting behavior changes from the Wenzel state to the Cassie state. The advancing water contact angle increases while the hysteresis decreases. Therefore, on the surface of our rough polymeric coating, an inefficient surface roughness may keep the water droplet in the Wenzel state which increases the contact angle hysteresis.

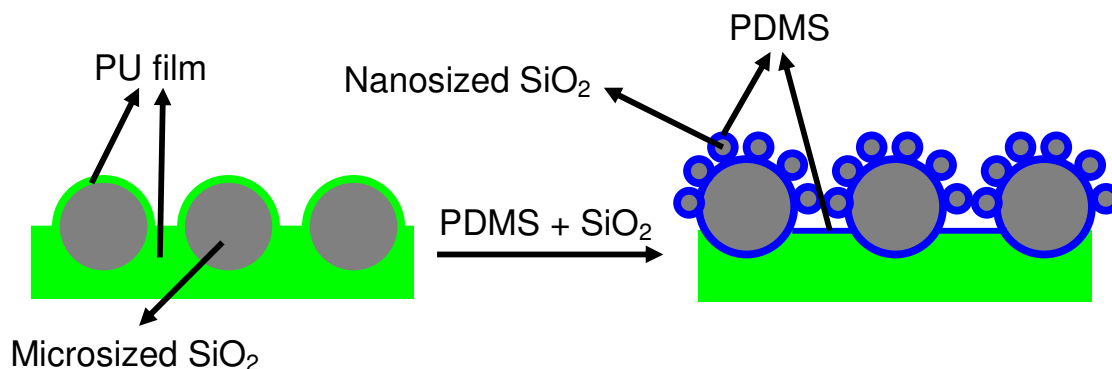
In order to further increase the surface roughness, two preliminary approaches have been attempted to create a structure with double roughness. One is depositing PDMS covered nanoparticles on rough PU film, and another is depositing PDMS covered nanoparticles on rough PDMS film.

## **2.4 Rough coatings with PDMS-covered nanoparticles**

Polydimethylsiloxane (PDMS) was chosen here for two reasons. First, it has a very low surface energy. A water droplet on a smooth PDMS surface has a water contact angle of about 105° and a very low contact angle hysteresis<sup>6</sup> which is typically less than 10°. Second, it is less water penetrable, due to its much longer chain than the perfluoroalkyl chain. Therefore, PDMS was used in the following approaches to eliminate surface reorganization.

Our first approach is to deposit PDMS covered nanoparticles on rough PU film as shown in Scheme 2.5. In this approach, the nanoparticles were applied to further increase the surface roughness.





**Scheme 2.5.** Depositing a mixture of nanoparticles and PDMS on rough PU film surface.

A mixture of vinyl-terminated poly(dimethylsiloxane), the cross-linker tetrakis(dimethylsiloxy)silane and the catalyst *cis*-dichlorobis(diethyl sulfide)platinum(II) was dissolved in toluene. Subsequently, a SiO<sub>2</sub> nanoparticle (12 nm) methanol dispersion was added to the mixture. The nanoparticle concentration in the solid mixture was 50 wt%. Coatings were prepared by spin-coating the mixture on the rough PU film surface and cured in an oven at 60 °C for 3 h.

The wettability of the film was checked by water contact angle measurements. The advancing water contact angle on the film is 130° with a water contact angle hysteresis about 110°. The significant hysteresis is probably due to incomplete coverage of PDMS on silica particles and polyurethane based coating. Therefore, rough PDMS based coating was used to replace PU to increase the chemical homogeneity of the film in our second approach.

First, a mixture of vinyl-terminated poly(dimethylsiloxane) and SiO<sub>2</sub> particles (0.9 μm) was dispersed in toluene by a sonifier for 2 min, then the cross-linker tetrakis(dimethylsiloxy)silane and the catalyst *cis*-dichlorobis(diethyl sulfide)platinum(II) were added to the mixture. The SiO<sub>2</sub> particle concentration in the final film was 50 wt %. Films were applied on clean aluminum panels by an automatic film applicator and then cured at 60 °C for 3 h. The thickness of the film is about 2 μm.

For this PDMS film with roughness on a micrometer scale, the advancing water contact angle on that is 150° with a water contact angle hysteresis about 45°. The sliding angle of a 20-μL water droplet is 22°. Comparing with the wettability of the rough

polymeric film we developed in 2.3, the contact angle hysteresis on the rough PDMS decreased rapidly. This may be due to the reason that the PDMS is less water penetrable, so the effect of the surface reorganization on this film is eliminated.

Next, a second PDMS layer with nanosized SiO<sub>2</sub> particles was applied on top of the first layer by spin-coating as we described previously. The advancing water contact angle on this coating is 155° with a water contact angle hysteresis about 35°. And the sliding angle of a 20-μL water droplet is 10°. The drawback of this PDMS film is its poor mechanical property.

## 2.5 Conclusions

It has been demonstrated in this chapter that polymeric films with low surface energy can be prepared by thermally curing a mixture of solventless liquid oligoesters and fluorinated isocyanates through the self-stratification process. Surface roughness and higher water advancing contact angle have been achieved by filling the low surface energy film with micrometer sized silica particles. However, the high contact angle hysteresis on both smooth and rough surfaces indicates that a polyurethane film enriched with fluorinated species at the surface may not be suitable for creating superhydrophobic films because of some intrinsic restrictions (the presence of polar groups which can interact with water molecules). A rough surface with a layer of PDMS on top has a much lower contact angle hysteresis. We conclude that creating a surface with double roughness and applying PDMS as a top layer may be a good approach to develop superhydrophobic coatings.

## References

1. Dettre, R. H.; Johnson, R. R., Jr. *Adv. Chem. Ser.* **1963**, *43*, 136.
2. Washo, B. D. *Org. Coat. Appl. Polym. Sci. Proc.* **1982**, *47*, 69.
3. Morra, M.; Occhiello, E.; Garbassi, F. *Langmuir* **1989**, *5*, 872.
4. Kunigi, Y.; Nonaku, T.; Chong, Y.-B.; Watanabe, N. *J. Electroanal. Chem.* **1993**, *353*, 209.
5. Ogawa, N.; Soga, M.; Takada, Y.; Nakayama, I. *Jpn. J. Appl. Phys.* **1993**, *32*, L614.

6. Onda, T.; Shibuichi, S.; Satoh, N.; Tsujii, K. *Langmuir* **1996**, *12*, 2125.
7. Yamauchi, G.; Miller, J. D.; Saito, H.; Takai, K.; Ueda, T.; Takazawa, H.; Yamamoto, H.; Nishi, S. *Colloids Surf., A* **1996**, *116*, 125.
8. Shibuichi, S.; Onda, T.; Satoh, N.; Tsujii, K. *J. Phys. Chem.* **1996**, *100*, 19512.
9. Tsujii, T.; Yamamoto, T.; Onda, T.; Shibuichi, S. *Angew. Chem., Int. Ed.* **1997**, *36*, 1011.
10. Tadanaga, K.; Katata, N.; Minami, T. *J. Am. Ceram. Soc.* **1997**, *80*, 1040.
11. Hozumi, A.; Takai, O. *Thin Solid Films* **1997**, *303*, 222.
12. Takai, O.; Hozumi, A.; Inoue, Y.; Komori, T. *Bull. Mater. Sci.* **1997**, *20*, 817.
13. Tadanaga, K.; Katata, N.; Minami, T. *J. Am. Ceram. Soc.* **1997**, *80*, 3213.
14. Sasaki, H.; Shouji, M. *Chem. Lett.* **1998**, 293.
15. Shibuichi, S.; Yamamoto, T.; Onda, T.; Tsujii, K. *J. Colloid Interface Sci.* **1998**, *208*, 287.
16. Hozumi, A.; Takai, O. *Thin Solid Films* **1998**, *332*, 54.
17. Chen, W.; Fadeev, A. Y.; Hsieh, M. C.; Öner, D.; Youngblood, J.; McCarthy, T. J. *Langmuir* **1999**, *15*, 3395.
18. Nakajima, A.; Fujishima, A.; Hashimoto, K.; Watanabe, T. *Adv. Mater.*, **1999**, *11*, 1365.
19. Youngblood, J. P.; McCarthy, T. J. *Macromolecules* **1999**, *32*, 6800.
20. Hopken, J.; Moller, M. *Macromolecules* **1992**, *25*, 1461.
21. Akiyama, S.; Kano, Y. In *Polymer Materials Encyclopedia*; Salamone, J. C., Ed.; 1996.
22. Yoon, S. C.; Ratner, B. D. *Macromolecules* **1986**, *19*, 1068.
23. Yoon, S. C.; Ratner, B. D.; Ivan, B.; Kennedy, J. P. *Macromolecules* **1994**, *27*, 1548.
24. Champan, T. M.; Marra, K. G. *Macromolecules* **1995**, *28*, 2081.
25. Ho, T.; Malik, A. A.; Wynne, K. J.; McCarthy, T. J.; Zhuang, K. H. Z.; Baum, K.; Honeychuck, R. V. *ACS Symp. Ser.* **1996**, *624*, 362.
26. Thomas, R. R.; Anton, D. R.; Graham, W. F.; Darmon, M. J.; Sauer, B. B.; Stika, K. M.; Swartzfager, D. G. *Macromolecules* **1997**, *30*, 2883.
27. Thomas, R. R.; Anton, D. R.; Graham, W. F.; Darmon, M. J.; Stika, K. M. *Macromolecules* **1998**, *31*, 4595.

28. Wang, J. G.; Mao, G. P.; Ober, C. K.; Kramer, E. J. *Macromolecules* **1997**, *30*, 1906.
29. Hwang, S. S.; Ober, C. K.; Perutz, S.; Iyengar, D. R.; Schneggenburger, L. A.; Kramer, E. J. *Polymer* **1995**, *36*, 321.
30. Kassis, C. M.; Steehler, J. K.; Betts, D. E.; Guan, Z. B.; Romack, T. J.; Desimone, J. M.; Linton, R. W. *Macromolecules* **1996**, *29*, 3247.
31. Sun, F.; Castner, D. G.; Mao, G.; Wang, M.; McKeown, P.; Grainger, D. W. *J. Am. Chem. Soc.* **1996**, *118*, 1856.
32. Affrossman, S.; Bertrand, P.; Hartshorne, M.; Kiff, T.; Leonard, D.; Pethrick, R. A.; Richards, R. W. *Macromolecules* **1996**, *29*, 5432.
33. Iyengar, D. R.; Perutz, S. M.; Dai, C.; Ober, C. K.; Kramer, E. J. *Macromolecules* **1996**, *29*, 1229.
34. Mason, R.; Jalbert, C. A.; O'Rourke Muisener, P. A. V.; Koberstein, J. T.; Elman, J. F.; Long, T. E.; Gunesin, B. Z. *Adv. Colloid Interface Sci.* **2001**, *94*, 1.
35. Winter, R.; Nixon, P. G.; Terjeson, R. J.; Mohtasham, J.; Holcomb, N. R.; Grainger, D. W.; Graham, D.; Castner, D. G.; Gard, G. L. *J. Fluorine Chem.* **2002**, *115*, 107.
36. Ming, W.; Tian, M.; Van de Grampel, R. D.; Melis, F.; Jia, X.; Loos, J.; Van der Linde, R. *Macromolecules* **2002**, *35*, 6920.
37. Van Benthem, R. A. T. M.; Hofland, A.; Peerling, H. W. I.; Meijer, E. W. *Prog. Org. Coat.* **2003**, *48*, 164.
38. Johnston, E.; Bullock, S.; Uilk, J.; Gatenholm, P.; Wynne, K. J. *Macromolecules* **1999**, *32*, 8173.
39. Ming, W.; Laven, J.; Van der Linde, R. *Macromolecules* **2000**, *33*, 6886.
40. Brongersma, H. H.; Gildenpfennig, A.; van de Grampel, R. D.; Laven, J.; et al. *Nucl. Inst. Meth. Phys. Res. B.* **2002**, *190*, 11.
41. Katano, Y.; Tomono, H.; Nakajima, T. *Macromolecules* **1994**, *27*, 2342
42. Wenzel, T. N. *J. Phys. Colloid Chem.* **1949**, *53*, 1466.
43. Cassie, A. B. D.; Baxter, S. *Trans. Faraday Soc.* **1944**, *40*, 546.



## Chapter 3

### Superhydrophobic coatings based on raspberry-like particles\*

**Abstract:** In this chapter, superhydrophobic films with a dual-size hierarchical surface structure were developed by depositing well-defined silica-based raspberry-like particles on an epoxy-based polymer matrix, followed by the surface modification with PDMS. On our superhydrophobic films, the advancing water contact angle is about 165°, and the roll-off angle of a 10 µL water droplet is about 2°. The dual-size surface structure which mimics the lotus leaf structure was examined by atomic force microscopy and scanning electron microscopy. The effect of the size ratio of raspberry particles on the wettability of film was studied.

---

\* Part of this Chapter has been published: Ming, W.; Wu, D.; van Benthem, R.; de With, G. Superhydrophobic films from raspberry-like particles, *Nano Lett.* **2005**, *5*, 2298-2301; and presented at ACS Meeting (Aug. 2005, Washington, DC): Ming, W.; Wu, D.; van Benthem, R.; de With, G. Biomimetic creation of superhydrophobic films, *Polym. Mater. Sci. Eng.* **2005**, *93*, 259.

### 3.1. Introduction

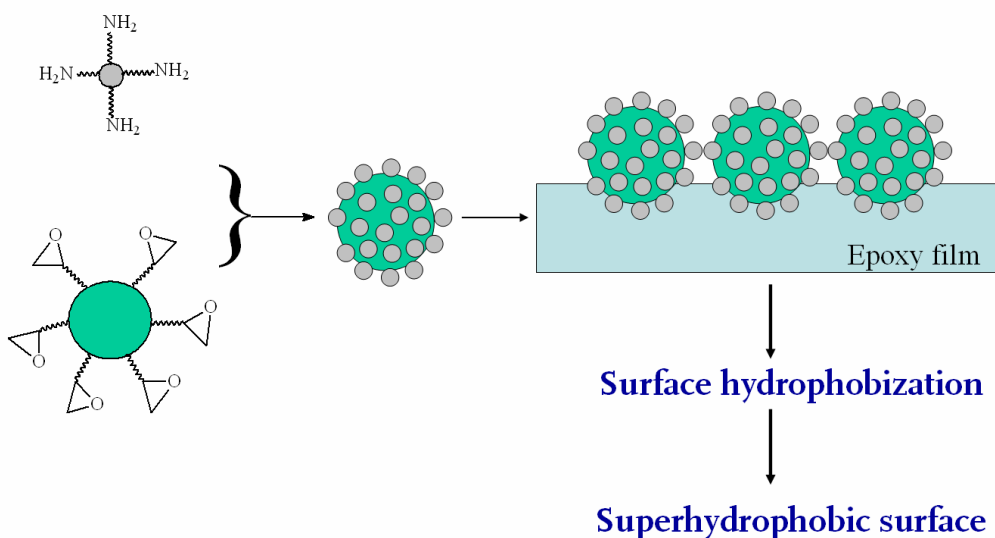
A superhydrophobic surface can be created by combining low surface energy and high surface roughness. As we mentioned at the end of Chapter 2, the polyurethane film enriched with fluorinated species at the surface may not be suitable for creating superhydrophobic films despite its low surface energy. In this chapter, we chose another material which also has low surface energy, but is less water penetrable, polydimethylsiloxane (PDMS), due to its much longer chain length than the perfluoroalkyl chain.

PDMS is well known for its low surface tension which makes it an attractive candidate for developing hydrophobic surfaces<sup>1-3</sup>. The low surface tension of PDMS comes from its unique structure. The PDMS backbone is a chain of alternating silicon and oxygen atoms, where each silicon atom has two methyl groups attached to it. This structure gives PDMS a flexible chain system in which steric packing restrictions are very low. Thus, methyl groups on the siloxane backbone are easily arranged into the lowest-surface energy configuration<sup>4</sup>. Well-packed methyl groups give low surface tension, which is about 22-24 mN/m at 20 °C<sup>5</sup>. A water droplet on a PDMS surface has a high water contact (about 105°) and a low contact angle hysteresis<sup>6</sup> (about 5°) which makes it a perfect candidate to create superhydrophobic surfaces.

Another important factor for a superhydrophobic surface is the surface roughness. There are many ways to make rough surfaces, such as etching<sup>7-11</sup>, lithography<sup>12,13</sup>, electrodeposition<sup>14,15</sup>, electro spinning<sup>16</sup>, use of templates<sup>3</sup> and so on. However, most of the methods are either expensive, require the use of a harsh chemical treatment, or are vulnerable to environment attack. Thus, a simple and robust procedure is requested.

As we mentioned in Chapter 1, Nature has given us many excellent examples to develop superhydrophobic surfaces. The dual-size roughness on the leaves of the sacred lotus plays a vital role for the superhydrophobicity of the leaf surface. On the other hand, according to Patankar's work<sup>17</sup>, the double-roughness structures or the slender pillars are appropriate surface geometries to develop a superhydrophobic surface. Since it is very difficult to develop a robust surface with slender pillars on top of a substrate in practice, our work is focused on creating a double-roughness structure.

In this chapter, we developed a simple, yet robust procedure for preparing surface with dual-size hierarchical structure from raspberry-like particles. The synthesis procedure is illustrated in Scheme 3.1. The key to introducing well-controlled dual-size roughness is the synthesis of raspberry-like particles. To synthesize raspberry-like particles, first, according to the Stöber method<sup>18</sup>, monodisperse silica particles with different sizes were prepared by hydrolysis and condensation of tetraethyl orthosilicate (TEOS) in a mixture of alcohol, water, and ammonia. Subsequently, different functional groups were attached on the silica particle surfaces. Subsequently, the raspberry-like silica particles were synthesized by attaching small particles on large ones via reactions between functional groups. After the raspberry-like particles were obtained, a surface with a dual-size hierarchical structure was developed by depositing raspberry-like particles on an epoxy based coating. Finally, a layer of PDMS was grafted on the top of the roughed surface to render the film surface hydrophobicity.



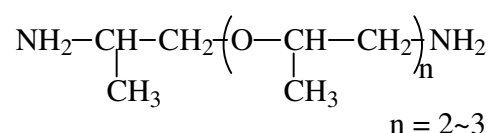
**Scheme 3.1.** Preparation of superhydrophobic films based on raspberry-like particles.



## 3.2. Experimental

### 3.2.1 Materials

Tetraethyl orthosilicate (TEOS) and aminopropyl terminated polydimethylsiloxane (DMS-A15, MW = 3000) were obtained from ABCR; monoglycidyl ether terminated polydimethylsiloxane (MW = 5000), trimethylolpropane triglycidyl ether (TPTGE), 3-glycidoxypropyl trimethoxysilane (GPS, 98%), 3-aminopropyltriethoxysilane (APS, 98%), 2,2-dihydroxy-1,3-indanedione (ninhydrin) and glutaraldehyde aqueous solution (25 wt%) were obtained from Aldrich; Jeffamine D-230 (a polyoxypropylene diamine, amine-hydrogen equivalent weight = 60, Scheme 3.2) was obtained from Huntsman. Ammonia solution (25%) was purchased from Merck. All of these chemicals were used without further purification.



**Scheme 3.2.** Molecular structure of Jeffamine D-230.

### 3.2.2 Raspberry-like particles from epoxy-amine chemistry

#### 3.2.2.1 Preparation of amino-functionalized silica nanoparticles

First, monodispersed silica particles of about 70 nm in diameter were prepared by polymerization of TEOS, according to the Stöber method<sup>18</sup>. Briefly, 6 mL of TEOS was added dropwise, under magnetic stirring, to a flask containing 15 mL of ammonia solution (25%, catalyst) and 200 mL of ethanol. The reaction was carried out at 60 °C for 5 h, followed by the addition of 0.3 mL of APS in 5 mL of ethanol. The stirring was continued for 12 h under N<sub>2</sub> atmosphere at 60 °C. The nanoparticles were separated by centrifugation and the supernatant was discarded. The particles were then washed by ethanol three times. White powders were vacuum-dried at 50 °C for 16 h.

An alternative one-step approach to the above two-step synthesis of amino-functionalized silica nanoparticles is described below:

A mixture of TEOS and APS in a volume ratio of 9:1 (4.5 mL TEOS and 0.5 mL APS), 4:1 or 1:1 was added dropwise, under magnetic stirring, to a flask containing 15 mL of ammonia solution (25%, catalyst) and 200 mL of ethanol. The reaction was carried

out at 60 °C for 16 h under N<sub>2</sub> atmosphere. The nanoparticles were separated by centrifugation and the supernatant was discarded. The particles were then washed by ethanol three times. The white powders were vacuum-dried at 50 °C for 16 h.

The existence of amine groups at the perimeter of silica nanoparticles was examined by the ninhydrin test<sup>19</sup>. The amino-functionalized silica particles were added into 5% ninhydrin aqueous solution at room temperature. The color of the particles turned from white to blue within a few min, indicating the successful grafting of amine moieties on the silica particle surface.

Monodispersed amino-functionalized silica particles of about 12 nm in diameter were prepared via the one-step reaction under same reaction condition but using methanol instead of ethanol as a reaction medium.

#### **3.2.2.2 Preparation of epoxy-functionalized silica microparticles**

Silica microparticles of 700 nm in diameter were synthesized first. At room temperature, 10 mL of TEOS was added dropwise, under magnetic stirring, to a flask containing 21 mL of ammonia solution, 75 mL of isopropanol, and 25 mL of methanol. After 5 h, the particles were separated by centrifugation, washed with distilled water/ethanol, and vacuum-dried at 50 °C for 16 h. Then 1.5 g of silica microparticles were redispersed into 40 mL of dry toluene and 0.2 g of GPS in 5 mL dry toluene was added dropwise to the silica suspension under vigorous stirring. The suspension was stirred at 50 °C under N<sub>2</sub> atmosphere for 24 h. The particles were then separated by centrifugation and washed with toluene three times. The washed powders were vacuum-dried at 50 °C for 16 h.

#### **3.2.2.3 Epoxy-amino approach to synthesize raspberry-like silica particles**

Amino-functionalized silica nanoparticles (70 nm, 0.4 g) were suspended in 20 mL of ethanol, and 0.6 g of epoxy-functionalized silica microparticles (700 nm) were suspended in 15 mL of ethanol, respectively. Afterwards, the silica microparticle suspension was added dropwise, under vigorous stirring, into the silica nanoparticle suspension. The suspension was refluxed for 24 h under N<sub>2</sub> atmosphere. The particles

were then separated by centrifugation and washed with ethanol. The powders were vacuum-dried at 50 °C for 16 h.

Raspberry-like silica particles (12 nm/700 nm) were synthesized by using a similar method. Amino-functionalized silica nanoparticles (12 nm) were grafted on epoxy-functionalized silica microparticles (700 nm) through amine-epoxy reactions.

### **3.2.3 Raspberry-like particles from aldehyde-amine chemistry**

#### **3.2.3.1 Preparation of amino-functionalized silica microparticles**

1.5 g of silica microparticles (700 nm) were redispersed into 40 mL of ethanol and 0.2 g of APS in 10 mL ethanol was added dropwise to the silica suspension under vigorous stirring. The suspension was stirred at 50 °C under N<sub>2</sub> atmosphere for 24 h. The particles were then separated by centrifugation and washed with ethanol three times. The washed powders were vacuum-dried at 50 °C for 16 h.

An alternative approach of one-step synthesis of amino-functionalized silica microparticles is described below:

A mixture of TEOS and APS a volume ratio of 9:1 (9 mL TEOS and 1 mL APS), 4:1 or 1:1 was added drop wise, under magnetic stirring, to a flask containing 21 mL of ammonia solution (25%, catalyst) 75 mL of isopropanol, and 25 mL of methanol. The reaction was carried out at 60 °C for 16 h under N<sub>2</sub> atmosphere. The microparticles were separated by centrifugation and the supernatant was discarded. The particles were then washed by ethanol three times. The white powders were vacuum-dried at 50 °C for 16 h.

#### **3.2.3.2 Preparation of aldehyde-functionalized silica microparticles**

Amino-functionalized silica microparticles (0.5 g) were dispersed into 100 mL phosphate buffer (pH 6.0), 1% glutaraldehyde solution in phosphate buffer (pH 6.0) was added. The suspension was stirred at room temperature under N<sub>2</sub> atmosphere for 3 h. The particles were then separated by centrifugation and washed with distilled water three times.

### **3.2.3.3 Aldehyde-amine approach to synthesize raspberry-like silica particles**

Amino-functionalized silica nanoparticles (0.1 g) were suspended in 100 mL phosphate buffer solution (pH 6, 6.5, 7, 7.5, respectively), and 0.5 g of aldehyde-functionalized silica microparticles were suspended in 100 mL of phosphate buffer solution, respectively. Afterwards, the silica microparticle suspension was added dropwise, under vigorous stirring, into the silica nanoparticle suspension. The suspension was stirred for 24 h under N<sub>2</sub> atmosphere. The particles were then separated by centrifugation and washed with distilled water.

### **3.2.4 Preparation of epoxy-amine films with dual-size surface roughness**

First, an epoxy-amine film with the epoxy in 10% excess was prepared on an aluminum substrate by the following procedure. 0.44 g of TPTGE and 0.24 g of Jeffamine D-230 were dissolved in 1 mL of toluene, with an epoxy/amino molar ratio of about 2.2:1. Afterwards, a film of about 30 μm (wet film thickness) was drawn down on an aluminum panel with an automatic film apparatus and then cured at 75 °C for 2 h. Next, 0.05 g of raspberry amino-functionalized silica particles was suspended in 1 mL ethanol. The suspension was deposited on the first epoxy layer by an automatic film apparatus (wet film thickness of about 60 μm) and then kept at 75 °C for 18 h. After cooling down, the film was flushed with ethanol in a sonicator to remove loose particles, and dried at room temperature.

### **3.2.5 Preparation of superhydrophobic films with PDMS**

The superhydrophobic film was obtained by grafting PDMS onto the double-structured film containing raspberry-like particles. The surface-roughened film was first reacted with amine-end-capped DMS-A15 at 80 °C for 4 h to ensure that any remaining epoxy groups from either epoxy-amine film or large silica particles were converted into terminal amine groups; after the reaction the film was thoroughly washed by toluene to remove unreacted DMS-A15. In the end, the film was reacted with monoglycidyl ether terminated polydimethylsiloxane at 80 °C for 4 h and followed by washing with toluene, resulting in a layer of PDMS covering the roughened surface.

For comparative purpose, a film containing only large or small silica particles was prepared as follows (reaction conditions are the same with above). An epoxy-amine film was prepared with 10% epoxy in excess, followed by the surface grafting of large silica particles (containing amino groups at surface). Loose large particles were removed by flushing with ethanol in a sonicator. Finally an epoxy-PDMS (monoglycidyl ether terminated polydimethylsiloxane) was grafted to the film.

### **3.2.6 Characterization techniques**

#### **Dynamic Light Scattering (DLS)**

The average particle size, particle size distribution and  $\zeta$ -potential were determined on a Malvern Zetasizer Nano ZS Instruments. The pH of the solution was adjusted by adding either HCl or NaOH using a Malvern MPT2 autotitrator. All the DLS measurements were performed at 20 °C.

#### **Transmission electron microscopy (TEM)**

The morphology of the raspberry-like particles was examined by TEM. The experiments were performed with a JEOL JEM-2000FX TEM at 80 kV. Traditional negative plates were used for the data recording. The negatives were digitized using a scanner (Agfa DUO Scanner) working in grade mode with 8-bits/channel of grayscale. The samples were prepared by dispersing silica particles in ethanol and depositing one drop of the dilute suspension on a copper grid coated with a carbon membrane.

#### **Scanning electron microscopy (SEM)**

SEM measurement was performed using a Philips XL-30 ESEM FEG environmental scanning electron microscopy (Philips, the Netherlands, now FEI Co.) in high-vacuum mode at an acceleration voltage of 2 kV, unless otherwise stated.

#### **Atomic force microscopy (AFM)**

All the AFM measurements were performed with Solver P47H (NT-MDT) in non-contact mode. The cantilever of choice was no-contact gold-coated NSG 11S, and a typical resonance frequency was 140 kHz.

The description of contact angle measurement is given in Chapter 2.

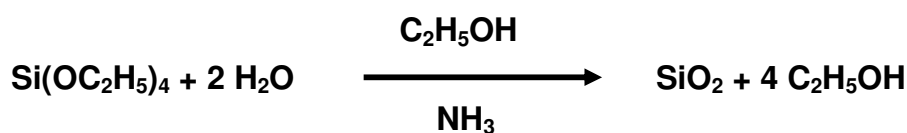
### Ninhydrin test

Add about 2 mg of the sample to 1 mL of solution of 0.2 g of ninhydrin in 50 mL of water. A blue to blue-violet color is given by  $\alpha$ -amine groups and constitutes a positive test.

## 3.3 Results and discussion

### 3.3.1 Two-step synthesis of modified silica particles

First, monodisperse silica particles (70 nm, 700 nm) were synthesized in this study according to the well-known Stöber method<sup>18</sup>. The preparation of monodisperse silica particles generally proceeds with the hydrolysis and condensation of TEOS in a mixture of alcohol, water and ammonia as a catalyst (Scheme 3.3). The final particle size can be adjusted by the initial concentrations of the reactant and reaction temperature. DLS results in Figure 3.1 show the particle size distributions which are centered at 70 nm or 700 nm. The PDI (polydispersity index) of the 70 nm and 700 nm nanoparticles are 0.058 and 0.035, respectively. The size and shape of the silica particles were checked by SEM. Figure 3.2 shows perfectly spherical silica particles with smooth particle surface.



**Scheme 3.3.** *Hydrolysis and condensation of TEOS.*

Scheme 3.4 shows the grafting of APS on the hydrated silica particle surface. Because this reaction occurs in a basic environment in the presence of water, the initial hydrolysis step can occur either in solution or at the silica particle surface. Hydrolyzed monomers then undergo condensation reactions to form dimers and larger oligomers. Subsequently, hydrolyzed APS monomers and oligomers adsorbed and reacted on the surface of silica particles. On the other hand, during the synthesis of epoxy modified silica particles in dry toluene, because of lack of water, the hydrolysis step may not have happened. GPS monomers were attached to the silica particle by direct reaction between the OCH<sub>3</sub> groups on GPS and the OH groups on the surface of silica particles, as shown in Scheme 3.5. To determine whether the amine group had been covalently bonded with the silica

surface, ninhydrin agent was added to the modified silica particles which had been carefully washed. A blue-violet color indicates the presence of amino groups. There was hardly any change in the size of the particles before and after the modification as verified with DLS.

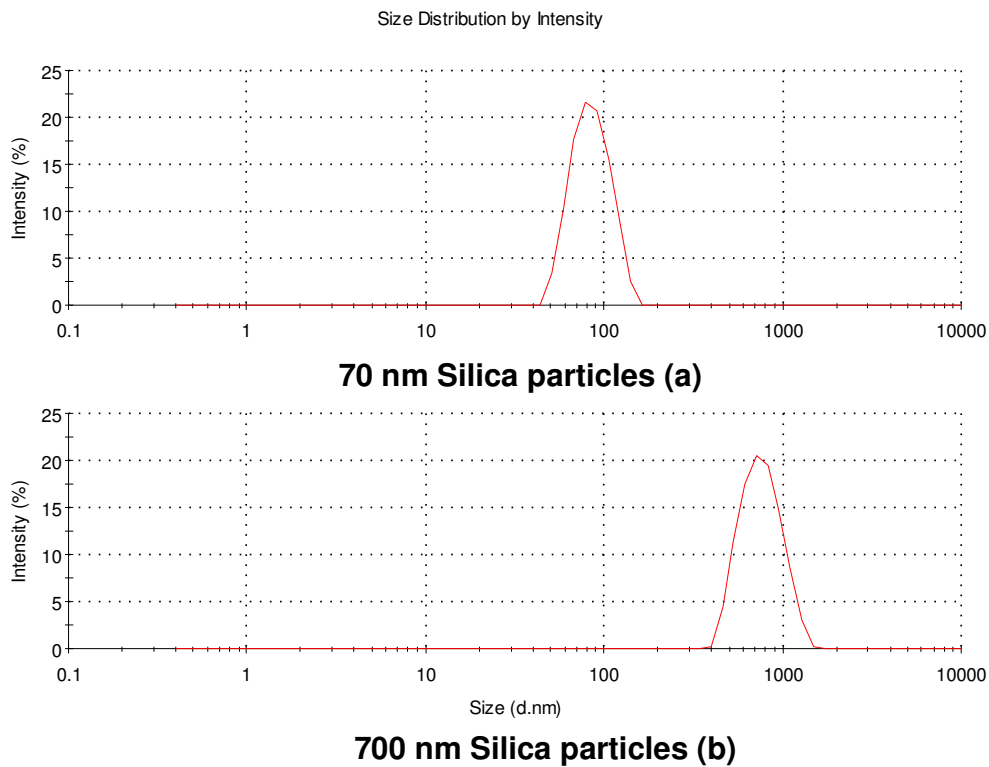


**Figure 3.1.** Particle size distribution of 70 nm (a) and 700 nm (b) silica particles in alcohol suspension. (d: the diameter of the particle)

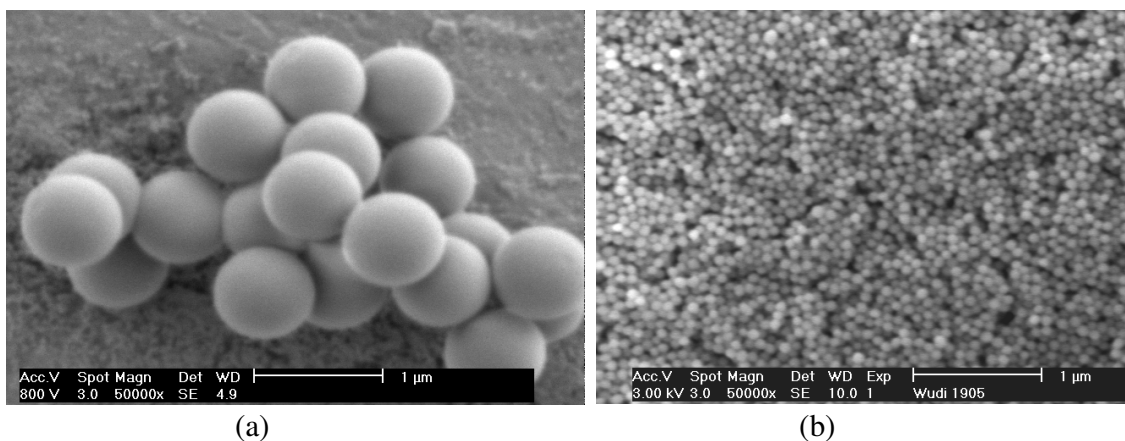
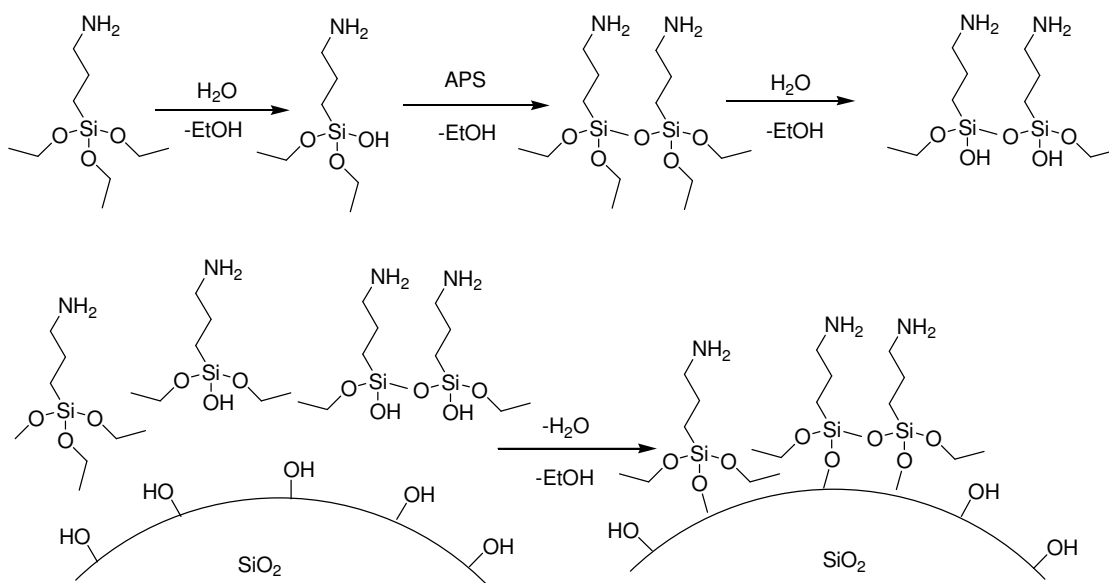
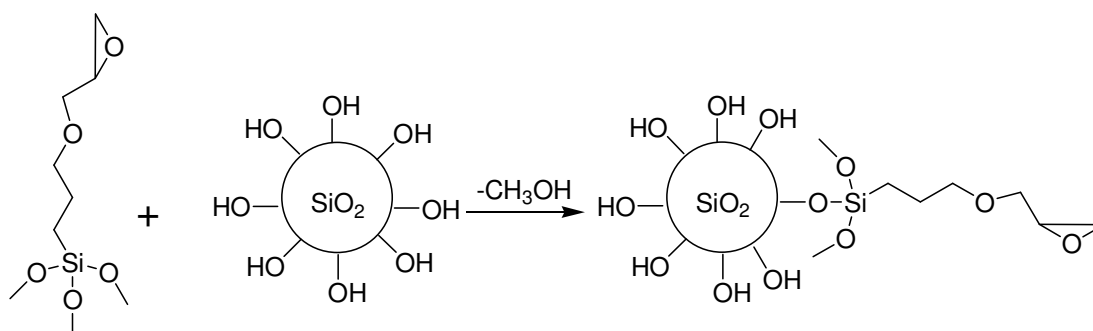


**Figure 3.2.** SEM images of (a) 700 nm and (b) 70 nm silica particles.



**Scheme 3.4.** Scheme of APS hydrolysis followed by condensation at silica particle surface.



**Scheme 3.5.** Illustration of GPS modification of silica particles.

### 3.3.2 One-step synthesis of amino-functionalized silica particles

In the one-step approach, we prepared amino-functionalized silica particles starting from mixtures of APS and TEOS. Van Blaaderen and Vrij<sup>20</sup> showed that the first order hydrolysis constants of TEOS and APS in n-propanol are  $6.0 \times 10^{-3} \text{ min}^{-1}$  and  $1.2 \times 10^{-3} \text{ min}^{-1}$ , respectively. They also assumed that the large difference in hydrolysis rate between TEOS and APS will not change by changing n-propanol to ethanol. Thus, when all the TEOS is hydrolyzed and converted into silica, the amount of hydrolyzed APS would still be small. Since the reaction rate between a hydrolyzed TEOS molecule and a



hydrolyzed APS molecule is probably much smaller than that between two hydrolyzed TEOS molecules, the amount of APS incorporated into the silica would be very small. APS is mainly grown on the silica surface. That means that only a small quantity of APS is needed to provide a silica surface with high amine group density. Van Blaaderen and Vrij also showed that it seems that the initial molar ratio of APS and TEOS does not have a strong effect on the particle morphology. By changing the APS/TEOS molar ratio from 0.4 to 0.65, they obtained perfect spheres with a smooth surface and a low polydispersity. The particle sizes were between 165 nm to 110 nm. In our research to synthesize micro-sized amine-functionalized silica particles (700 nm), we found that the particles change from monodispersed smooth spherical particles to agglomerates of much smaller particles with rough surfaces as the APS/TEOS molar ratio increases in the reaction mixture. When the molar ratio of APS/TEOS is 1:9, monodisperse spherical silica particles were obtained. However, as the molar ratio of APS/TEOS increased to 1:4, the spherical silica particles stick to each other. When the APS/TEOS molar ratio further increased to 1:1, agglomerates of smaller particles appeared (Figure 3.3c). The possible reason is that when the APS concentration is very high, first, smaller silica particles coated with APS will form mainly by TEOS. A large amount of APS will hydrolyze and self-condense in reaction solution, and subsequently glue smaller silica particles together.

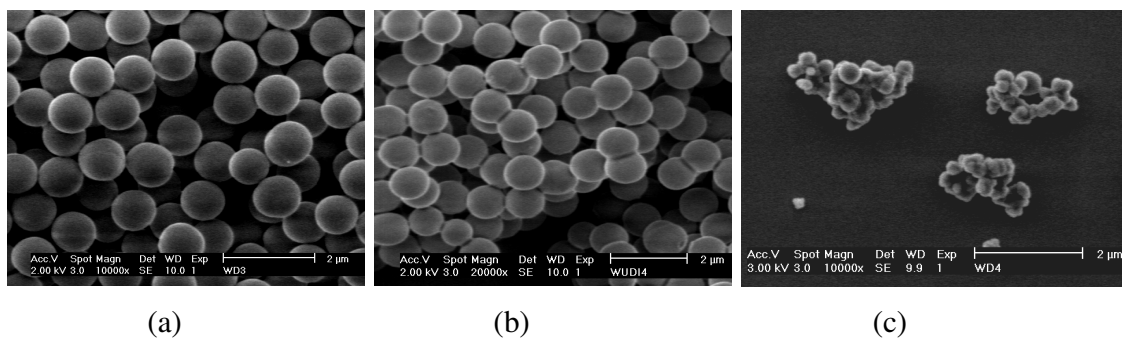


**Figure 3.3.** SEM images of amine modified silica particles synthesized by one-step approach with different APS/TEOS ratio: (a) 1:9, (b) 1:4, and (c) 1:1.

### 3.3.3 Synthesis of raspberry-like particles

The raspberry-like particles were synthesized by either epoxy-amine reaction or aldehyde-amine reaction. We estimated the numbers of nanoparticles that could pack

onto the surface of a microparticle by assuming that the nanoparticles are closely packed on the surface. The resulting value was used to determine the minimum number of nanoparticles needed in suspension for each microparticle present. We subsequently convert the number ratio between nano- and microparticles to weight ratio. For example, to completely cover a 700 nm diameter silica particle with 70 nm silica particles, we calculated that approximately a 362:1 number ratio or 1:2.76 weight ratio of nanoparticles to microparticles should be used.

For the epoxy-amine approach, the epoxy-functionalized monodisperse silica particle about 700 nm and amine-functionalized silica particles of about 70 nm were prepared, respectively. The small particles were then covalently grafted onto the bigger ones via the reaction between epoxy and amine groups, leading to raspberry-liked silica particles of uniform size with dangling amine groups at the surface. TEM images of the raspberry-like particles are shown in Figure 3.4. The 70 nm silica particles were packed on the surface of the microparticles. Some loose small particles are present, probably because of physical adsorption.

However, the aldehyde-amine approach proved unsuccessful. We chose a slightly acidic reaction medium for two reasons. First, the amine-aldehyde reaction is acid catalyzed. The unshared pair of electrons on an amine nitrogen is not sufficiently nucleophilic to attack the carbonyl group without help from an  $H^+$ . On the other hand, if too much acid is put into the reaction medium, the reaction stops because all amine will be protonated. However,  $\zeta$ -potential measurements showed that both amino-functionalized silica particles and aldehyde-functionalized silica particles have positive charge at pH below 7. For example, when the pH is 6.5, the  $\zeta$ -potential of amino-functionalized silica particles and aldehyde-functionalized silica particles is +50 mV and +25 mV, respectively (the positive charge on the aldehyde-functionalized silica particle comes from the  $-N=$  group in the middle of the grafted chain, but it gives less positive charge than  $NH_2$  group on the amino-functionalized silica). Therefore, the particles will repel each other preventing further reactions. We also tried to make the aldehyde-amine reaction in slightly basic reaction medium. It was unsuccessful because the unshared pair of electrons on an amine nitrogen is not sufficiently nucleophilic to attack the carbonyl group.

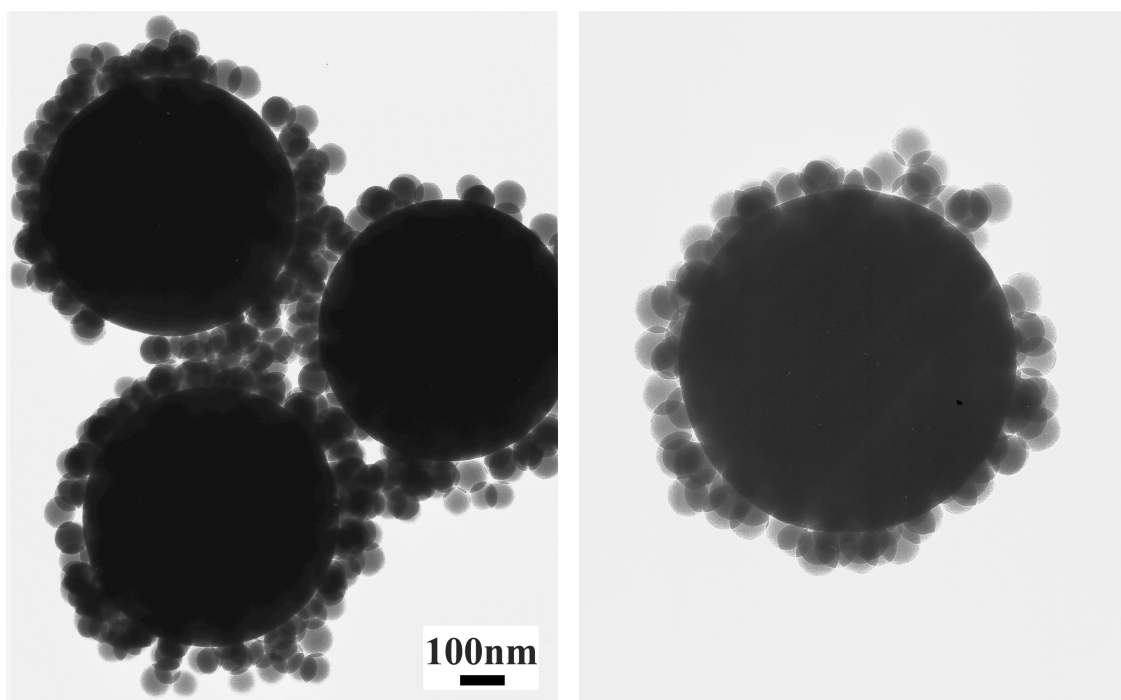


**Figure 3.4.** *Transmission electron microscopy (TEM) photos of raspberry-like silica particles (left) and an enlarged single raspberry-like silica particle(right).*

### 3.3.4 Preparation of superhydrophobic coatings

First, a conventional polymer film was applied on aluminum substrates based on thermal curing of a mixture of an epoxy and a diamine with the epoxy in 10% excess. Thus, there are epoxy functional groups left on the film for further reaction. The amine-functionalized raspberry particles (dispersed in ethanol) are then deposited on the epoxy film via again epoxy-amine reaction at 75 °C. Loose particles can be easily flushed away with ethanol or water, leaving one layer of the raspberry particles chemically bonded to the epoxy-amine films. Possibly remaining epoxy groups at the surface of large particles and epoxy-amine films are further reacted with an amine-bifunctional PDMS. In the end, epoxy-end-capped PDMS is grafted to the particles to bring hydrophobicity to the surface.

The wettability of the coating was checked by water contact angle (CA) measurements. The advancing water CA on a smooth epoxy-amine film (surface modified with PDMS) is  $107 \pm 2^\circ$  (Figure 3.5a), with a CA hysteresis of about  $40^\circ$ . When only large silica particles ( $\sim 700$  nm in diameter) are deposited (surface also modified

with PDMS) on the epoxy-amine film, there is an increase of the water advancing CA, reaching  $151 \pm 2^\circ$  (Figure 3.5b), but at the same time, the CA hysteresis also increases dramatically to about  $57^\circ$ . Similarly, when only 70 nm silica particles are introduced to the film surface, the advancing/receding CAs are  $148^\circ/85^\circ$ , respectively. Even when the film is turned upside down, the water droplet would stay pinned to the film surface. However, for the film containing raspberry particles (surface modified with PDMS), the advancing CA of water further increases to  $165 \pm 1^\circ$  (Figure 3.5c); the CA hysteresis is shown to be about  $4^\circ$ . More importantly, the roll-off angle of a 10- $\mu$ L water droplet on the surface is  $3 \pm 1^\circ$  (Figure 3.6). By incorporating raspberry particles with surface modified by PDMS, a conventional epoxy-amine film has been successfully turned superhydrophobic.

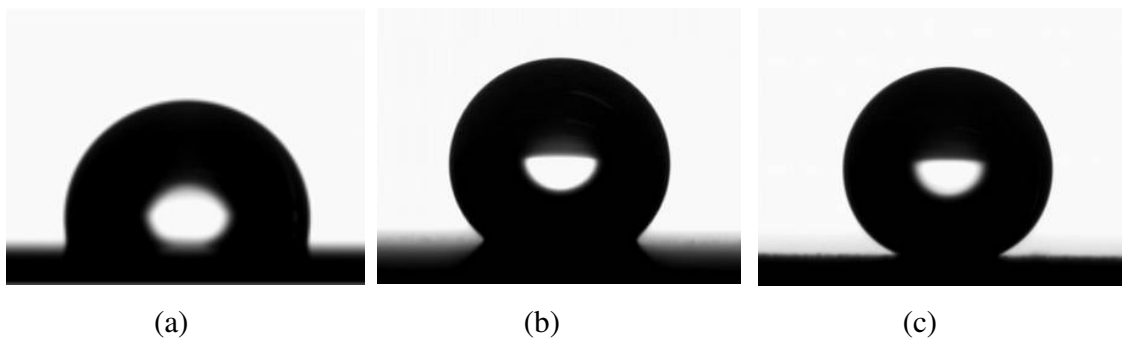


**Figure 3.5.** Water droplets of 5  $\mu$ L on films containing (a) no particles, (b) large silica particles, and (c) raspberry particles.

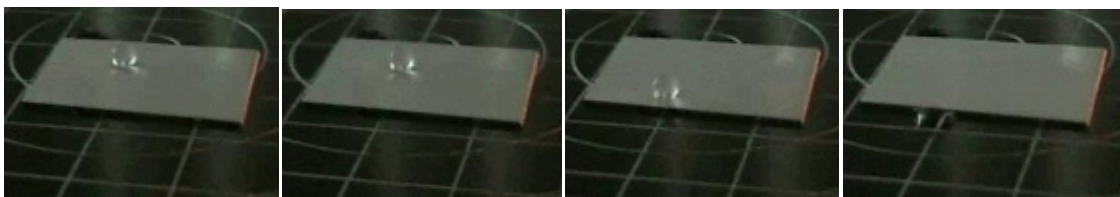


**Figure 3.6.** A water droplet (10  $\mu$ L) rolls off the film as the tilting angle increases from 0 to  $1.8^\circ$ .

On the other hand, the water CAs were also checked on the film containing raspberry-like particles before it was modified with a layer of PDMS. The advancing and receding CAs are only  $22^\circ$  and  $6^\circ$ , respectively, significantly lower than the CAs of water on the corresponding smooth epoxy-amine film (advancing/receding CA:  $66/30^\circ$ ). This

implies that, to make a surface superhydrophobic, it is necessary to combine a proper surface roughness with proper chemistry.

It is well known that surface roughness can not only amplify the wettability but also dramatically affect the contact angle hysteresis on a surface<sup>21-26</sup>. Here, we used atomic force microscope (AFM) to examine the film surfaces with and without particles. With no particles in the films, the smooth film surface appears to be featureless. With the large silica particles incorporated into the film, a layer of silica particles can be easily observed by AFM (Figure 3.7a&c). The surface roughness is apparently due to the existence of the silica particles; the typical peak-valley distance of about 400 nm (Figure 3.7b), roughly the radius of a silica microparticle. When raspberry particles are introduced to the film, the topographic image (Figure 3.6d&f) clearly shows a two-level structure: the micrometer-level structure can be ascribed to the large silica particles that are the core of raspberry particles, while on each of the micrometer-level structure there is a finer structure at a sub-micrometer (about 70 nm) level. The peak-valley distance is typically about 500 nm (Figure 3.7e). Obviously, the topographic feature of raspberry particles is completely preserved in the superhydrophobic film. This dual-size hierarchical structure resembles the surface of a lotus leaf<sup>12,17,27,28</sup>, as clearly demonstrated by the 3-D image in Figure 3.7f.

As we described in Chapter 1 and Chapter 2, two distinct wetting behaviors exist on a rough hydrophobic surface. When the roughness factor<sup>21</sup> ( $r$ ) is low, the water droplet behavior follows the Wenzel's model<sup>21</sup>; both advancing CA and CA hysteresis increase as  $r$  increases. However, as  $r$  further increases passing a critical level, the water droplet behavior will follow the Cassie model<sup>22</sup>. As  $r$  increases, the advancing CA increases while the CA hysteresis decreases. Besides a high enough advancing CA, a very small CA hysteresis is necessary to make a superhydrophobic surface with a very low roll-off angle of water droplet. Our films containing only large silica particles, although the surface roughness factor  $r$  increases significantly as compared to a smooth surface, are still in a regime where the Wenzel behavior dominates, resulting in enlarged CA hysteresis<sup>23</sup> (from 40 to 57°; the water droplet remains pinned at the surface even when the film is tilted to a high angle). The surface roughness factor  $r$  has to surpass a certain level to enter the Cassie regime, in which the difference between advancing and receding

CA minimizes. The dual-size surface structure at the lotus leaf surface amplifies the surface roughness factor to reach the Cassie regime. Similarly, in our double-structured films containing raspberry particles, the surface roughness factor  $r$  is also drastically increased by the existence of raspberry particles, effectively making our films superhydrophobic and allowing a 10- $\mu\text{L}$  water droplet roll off the surface when tilted at  $2^\circ$ .

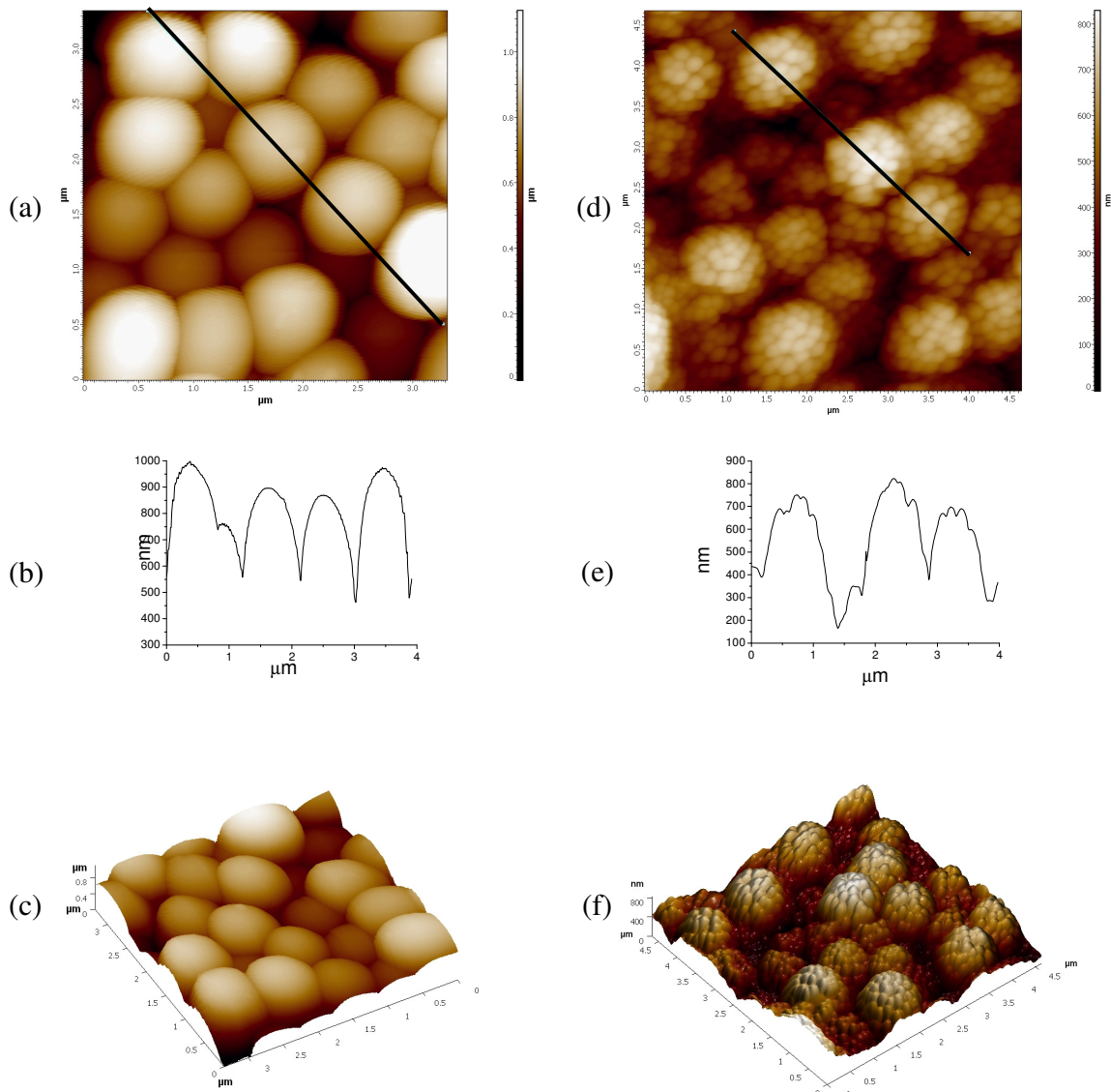


**Figure 3.7.** AFM images for films containing large particles: (a) height image, (b) topographic profile from (a), and (c) 3-D image, and for films containing raspberry: (d) height image, (e) topographic profile from (d), and (f) 3-D image.

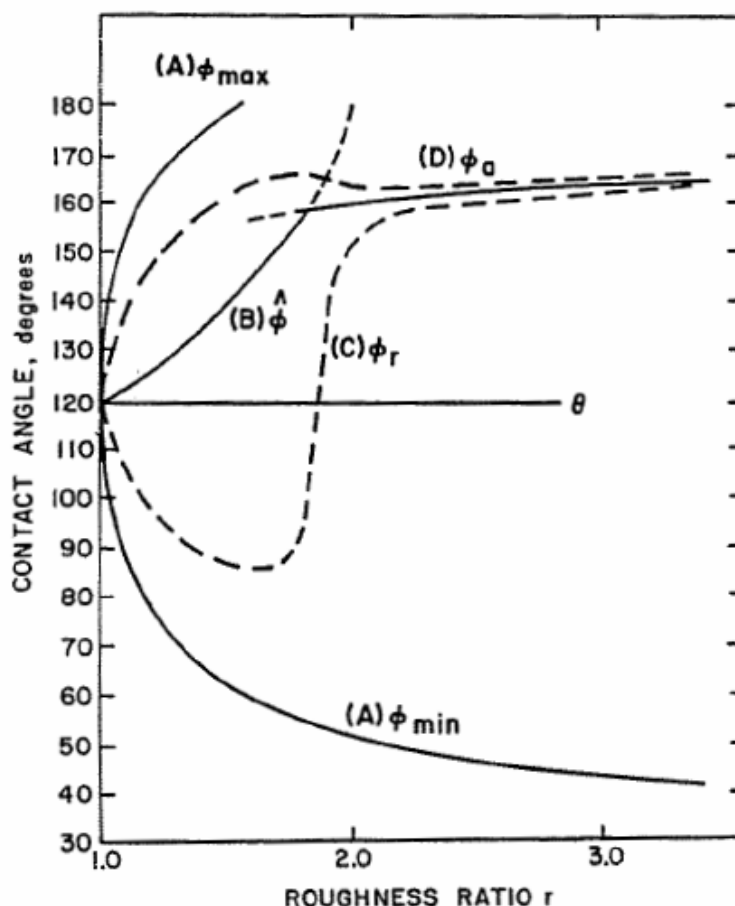


**Figure 3.8.** Predicted water CA on rough surface with  $120^\circ$  intrinsic water CA<sup>23</sup>. A: Maximum and minimum possible angles. B: Most probable contact angles. (Lower: Calculated from Wenzel's equation; Upper: Calculated from Cassie and Baxter's equation.) C: Possible curve of receding angles. D: Possible curve of advancing angles.

We did preliminary quantitative analysis on the basis of AFM images. For the film containing only large silica particles, the root-mean-square roughness ( $S_q$ ) is  $173 \pm 25$  nm and  $r = 1.45 \pm 0.05$ . For the film containing raspberry-like particles,  $S_q = 185 \pm 20$  nm and  $r = 1.54 \pm 0.09$ , respectively. The increase in  $r$  seems to be small. However, we believe the real  $r$  on the film containing raspberry-like particles may be higher than the measured one because the AFM tip may not be able to completely follow the surface of nanoparticles. On the other hand, from Johnson and Dettre's work<sup>23</sup>, we know that a water droplet sitting on a hydrophobic surface has a sharp transition from the Wenzel regime to the Cassie regime as  $r$  increases above a certain value. For example, they predicted the changing of advancing CA and receding CA on a film with intrinsic CA

about  $120^\circ$  (Figure 3.8). On this curve, CA hysteresis decreases rapidly for  $r$  above 1.8, which indicates the sharp transition between the Wenzel regime and the Cassie regime.

### 3.3.5 Superhydrophobic coatings containing raspberry-like particles with different size ratio

As we mentioned above, we synthesized raspberry-like particle by grafting small particles onto large particles. By using the Stöber method, the particle size can be controlled. Therefore, raspberry-like particles with different size ratio can be obtained. In order to study the size ratio effect on the wettability of our superhydrophobic coatings, raspberry-like particles with size ratio 12 nm/700 nm were synthesized by a similar method as we synthesized raspberry-like particles with the size ratio of 70 nm/700 nm. Similar superhydrophobic surfaces were obtained. Figure 3.9 shows a superhydrophobic surface containing raspberry-like particles with size ratio 12/700, and an image of a water droplet on top of it. The raspberry-like particle is not ideal because the 12 nm silica particles were slightly pre-coagulated in the mixture of reaction. On this surface, the advancing water CA is  $158 \pm 0.8^\circ$  and the CA hysteresis is about  $5^\circ$ , which is similar to the water contact angles on the superhydrophobic coating containing raspberry-like particles with size ratio 70/700 (advancing/receding CA:  $165^\circ/161^\circ$ ).

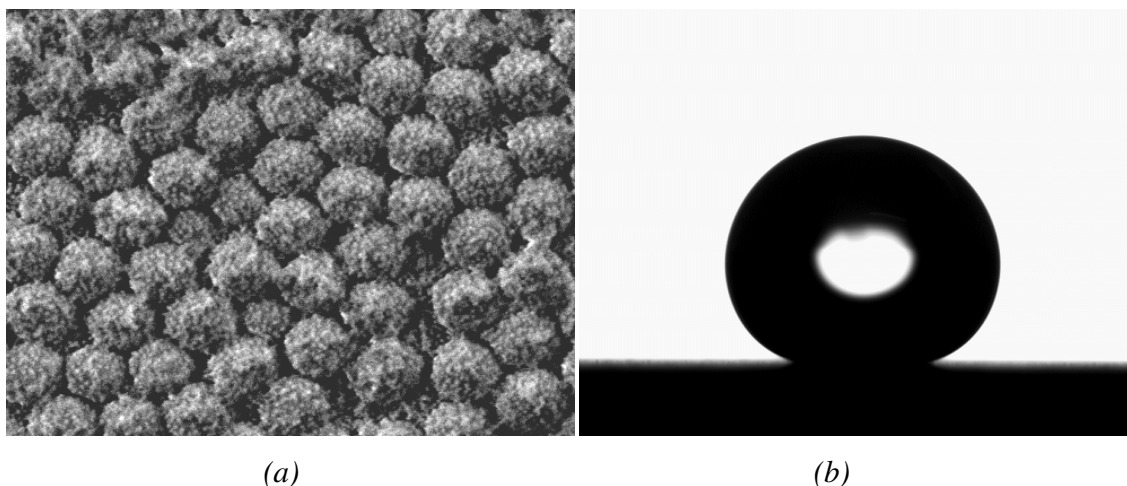


**Figure 3.9.** (a) SEM image of a film containing raspberry-like particles (12 nm/700 nm), and (b) a water droplet of  $5 \mu\text{L}$  on top of this surface.



### 3.4 Modeling study for superhydrophobicity

We also tried to understand the effect of dual-size structure on the surface wettability from a modeling perspective. A free energy description of water droplets on a single size and a double size structure has been detailed in Bart van Loenen's Master thesis<sup>29</sup>. The major findings are summarized below:

When a water droplet rests on a solid surface, the total Helmholtz energy of the system consists of three types of energy contributions: bulk contributions, interfacial contributions and line tension contributions. The energy will be minimized in the equilibrium position due to thermodynamic considerations. The total energy is displayed in equation 3.1. From literature the bulk and contact line contribution can be neglected<sup>30-35</sup>, and the interfacial contributions can be calculated as equation 3.2.

$$F_{\text{total}} = F_{\text{bulk}} + F_{\text{interface}} + F_{\text{line}} \quad (3.1)$$

$$F_{\text{interface}} = \gamma_{\text{sl}} \cdot \Omega_{\text{sl}} + \gamma_{\text{lv}} \cdot \Omega_{\text{lv}} + \gamma_{\text{sv}} \cdot \Omega_{\text{sv}} \quad (3.2)$$

Where  $\gamma_{\text{sl}}$ ,  $\gamma_{\text{lv}}$ ,  $\gamma_{\text{sv}}$  are interfacial energy of solid-liquid interface, liquid-vapor interface and solid-vapor interface, respectively. And  $\Omega_{\text{sl}}$ ,  $\Omega_{\text{lv}}$ ,  $\Omega_{\text{sv}}$  are total area of solid-liquid interface, liquid-vapor interface and solid-vapor interface, respectively.

When the energy relative to the non-wetted case where  $\Omega_{\text{sv}}$  is infinite is calculated, equation 3.3 is formed.

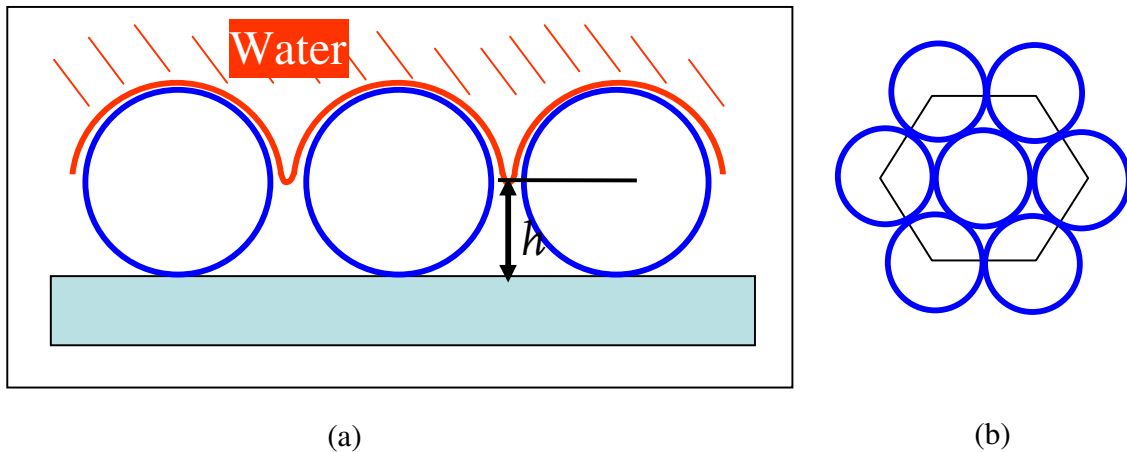
$$\Delta F_{\text{interface}} = \gamma_{\text{lv}} \cdot \Omega_{\text{lv}} + (\gamma_{\text{sl}} - \gamma_{\text{sv}}) \cdot \Omega_{\text{sl}} \quad (3.3)$$

When equation 3.3 is modified to include the Wenzel and Cassie-Baxter considerations, equation 3.4 is obtained<sup>36</sup>. The parameters  $f_{\text{sl,CB}}$  (the fraction of the solid surface that is wetted by the liquid) and  $f_{\text{lv,CB}}$  (entrapped vapor fraction) are related to the surface structure.

$$\Delta F_{\text{interfacial}} = \gamma_{\text{lv}} \cdot (\Omega_{\text{lv}} + f_{\text{lv,CB}} \cdot \Omega_{\text{sl}}) + f_{\text{sl,CB}} \cdot R \cdot (\gamma_{\text{sl}} - \gamma_{\text{sv}}) \cdot \Omega_{\text{sl}} \quad (3.4)$$

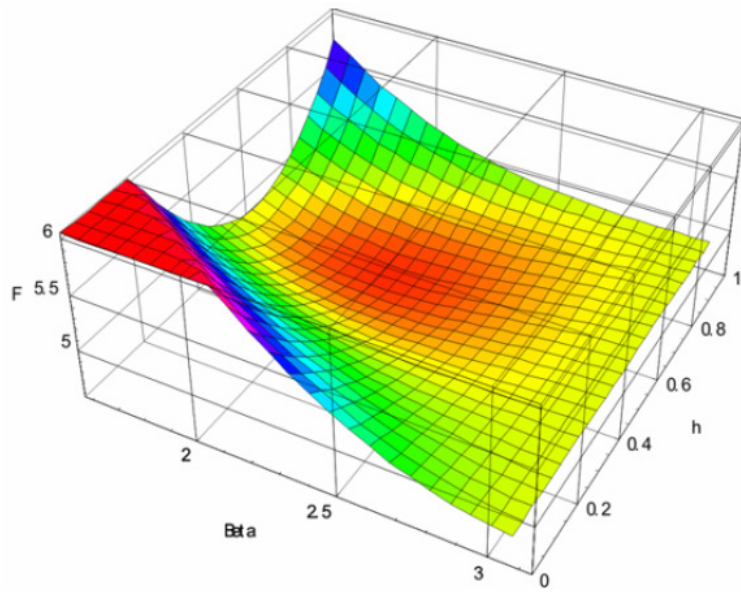
The free energy "landscape"<sup>29</sup> of a system where a water droplet rests on a surface composed of a layer of single size particles or raspberry-like particles can be calculated on the basis of the equation 3.4.

When we consider a water droplet rests on a surface composed of a layer of spheres, two important parameters need to be taken into account: relative air height ( $h$ ) beneath the water, and the packing factor of spheres ( $\eta$ ). When  $h = 0$ , water totally fills the gaps between the spheres, and when  $h = 1$ , the water droplet is on the top of the spheres. For a maximum hexagonal packing of sphere,  $\eta = 0.907$ . The parameter  $\eta$  decreases when the packing becomes loose (Scheme 3.6).

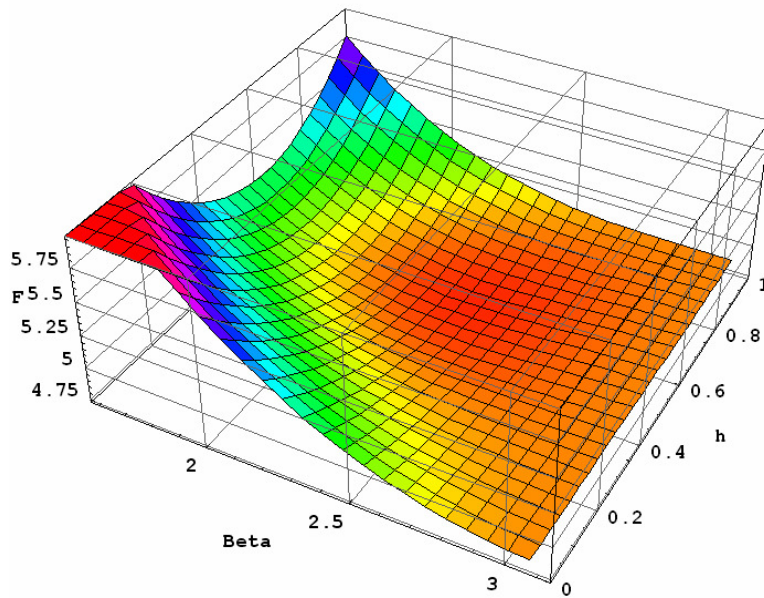


**Scheme 3.6.** (a) A water droplet sits on a surface composed of a layer of spheres, and (b) A maximum hexagonal packing of spheres.  $\eta = 0.907$ .

First, the surface composed of a layer of single-size spheres was investigated. Assuming the surface is composed of pure PDMS, which theoretically corresponds to an intrinsic water contact angle of  $105^\circ$  on the flat PDMS surface. Figure 3.10 shows the total free energy ( $F$ ) for a system (with a particle packing factor: 0.9) as a function of the apparent contact angle ( $\beta$ , in radian) and the relative air height ( $h$ ). We can find an energy minimum at  $\beta = 121^\circ$  and  $h = 0.64$ . If the particle packing factor is reduced to 0.5,  $\beta$  increases further to  $137^\circ$ . Obviously, the single-size particle structure can effectively enhance the surface hydrophobicity, which is in agreement with many experimental results and the Wenzel's prediction<sup>21</sup>.

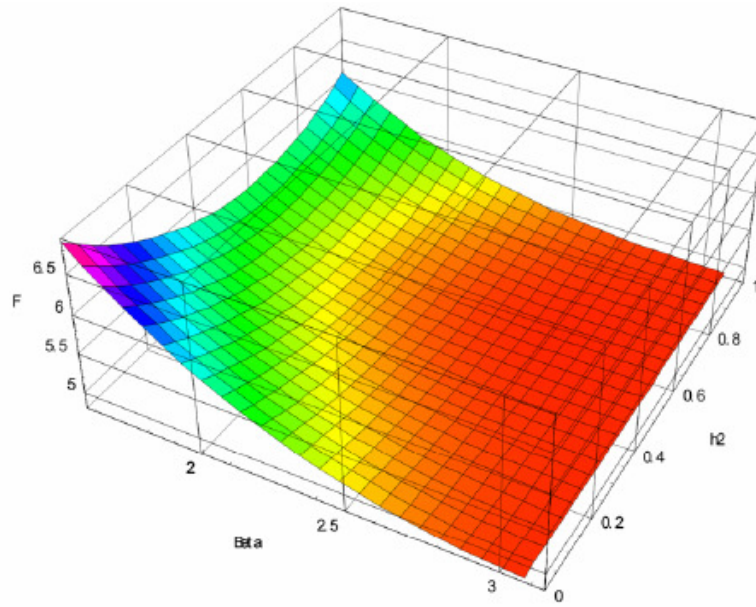


(a)

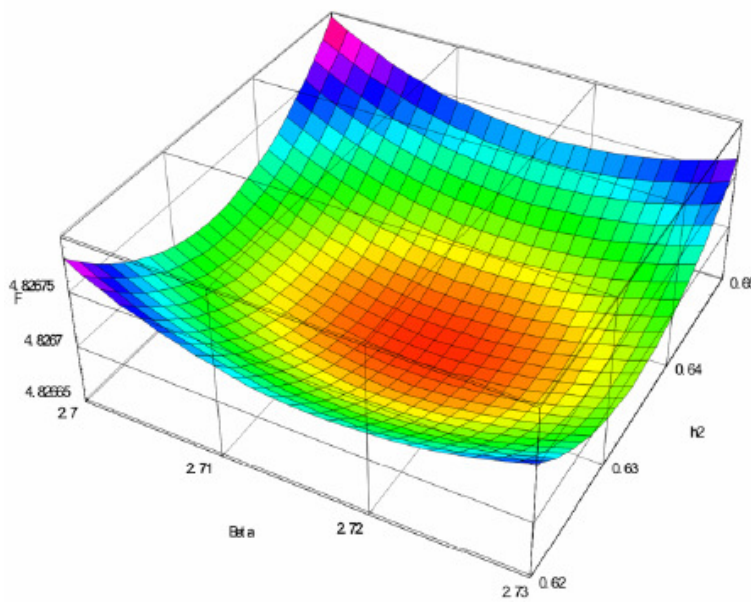


(b)

**Figure 3.10.** Free energy 'landscape' of a water droplet resting on a structured surface composed of single-size particles. (a)  $\eta = 0.9$ , and (b)  $\eta = 0.5$ .



(a)



(b)

**Figure 3.11.** (a) Free energy ‘landscape’ of a water droplet resting on a structured surface composed of raspberry-like particles.  $\eta_1 = \eta_2 = 0.5$ , and (b) zoom-in view of (a) to show the global energy minimum.

Next, the free energy on the dual-size structure from raspberry-like particles was examined. To simplify the calculation, we started with a fixed  $h_1$  (air height relative to larger particles). Figure 3.11 gives the free energy ‘landscape’ of a water droplet resting

on a surface with dual-size structure. ( $\eta_1 = \eta_2 = 0.5$ ). From Figure 3.11, the global energy minimum is found at  $\beta = 163^\circ$ , which increased significantly from that on a single-size structure ( $\beta = 137^\circ$ ) and is in good agreement with our experiment results ( $165^\circ$ ). It is interesting to notice that, as the packing factors for both large and small particles decrease, the surface becomes more water-repellent since the ratio of vapor-liquid interface increases. On the other hand, the packing factor cannot be too small; otherwise, the gravity of the water droplet cannot be neglected and the low-energy state becomes unstable, leading to the collapse of the water droplet.

The modeling study also indicates that for a size ratio between larger and smaller particle below 10, the apparent water contact angle increases as the size ratio increases<sup>29</sup>. As the size ratio is above 10, further increasing the size ratio does not have a significant effect on the wettability of the surface, which has also been experimentally demonstrated in this chapter.

### 3.5 Conclusions

Inspired by Mother Nature, we successfully developed superhydrophobic films based on conventional silica particles and epoxy films in an effort to mimic the two-level surface structure of lotus leaves. The results of water contact angle measurements indicate that the water droplets sitting on this superhydrophobic surface remain in the Cassie regime. The dual-size surface structure from raspberry-like particles on our superhydrophobic films was proved by AFM and SEM observations. Comparing the results from our experimental data and modeling study, we draw the conclusion that the size ratio of raspberry particles does not have a significant effect on the wettability of film when it is more than 10. The simplicity of this procedure may make widespread applications of so-prepared superhydrophobic films possible.

## References:

1. Khorasani, M.Y.; Mirzadeh, H.; Kermani, Z. *Appl. Surf. Sci.* **2005**, *242*, 339.
2. Jin, H. M.; Feng, X. J.; Xi, J. M.; Zhai, J.; Cho K.W.; Feng, L. *et al.*, *Macromol. Rapid Commun.* **2005**, *26*, 1805.
3. Sun, M. H.; Luo, C. X.; Xu, L. P.; Ji, H.; Qi, O. Y.; Yu D. P. *et al.*, *Langmuir* **2005**, *21*, 8978.
4. Mark, J. E. *Macromolecules* **1978**, *11*, 627.
5. Shafrin, E. G.; Zisman, W. A. *J. Phys. Chem.* **1969**, *64*, 523.
6. Noll W. Chemistry and technology of silicones. London. Academe Press; **1960**
7. Shiu, J. Y.; Kuo, C. W.; Chen, P. Proceedings of SPIE, Smart Materials III, **2005**, *5648*, 325.
8. Teshima, K.; Sugimura, H.; Inoue, Y.; Takai, O.; Takano, A. *Appl. Surf. Sci.* **2005**, *244*, 619.
9. Song, X. Y.; Zhai, J.; Wang, Y. L.; Jiang, L. *J. Phys. Chem. B* **2005**, *109*, 4048.
10. Qian, B. T.; Shen, Z. Q. *Langmuir* **2005**, *21*, 9007.
11. Guo, Z. G.; Zhou, F.; Hao, J. G.; Liu, W. M. *J. Am. Chem. Soc.* **2005**, *127*, 15670.
12. Furstner, R.; Barthlott, W.; Neinhuis, C.; Walzel, P. *Langmuir* **2005**, *21*, 956.
13. Callies, M.; Chen, Y.; Marty, F.; Pepin, A.; Quere, D. *Microelectron Eng.* **2005**, *78*, 100.
14. Zhang, X.; Shi, F.; Yu, X.; Liu, H.; Fu, Y.; Wang Z. Q.; *et al.*, *J. Am. Chem. Soc.* **2004**, *126*, 3064.
15. Shirtcliffe, N. J.; Mchale, G.; Newton, M. I.; Chabrol, G.; Perry C. C. *Adv. Mater.* **2004**, *16*, 1929.
16. Jiang, L.; Zhao, Y.; Zhai, J. *Angew. Chem. Int. Ed.* **2004**, *43*, 4338.
17. Patankar, N. A. *Langmuir* **2004**, *20*, 8209.
18. Stöber, W.; Fink, A.; Bohn, E. *J. Coll. Interface Sci.* **1968**, *26*, 62.
19. Nakada, S.; Sawatari, C.; Tamura, K.; Yagi, T. *Coll. Poly. Sci.* **2001**, *279*, 754.
20. Van Blaaderen, A.; Vrij, A. *J. Coll. Interface Sci.* **1993**, *156*, 1
21. Wenzel, R. N. *Ind. Eng. Chem.* **1936**, *28*, 988; *J. Phys. Colloid Chem.* **1949**, *53*, 1466.
22. Cassie, A. B. D.; Baxter, S. *Trans. Faraday Soc.* **1944**, *40*, 546.
23. Johnson, R. E.; Dettre, R. H. *Adv. Chem. Ser.* **1963**, *43*, 112 & 136.

24. Herminghaus, S. *Europhys. Lett.* **2000**, *52*, 165.
25. Oner, D.; McCarthy, T. J. *Langmuir* **2000**, *16*, 7777.
26. Lafuma, A.; Quéré, D. *Nature Mater.* **2003**, *2*, 457.
27. a) Barthlott, W.; Neinhuis, C. *Planta* **1997**, *202*, 1; (b) Neinhuis, C.; Barthlott, W. *Annals of Botany* **1997**, *79*(6), 667.
28. Feng, L.; Li, S.; Li, Y.; Li, H.; Zhang, L.; Zhai, J.; Song, Y.; Liu, B.; Jiang, L.; Zhu, D. *Adv. Mater.* **2002**, *14*, 1857.
29. van Loenen, B. Nature-inspired (super)lyophobic surfaces: a modeling approach. Master thesis, Eindhoven University of Technology, March **2007**.
30. Vrancken, R. Geometry of micro-transfer printed polymerized mesogen structures, Master thesis, Eindhoven University of Technology, June 28, **2006**, MBX 2006-04.
31. Marmur, A. *Langmuir*, 2003, *19*, 8343.
32. Briant, A.J.; Wagner, A.J.; Yeomans, J.M. *Phys. Rev. E*, **2004**, *69*, 31602.
33. Werner, O.; Wågberg, L.; Lindström, T. *Langmuir* **2005**, *21*, 12235.
34. Li, W.; Amirfazli, A. *J. Colloid Interface Sci.* **2005**, *292*, 195.
35. Jopp, J.; Grüll, H.; Yerushalmi-Rozen, R. *Langmuir* **2004**, *20*, 10015.
36. Johnson, R.E.; Dettre, R. H. *Contact Angle, Wettability and Adhesion; Advances in Chemistry Series 43*, ACS, Editor: R.E. Gould, **1964**.

## Chapter 4

### Superhydrophobic surfaces by a layer-by-layer approach<sup>\*</sup>

**Abstract:** A layer-by-layer (LbL) approach was developed to prepare superhydrophobic surfaces, with the aim of improving mechanical robustness of the films. Epoxy-based films were partially pre-cured to a varied extent, followed by the deposition of silica microparticles. After that, the films were completely cured. Microparticles became partially embedded into the polymer matrix. Subsequently, silica nanoparticles were grafted on the microparticle surface through amine-epoxy reactions. Finally, the surfaces were modified with a layer of PDMS to render their superhydrophobicity. However, the adhesion between nanoparticles and microparticles is still weak. Thus, to further increase the robustness of the film, the films were treated with  $\text{SiCl}_4$ , which cross-linked the nano- and microparticles together. The films were then modified with perfluoroalkylsilane, leading to superhydrophobic films. On this superhydrophobic surface, the advancing water contact angle was about  $156 \pm 0.5^\circ$ , with a CA hysteresis of about  $4^\circ$ . Pull-off tests and the paper tissue rubbing abrasion test on these films show that the mechanical robustness of the superhydrophobic film has been improved.

---

<sup>\*</sup> Part of this Chapter will be submitted for publication: Wu, D.; Ming, W.; van Benthem, R.A.T.M.; de With, G. Mechanically robust superhydrophobic surfaces by a layer-by-layer approach, to be submitted to *Langmuir*, 2007.



## 4.1 Introduction

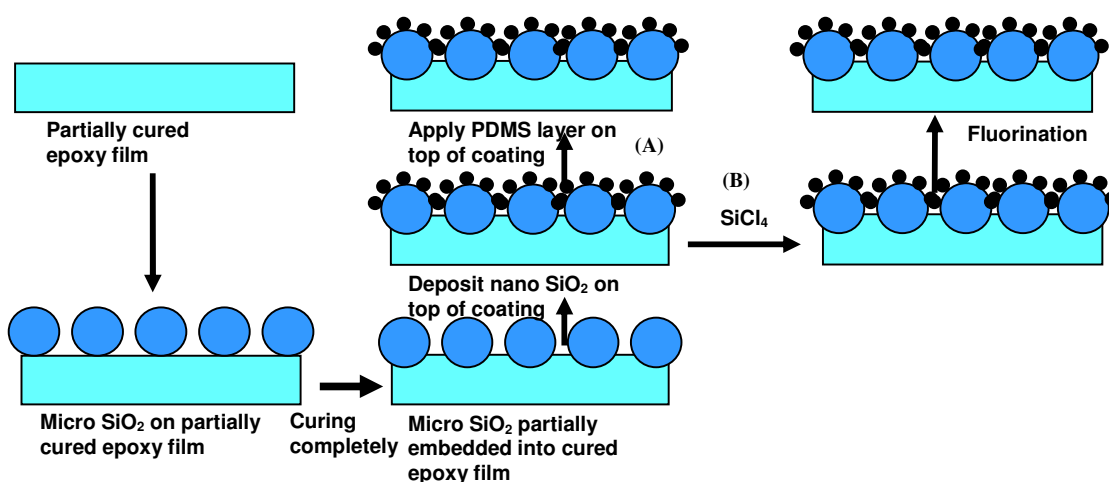
In Chapter 3, we described a method to obtain superhydrophobic films with a dual-size hierarchical structure by using raspberry-like particles. On the surface of such a film, the advancing water contact angles was about  $165^\circ$ , and the roll-off angle of a  $10\text{-}\mu\text{L}$  water droplet was about  $2^\circ$ . However, it had a drawback. Despite there was chemical bonding between microparticles and epoxy, microparticles and nanoparticles, PDMS and nanoparticles, the film was not robust enough to withstand rubbing by paper tissue or finger nails. This was due to that there are only point contacts between the particles and epoxy. Therefore, in this chapter, we aimed at developing a new method to create more robust superhydrophobic surfaces.

The layer-by-layer (LbL) assembly technique is a simple way to fabricate various kinds of surfaces with tailored chemical composition and architecture in micro- and nanoscales<sup>1-5</sup>. Recently, the LbL assembly technique has been used to develop superhydrophobic surfaces<sup>6-13</sup>. For example, Zhai *et al.*<sup>9</sup> used an LbL technique to create a surface with honeycomb-like microporous structure followed by covering the microporous structure with nanoparticles. Cho and co-workers<sup>11</sup> fabricated a superhydrophobic surface by depositing silica nanoparticles on a poly(allylamine hydrochloride) film surface containing poly(acrylic acid) coated  $\text{ZrO}_2$  nanoparticles followed with a simple fluorination. Bravo *et al.*<sup>14</sup> developed a transparent superhydrophobic film based on silica nanoparticles. They used the LbL assembly method to control the placement and level of aggregation of differently sized nanoparticles. Zhang *et al.*<sup>15</sup> reported a method to prepare a micro- and nanostructured hierarchical surface for use as a superhydrophobic surface by depositing LbL assembled multilayer films on a silica-sphere-coated substrate.

Most of these LbL approaches use electrostatic adsorbing techniques to deposit particles on top of a substrate or larger particles. In this chapter, we report an LbL approach to develop a robust superhydrophobic coating by using epoxy-amine chemistry. The process is illustrated in Scheme 4.1. First, a layer of a partially pre-cured epoxy was prepared. Then, a single layer of epoxy-modified silica microparticles was spin-coated on the top of the epoxy film. After that, the film was fully cured. Therefore, a completely cross-linked epoxy film with microparticles partially embedded was formed. Next,

amine-modified silica nanoparticles were deposited onto the single-layer microparticles. The last step was to apply a PDMS layer on top of the coating, as shown in the route A in Scheme 4.1.

An alternative approach was investigated in order to further improve the robustness of the coating. After the amine-modified silica nanoparticles were deposited onto the cross-linked epoxy film with microparticles partially embedded, the film was briefly immersed into a  $\text{SiCl}_4$  solution, followed by washing with toluene, and drying. In this way, a cross-linked stable silica-sphere-coated substrate was obtained. The substrate was then chemically modified with a perfluorodecyltrichlorosilane (Scheme 4.1B).



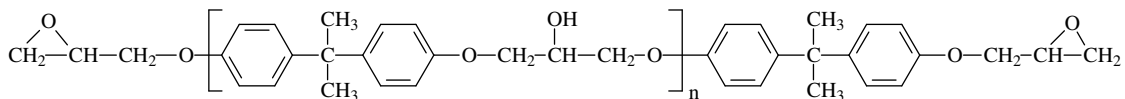
**Scheme 4.1.** Preparation of superhydrophobic film by LbL approach.

## 4.2 Experimental

### 4.2.1 Materials

Amine-modified silica particles (12 nm, 50 nm) and epoxy-modified silica particles (800 nm) were synthesized as described in Chapter 3. Aminopropyl terminated polydimethylsiloxane (DMS-A15) were obtained from ABCR; Monoglycidyl ether terminated polydimethylsiloxane (MW = 5000), 1H,1H,2H,2H-perfluorodecyl trichlorosilane, and silicon tetrachloride were obtained from Aldrich; Jeffamine D-230 (a polyoxypropylene diamine, amine-hydrogen equivalent weight = 60) was obtained from

Huntsman. Epikote 1004 (Scheme 4.2, a solid epoxy resin produced from bisphenol A and epichlorohydrin; the epoxy group content in this resin is about 1100 ~1240 mmol/kg) was purchased from Shell Chemicals U.K. Limited.



**Scheme 4.2.** Molecular structure of the Epikote 1004.

#### 4.2.2 Preparation of partially cured epoxy coatings

Epikote 1004 1.73 g (2 mmol epoxy) was first dissolved into 10 mL butyl acetate at 70 °C. Jeffamine D-230 0.13 g (1.1 mmol amine) was then dissolved into the Epikote 1004 solution. The mixture was spin-coated on a 2 x 2 cm<sup>2</sup> silicon wafer at 1000 rpm for 15 s with a spin-coater (KW-4A, Chemat Technology) at room temperature. The epoxy films were pre-cured in an oven at 100 °C for different periods of time (10 min, 20 min, 30 min or 16 h, respectively). The epoxy conversion was followed by ATR-FTIR on a BioRad Excalibur Spectrophotometer.

#### 4.2.3 Preparation of epoxy coatings with silica microparticles

A single layer of epoxy-modified silica microparticles (800 nm) was spin-coated on the top of epoxy film from a 10 % (w/v) silica suspension in ethanol at 1000 rpm for 10 s. The coating was then cured in an oven at 100 °C for 16 h.

#### 4.2.4 Preparation of superhydrophobic surfaces

##### 4.2.4.1 Preparation of superhydrophobic surfaces with PDMS

Amine-modified silica nanoparticles (50 nm, 12 nm, respectively) were deposited onto the single-layer microparticles by immersing the substrates into 1 % (w/v) nanosilica suspension for 24 h at 60 °C followed by washing with ethanol. The surface-roughened film was then reacted with amine-end-capped DMS-A15 at 80 °C for 4 h to ensure that any remaining epoxy groups from either the epoxy-amine film or large silica particles were converted into terminal amine groups; after the reaction the film was thoroughly washed by toluene to remove unreacted DMS-A15. In the end, the film was reacted with

monoglycidyl ether terminated polydimethylsiloxane at 80 °C for 4 h and followed by washing with toluene, resulting in a layer of PDMS covering the roughened surface.

#### **4.2.4.2 Superhydrophobic surfaces with perfluorodecyltrichlorosilane modification**

After depositing nanoparticles on the microparticle surfaces, the film was immersed in a toluene solution of SiCl<sub>4</sub> (1 wt %) for 5 min, followed by washing with toluene, and drying with an air flow. The substrate was then transferred to a dry toluene solution of 1*H*,1*H*,2*H*,2*H*-perfluorodecyltrichlorosilane (1 wt %) for 30 min in a glove box. After that, the samples were rinsed with dry toluene to remove the excess perfluorodecyltrichlorosilane and dried again.

#### **4.2.5 Characterization techniques**

##### **Pull-off test**

Prior to the pull-off measurements, the samples were coated with a 10 nm thick gold layer. The sputtering was done at Moorfield MiniLab sputter system under 1.33 Pa Ar<sup>+</sup> plasma using an RF power of 60 W. The employed background pressure was 3×10<sup>-4</sup> Pa.

For the pull-off measurements, pull-off studs (stainless steel,  $d = 8$  mm) were glued to the metalized samples by 3M DP 460 epoxy glue (cured for 24 h at room temperature). After solidification of the glue, the precut around the stud is made (Figure 4.1). The samples thus prepared are then clamped in the tensile machine (TesT 810) and connected to the load cell via a long cable to make sure the force application angle is 90° at any moment. Subsequently, the clamped sample is moved downwards at a constant speed until the fracture occurs. The tests were performed in an air at room temperature using a tensile machine cross-head velocity of 1 mm/min.

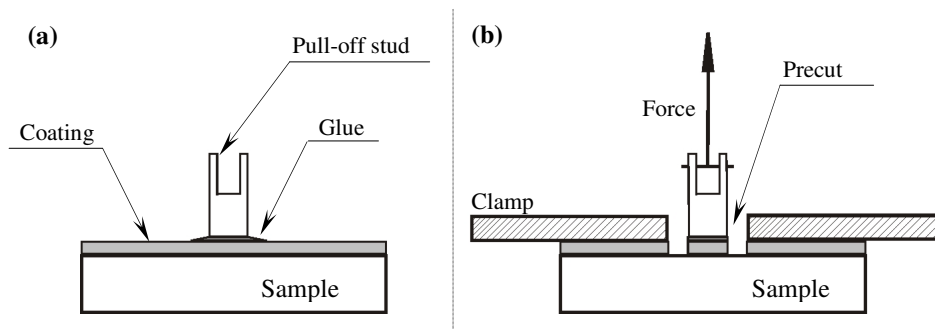


**Figure 4.1.** a) Schematic drawing of the pull-off test specimen and b) drawing of the pull-off test specimen, with a precut, in the clamping system.

The descriptions of scanning electron microscopy (SEM), contact angle measurement and ATR-FTIR measurements are given in previous chapters.

## 4.3 Results and discussion

### 4.3.1 Preparation of partly cured epoxy coatings

The conversion of the epoxy film was investigated by real-time ATR-FTIR. The evolution of IR spectra of the reaction mixture of Epikote 1004 and Jeffamine D-230 at 100 °C is shown in Figure 4.2. The peak at 915 cm<sup>-1</sup>, corresponding to the oxirane ring deformation of the epoxy group, decreased steadily as the curing reaction proceeded. On the other hand, the peak at 833 cm<sup>-1</sup>, corresponding to the phenyl group, remained the same throughout the reaction. This peak therefore can be used as an internal standard. The relative conversion ( $\alpha$ ) of the epoxy groups denoting the degree of curing at time  $t$  was calculated by the following equation:<sup>16</sup>

$$\alpha = 1 - \frac{(A_{epoxy} / A_{ref})_t}{(A_{epoxy} / A_{ref})_0} \quad (4.1)$$

Where  $A$  is the absorbance of the epoxy group; the subscripts 0 and  $t$  denote the reaction time 0 and  $t$ , respectively; the subscripts epoxy and ref denote the characteristic epoxy and reference peak, respectively.

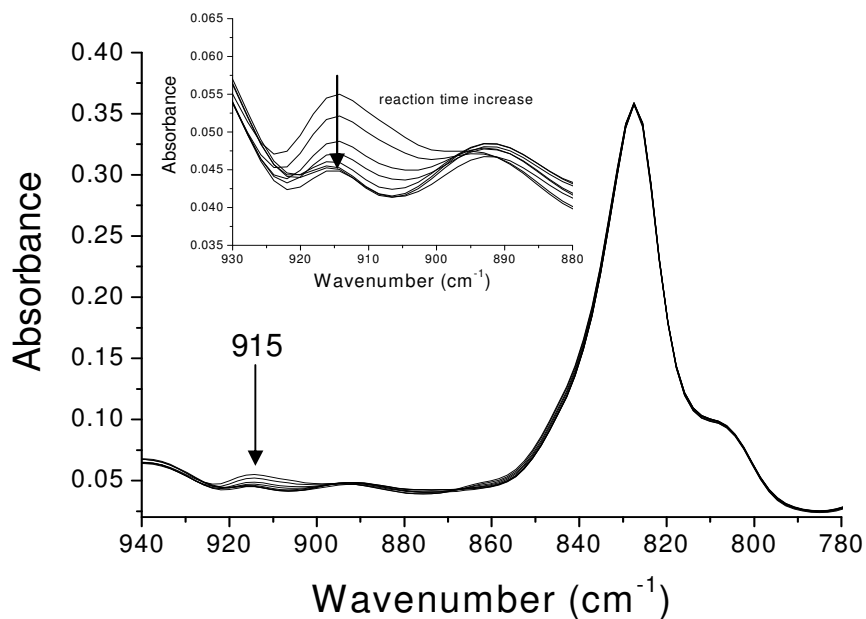


**Figure 4.2.** Real-time ATR-FTIR spectra for the thermal curing of Epikote 1004 at 100 °C.

Figure 4.3 shows the conversion of epoxy group vs. time at 100 °C. From this curve, we calculated the degree of epoxy conversion at 10 min, 20 min, and 30 min to be 44%, 57% and 65%, respectively. The conversion of epoxy group is in agreement with previous reports<sup>16-18</sup>.

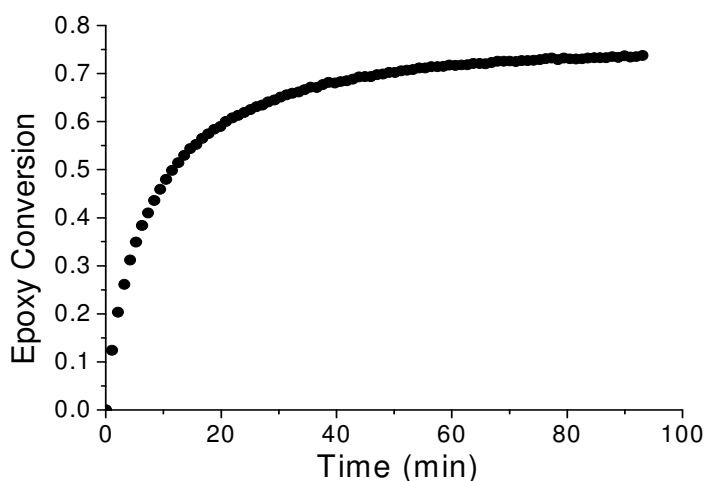


**Figure 4.3.** Conversion of epoxy group during thermal curing of Epikote 1004 at 100 °C

### **4.3.2 Characterization of epoxy coatings with silica microparticles**

Silica microparticles were deposited on uncured, 10 min, 20 min, 30 min pre-cured and 16 h cured epoxy films (film 4A to 4E), respectively, followed by a complete curing at 100 °C overnight. The topography of the films was checked by SEM. As shown in Figure 4.4, silica particles were completely embedded into the polymer matrix on the uncured film 4A, and the coating surface was rather smooth. As we know the adhesion forces between particles and polymer matrix mainly come from the amine-epoxy bonds between them. A large contact area gives a stronger adhesion. Therefore, the film 4A was likely to be the most robust film among them. However, the surface roughness was very low. On the other hand, silica particles were on the top of the polymer coating on the fully cured film 4E. This indicates the adhesion force between particles and polymer matrix of this film was very low although the surface roughness was very high. Neither of them was suitable to develop a robust superhydrophobic coating. On the films 4B, 4C and 4D, particles were partially embedded into the polymer matrix which gives the coating both mechanical stability and surface roughness. For instance, about 75%, 50%, and 30% of individual spheres was embedded into the polymer matrix on the films 4B, 4C and 4D, respectively.

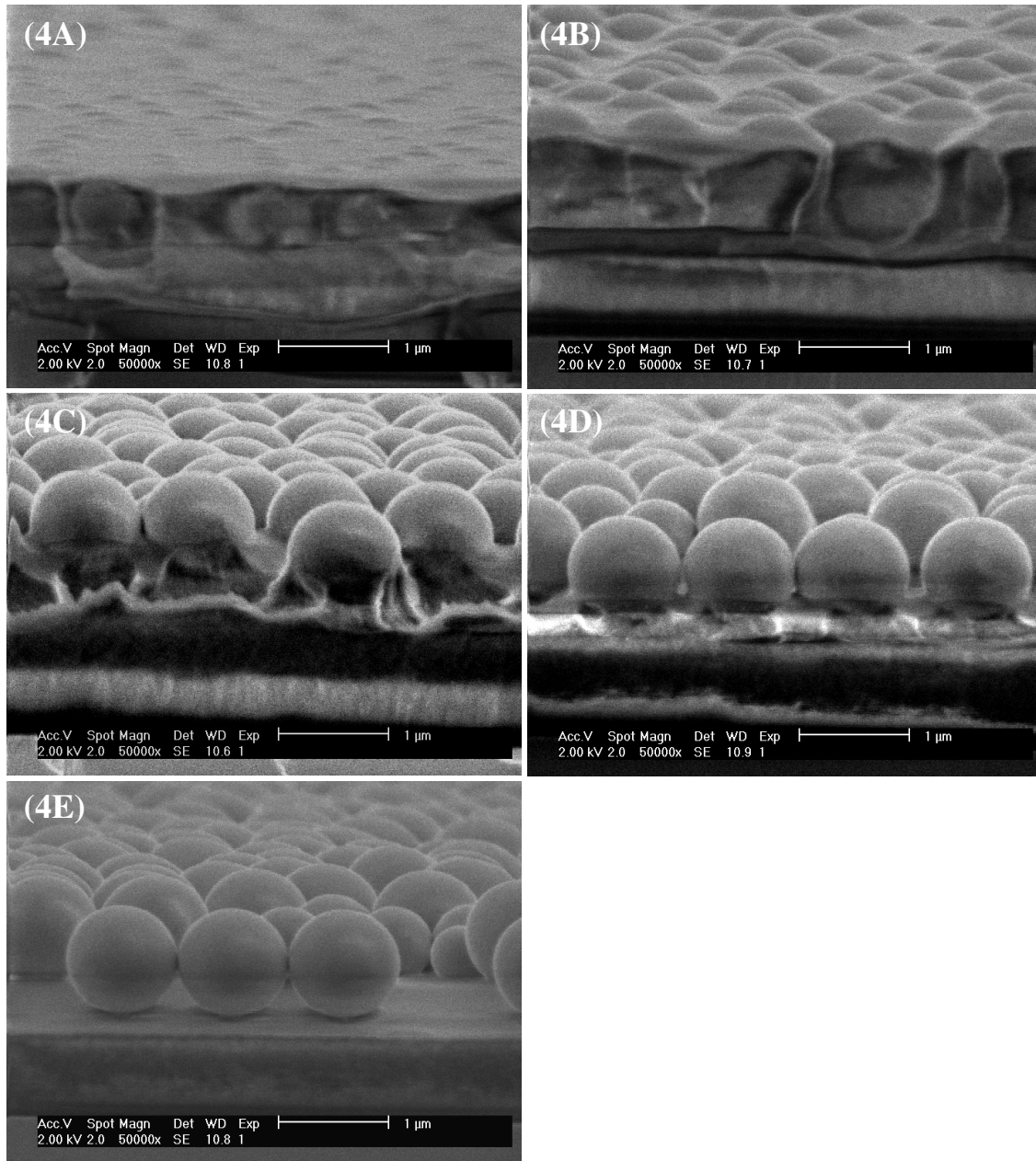


**Figure 4.4.** SEM images of silica microparticles on uncured, 10 min, 20 min, 30 min pre-cured, and 16 h cured epoxy film (film 4A to 4E), followed by a complete curing at 100 °C overnight.

#### 4.3.3 Surface wettability on single-sized structured surfaces

It is well known that surface roughness can amplify the hydrophobicity on a hydrophobic surface. Table 4.1 shows water contact angles on film 4A to film 4E after

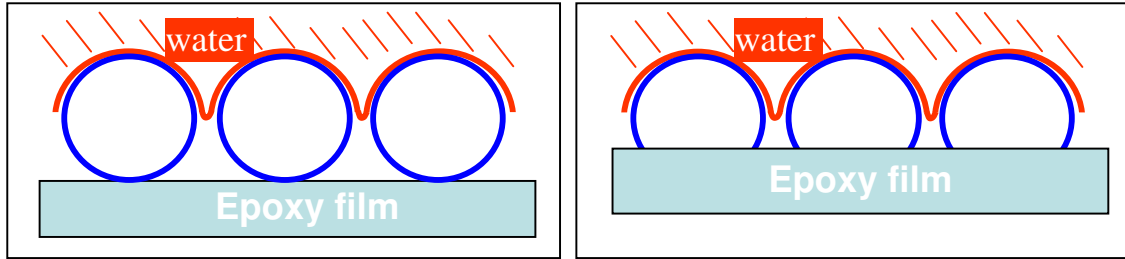


they are modified by PDMS. The advancing and receding water CAs on film 4A are 109° and 74°, respectively. These values are slightly higher than the CA on the smooth PDMS modified epoxy film (Chapter 3). It indicates that very low surface roughness only increases the hydrophobicity slightly. As the pre-curing time increases from film 4A to film 4E, both advancing CA and receding CA increase until the advancing CA reaches the maximum value for film 4C, and the receding CA reaches the maximum value for film 4D. Further increase of the pre-curing time during film formation does not increase the CA anymore, which indicates that for film 4C and film 4D, the maximum amplified wettability has been achieved. Further increase of the pre-curing time can only compromise the robustness of the films.

**Table 4.1.** Water contact angles on the PDMS modified films (4A-4E).

	Film 4A	Film 4B	Film 4C	Film 4D	Film 4E
$\theta_A$ (°)	109.2 ± 0.3	114.4 ± 0.6	149.1 ± 0.2	147.2 ± 0.3	148.2 ± 0.5
$\theta_R$ (°)	74.2 ± 0.4	72.2 ± 0.7	89.1 ± 0.5	99.6 ± 0.4	99.5 ± 0.7

As we mentioned in Chapter 1, when a water droplet sits on a rough, hydrophobic surface, and air remains underneath the water, the water droplet is in the Cassie state. From modeling studies in our laboratory, we know that the water contact angle in the Cassie state only depends on the air/liquid interface area ratio ( $1-f$ , as given in Chapter 1) and the surface energy of the solid surface. The air volume underneath the water doesn't directly affect the contact angle. From SEM images, we found that if the water droplets remains above an air pocket, the air/liquid interface area ratio on film 4C (one third of a particle is embedded into the polymer matrix), 4D, and 4E are almost the same (Scheme 4.2). So the roughness effect on the water contact angle of those surfaces would be similar. However, film 4C and 4D will be much more robust than film 4E due to the larger contact area between the particles and the polymer matrix which gives stronger adhesion.



**Scheme 4.2.** Scheme images of the air/liquid interface area ratio on a surface covered by spheres. Left: spheres sit on top of an epoxy substrate. Right: spheres are partially embedded into the epoxy substrate.

#### 4.3.4 Adhesion between particles and polymer matrix

The adhesion between particles and polymer matrix was investigated by the pull-off test. Before pull-off testing, film 4C, film 4D and film 4E (without PDMS top layer) were coated with a 10 nm thick gold layer, respectively. In the pull-off test, the pulling force was measured until fracture occurred. The fracture stress ( $\sigma_c$ ) was calculated as follows:

$$F_{\text{pull-off}} = \sigma_c A \quad (4.2)$$

where  $A$  is the pulled surface area (set to  $0.48 \text{ cm}^2$  here) and  $F_{\text{pull-off}}$  is the pulling force when fracture occurs.

Thus, the experimentally determined fracture stresses (from single measurements) of film 4C, film 4D and film 4E are 260, 240 and  $120 \text{ N/cm}^2$ , respectively.

After the pull-off test, the damage of the sample surfaces was checked by SEM. Figure 4.5 shows the surfaces of films with different pre-curing time before and after pull-off tests. Before the pull-off test, each surface is covered by particles, while after the pull-off testing, varying levels of damage are shown on the sample surface depending on different pre-curing time. As shown by SEM, after pull-off testing, all the particles were removed from the surface of film 4E. The SEM image also indicates that the fracture on film 4E occurred at the interface between particles and polymer matrix.

In contrast, nearly all the particles remain on the surface for film 4C, and a small part of particles were removed from the surface of film 4D (the image in the inset of Figure 4.5 shows a single particle that was pulled out from the polymer matrix). Moreover, the SEM results show that the fracture on both film 4C and film 4D occurred mainly on the interface between the particles and the gold layer, which indicates that the adhesion

between particles and polymer matrix is even stronger than that between particle/gold layer.

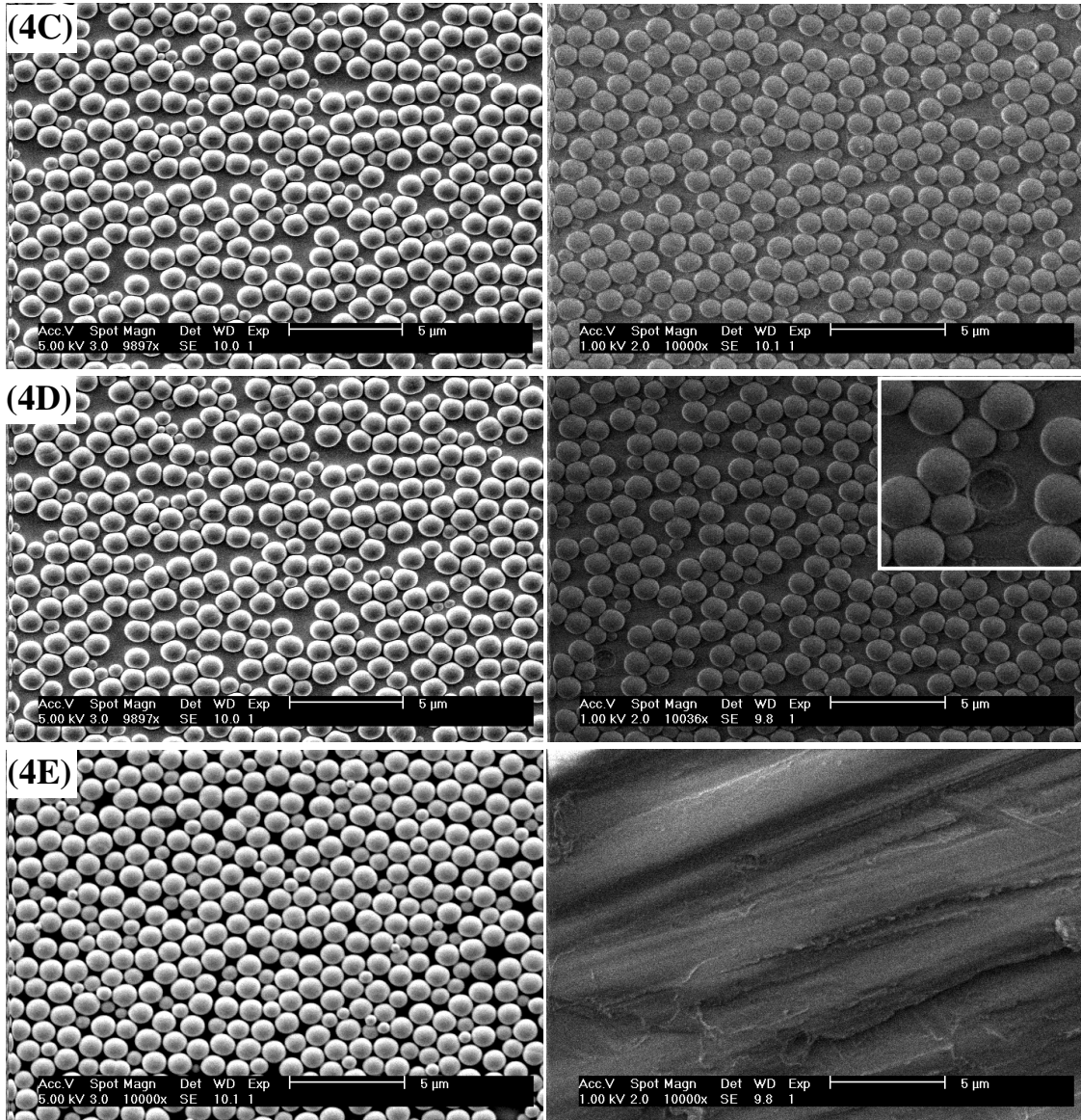


**Figure 4.5.** SEM images of film 4C, film 4D and film 4E before pull-off test (left), respectively; and after pull-off test (right). The inset in the right middle image shows a zoom-in image of one particle having been pulled off from the polymer matrix.

The SEM images also show that the silica particles were not perfectly packed due to the presence of smaller particles. Thus, small polymer/gold interfaces could be formed

after deposition of the gold layer, so that these interfaces may also contribute to the pull-off force. This may give an explanation why the fracture stress of film 4E was 120 N/cm<sup>2</sup>, although we suppose there was only weak force between the particles and the polymer matrix because of the point contacts.

To summarize the adhesion between particles and the polymer matrix on the films which were prepared under different pre-curing times, Table 4.2 is given below.

**Table 4.2.** Stability of films which were prepared under different pre-curing times.

Film	Pre-curing time (min)	Surface damage after pull-off test	Fracture stress (N/cm <sup>2</sup> )
4A	0	unchecked	unchecked
4B	10	unchecked	unchecked
4C	20	No damage	260
4D	30	Slight damage	240
4E	Completely cured	Full damage	120*

\*The high fracture force may come from the energy needed to break polymer/gold interfaces.

#### 4.3.5 Superhydrophobic coatings from layer-by-layer approach

The superhydrophobic coating was developed by depositing silica nanoparticles (12 nm, 50 nm, respectively) on the top of film 4C, followed by applying a layer of PDMS. Figure 4.6 shows SEM images of the final superhydrophobic coating (50 nm/ 800 nm). Figure 4.6 clearly shows that nanoparticles covered the top half of microparticles, forming a dual-size structure that mimics the lotus leaf surface. Figure 4.6B shows the cross-section of the film. The particles are partially embedded into the polymer matrix which increases the mechanical stability of the coating.

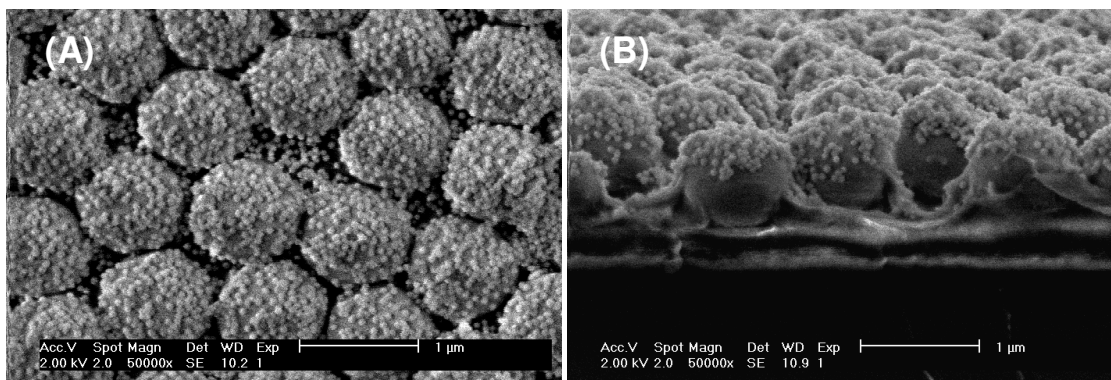


**Figure 4.6.** SEM images of superhydrophobic coating based on film 4C: (A) top view, and (B) side view.

The wettability of the film was measured by contact angle (CA) of water on the surface. Figure 4.7 shows the image of a 10- $\mu$ L water droplet on the surface containing 50 nm/ 800 nm dual-size structure. The advancing water CA on the film is  $161.2 \pm 0.4^\circ$ , with a CA hysteresis of about  $5.0 \pm 0.8^\circ$ . On the surface containing 12 nm/700 nm dual-size structures, the advancing water CA is  $157.2 \pm 0.5^\circ$  and the water CA hysteresis is  $4.5^\circ$ . The wettability on these two films is similar, and the explanation has been given in Chapter 3.

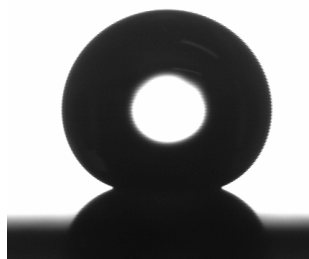


**Figure 4.7.** Image of a 10- $\mu$ L water droplet on the superhydrophobic coating with dual-size surface structure (Film 4C covered with nanoparticles and with PMDS surface modification, Figure 4.5).

As discussed above, we know the adhesion force between microparticles and polymer matrix is strong when particles are partially embedded into the polymer matrix. However, to obtain a robust film with dual-size surface structure, the adhesion forces between nano- and microparticles are also important. Thus, the pull-off test was applied on the surface of a film with double-size surface structure. Figure 4.8 gives the image of a surface with dual-size structure before and after pull-off test. These images show clearly that

nanoparticles were peeled off from the surface of microparticles during the pull-off test. Therefore, we need to improve the adhesion force between nano- and microparticles and among nanoparticles in order to obtain a robust coating.

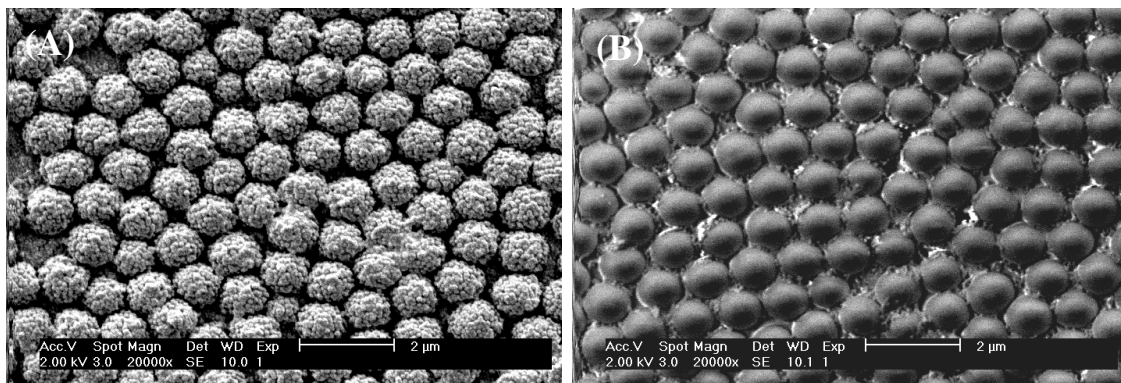
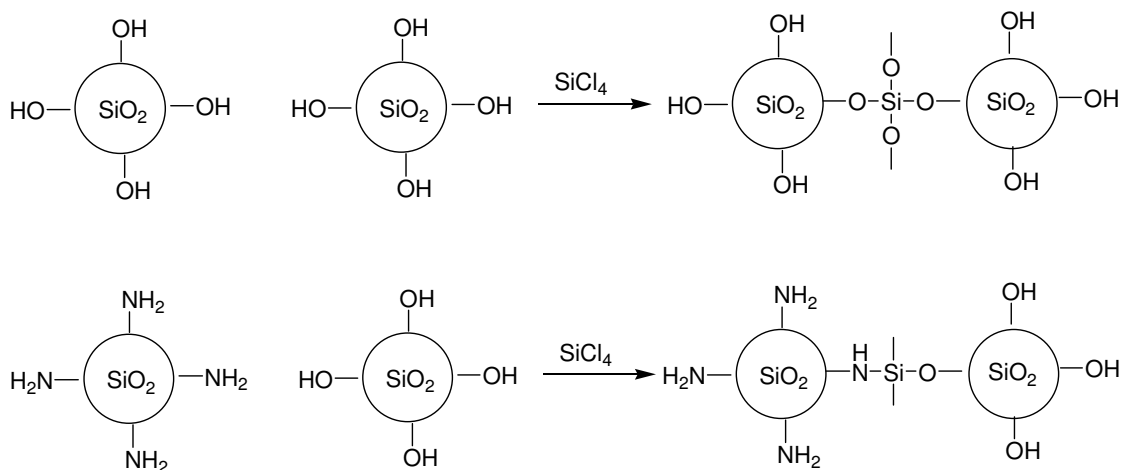


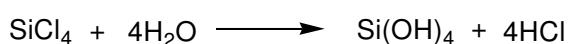
**Figure 4.8.** SEM images of a surface with dual-size structure (50 nm/800 nm, no PDMS modification) based on Film 4C before (A) and after (B) pull-off test.

#### 4.3.6 SiCl<sub>4</sub>-strengthened superhydrophobic coatings

We increased the adhesion force between nano and microparticles and among nanoparticles by using SiCl<sub>4</sub> as a cross-linker<sup>15,19</sup>. The possible reactions are given below:



Or the SiCl<sub>4</sub> molecules are reacted with pre-adsorbed water molecules on a silica surface,



Subsequently, the  $\text{Si(OH)}_4$  molecules will self-condense and the hydroxyl groups on  $\text{Si(OH)}_4$  will also react with both remaining hydroxyl groups on silica microparticles and the amine groups on silica nanoparticles. Thus,  $\text{SiCl}_4$  cross-link nano- and microparticles together. After cross-linking, the surface was modified with *1H,1H,2H,2H*-perfluorodecyltrichlorosilane to obtain superhydrophobicity.

The pull-off test was applied on this coating. Figure 4.9 shows the SEM images of the  $\text{SiCl}_4$ -strengthened coating before and after pull-off test. It clearly shows that after pull-off test, the nanoparticles were still attached on the microparticle surface.

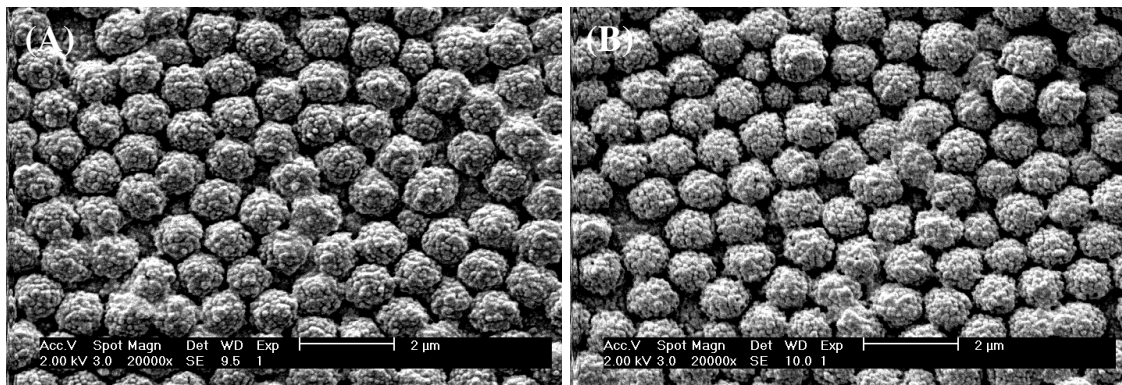


**Figure 4.9.** SEM images of a surface with double-size structure (50 nm/800 nm, no  $R_f$ -silane modification) based on Film 4C after cross-linked by  $\text{SiCl}_4$  before (A) and after (B) pull-off test.

To check the hydrophobicity and stability of the film, water contact angles on the film were checked before and after the films were gently rubbed with soft tissue paper. Before the tissue rubbing test, the advancing CA on the film is  $156 \pm 0.5^\circ$ , with a CA hysteresis of about  $4^\circ$ . After the tissue rubbing abrasion test, the advancing CA on the film is  $154 \pm 0.3^\circ$ , and CA hysteresis is about  $9^\circ$ . The hydrophobicity of the film is only slightly reduced. In contrast, after the same tissue rubbing abrasion test, the advancing CA on the film without  $\text{SiCl}_4$  treatment decreased from about  $161^\circ$  to  $145^\circ$ . Moreover, the CA hysteresis increased from  $4^\circ$  to  $32^\circ$ .

The superhydrophobic films prepared by modification of a rough surface with *1H,1H,2H,2H*-perfluorodecyltrichlorosilane also show lipophobicity which will be described in detail in Chapter 5.

## 4.4 Conclusions

In this Chapter, we demonstrated that a robust superhydrophobic coating can be developed by an LbL assembly technique. Before depositing a layer of silica microparticles on it, an epoxy-based film was partially pre-cured; subsequently, the film was completely cured. On the surface of this superhydrophobic coating, silica microparticles were partly embedded into the polymer matrix which increases the adhesion between the particles and the polymer matrix. The adhesion force was examined by pull-off test. Nanoparticles were grafted on the microparticle surface by amine-epoxy reactions. The adhesion between nano- and microparticles and among nanoparticles was enhanced by using  $\text{SiCl}_4$  as a cross-linker which was proved by the pull-off tests and SEM measurements. Contact angle measurement indicates that the  $\text{SiCl}_4$ -strengthened superhydrophobic coating maintains its superhydrophobicity after a paper tissue rubbing test.

## References

1. Decher, G.; Hong, J. D. *Makromol. Chem. Macromol. Symp.* **1991**, *46*, 321.
2. Decher, G. *Science* **1997**, *277*, 1232.
3. Zhang, X.; Shen, J. C. *Adv. Mater.* **1999**, *11*, 1139.
4. Hammond, P. T. *Adv. Mater.* **2004**, *16*, 1271.
5. Bertrand, P.; Jonas, A.; Laschewsky, A.; Legras, R. *Macromol. Rapid Commun.* **2000**, *21*, 319.
6. Zhang, X.; Shi, F.; Yu, X.; Liu, H.; Fu, Y.; Wang, Z.; Jiang, L.; Li, X. *J. Am. Chem. Soc.* **2004**, *126*, 3064.
7. Zhao, N.; Shi, F.; Wang, Z.; Zhang, X. *Langmuir* **2005**, *21*, 4713.
8. Jiang, Y. G.; Wang, Z. Q.; Yu, X.; Shi, F.; Xu, H. P.; Zhang, X. *Langmuir* **2005**, *21*, 1986.
9. Zhai, L.; Cebeci, F. C.; Cohen, R. E.; Rubner, M. F. *Nano Lett.* **2004**, *4*, 1349.
10. Zhai, L.; Berg, M. C.; Cebeci, F. C.; Kim, Y.; Milwid, J. M.; Rubner, M. F.; Cohen, R. E. *Nano Lett.* **2006**, *6*, 1213.



11. Han, J. T.; Zheng, Y.; Cho, J. H.; Xu, X.; Cho, K. *J. Phys. Chem. B* **2005**, *109*, 20773.
12. Jisr, R. M.; Rmaile, H. H.; Schlenoff, J. B. *Angew. Chem., Int. Ed.* **2005**, *44*, 782.
13. Ji, J.; Fu, J. H.; Shen, J. C. *Adv. Mater.* **2006**, *18*, 1441.
14. Bravo, J.; Zhai, L.; Wu, Z. Z.; Cohen, R. E.; Rubner, M. F. *Langmuir* **2007**, *23*, 7293.
15. Zhang, L.B.; Chen, H.; Sun, J.Q.; Shen, J. C. *Chem. Mater.* **2007**, *19*, 948.
16. Karayannidou, E.G.; Achilias, D.S.; Siderdou, I.D. *European Polym. J.* **2006**, *42*, 3311.
17. Mijovic, J.; Andjelic, S. *Polymer* **1996**, *37*, 1295.
18. Musto, P.; Martuscelli, E.; Ragosta, G.; Russo, P.; *J. Appl. Polym. Sci.* **1999**, *74*, 532.
19. Kurumoto, N.; Yamada, T.; Uchino, T. *J. Non-Crystalline Solids* **2007**, *353*, 684.

## Chapter 5

### Lipophobicity on superhydrophobic surfaces\*

**Abstract:** In this chapter, we examine the lipophobicity on the superhydrophobic films with dual-size surface roughness. A surface with a dual-size roughness structure was modified with 1*H*,1*H*,2*H*,2*H*-perfluorodecyltrichlorosilane. The advancing CA for pure water on this film is 168° with a CA hysteresis as low as 2°. Mixtures of ethanol and pure water were used as probe liquids; the contact angles and contact angle hystereses of these probe liquids on the superhydrophobic surfaces were examined. Moreover, on this surface, wettabilities of several hydrophobic liquids (hexadecane, oleic acid and sunflower oil) were checked. The static hexadecane CA is 125°, which indicates that the surface is also lipophobic. The modeling results show that it is possible to achieve superlipophobicity on the fluorinated surface with a dual-size structure.

---

\* Part of this Chapter has been presented at ACS Meeting (Aug. 2007, Boston): Wu, D.; Vrancken, R. J.; van Loenen, B.G.H.; van Benthem, R.A.T.M.; de With, G.; Ming, W. Lipophobicity on hierarchically structured superhydrophobic surfaces, *Polym. Mater. Sci. Eng.* **2007**, *97*, 418-419.

## 5.1 Introduction

Inspired by the superhydrophobic behavior of plant and insect surfaces, recently there have been many attempts to prepare artificial superhydrophobic surfaces. In Chapters 2, 3 and 4, we described different methods to develop superhydrophobic coatings. However, there are so far very few investigations dealing with oil repellency of a hierarchically structured surface<sup>1-5</sup>. Oil repellency is a very important property for a surface to maintain self-cleaning property. If a self-cleaning surface is not oil repellent, when it is in a dirty environment, oily materials can accumulate on the surface, eventually fill the textures, leading to the loss of the superhydrophobic and self-cleaning properties. Thus, in this chapter, we will examine the possibility to obtain lipophobic surfaces.

As we discussed in Chapter 1, wettability of solid surfaces with a liquid in air is governed by two factors. One is the chemical factor of the solid surface and the liquid, and the other is the geometrical factor of the solid surface. If we keep the geometrical factor of the solid surface unchanged, lowering the surface energy of the solid surface can further increase the hydrophobicity of a surface, and may even make it superlipophobic. A surface covered with close packed  $-CF_3$  group gives the lowest known surface energy ( $\sim 6 \text{ mN/m}$ )<sup>2</sup>, therefore, in this Chapter, we try to develop a self-assembled monolayer of *1H,1H,2H,2H*-perfluorodecyltrichlorosilane on the surface with a dual-size hierarchical structure .

Self-assembled monolayers (SAMs) are molecular assemblies that are formed spontaneously by the immersion of an appropriate substrate into a solution of an active surfactant in an organic solvent (Figure 5.1)<sup>6</sup>. This simple process makes self-assembled monolayers inherently manufacturable and thus technologically attractive for building superlattices and for surface engineering. The order in these two-dimensional systems is produced by a spontaneous chemical synthesis at the interface as the system approaches equilibrium.

SAMs of alkylchlorosilanes require hydroxylated surfaces as substrates for their formation. The mechanism of monolayer formation is believed to proceed by the initial conversion of Si-Cl groups in the silane molecule to Si-OH groups. Water, which is either bound to the surface of the substrate or present in the solution, hydrolyzes the chlorosilanes to form silanols<sup>7-9</sup>. These silanols then form stable bonds to the silica upon

reacting with the surface silanols and release water. Under ideal conditions, a Langmuir-like monolayer is formed on the hydrophilic surface in the presence of a thin water film. A cross-linked surface assembly is then formed by condensation reactions between the OH groups from the silane molecules with those on the oxide surface or from neighboring silanes.

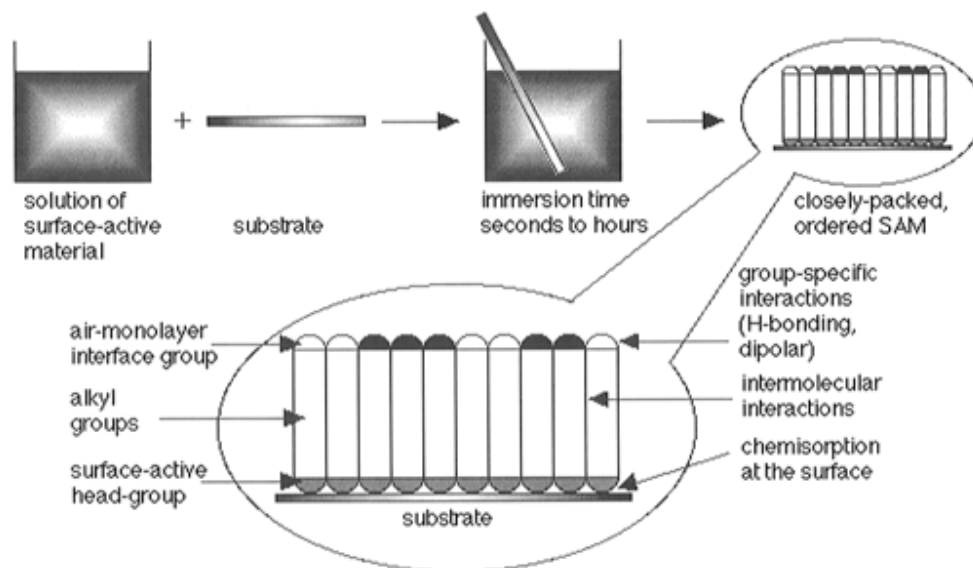


**Figure 5.1** *Self-assembled monolayers are formed by immersing a substrate into a solution of the surface-active material. The driving force for the spontaneous formation of the 2D assembly includes chemical bond formation of molecules with the surface and intermolecular interaction<sup>6</sup>.*

## 5.2 Experimental

### 5.2.1 Materials

Hexadecane was obtained from Sigma, oleic acid was purchased from Merck, and 1*H*,1*H*,2*H*,2*H*-perfluorodecyltrichlorosilane and sunflower oil were obtained from Aldrich.

### 5.2.2 Preparation of surface-fluorinated superhydrophobic films

The films with a dual-size hierarchical structure were prepared as we described in Chapter 3 and Chapter 4. Subsequently, the surface-fluorinated films were prepared as

follows. First, toluene was dried via distillation in the presence of active molecular sieves. In a glove box, a solution of 0.5 mL of 1*H*,1*H*,2*H*,2*H*-perfluorodecyl trichlorosilane in 50 mL of dry toluene was prepared. The surface-roughened films were dried and added to the solution and left for 30 min. Subsequently, the samples were rinsed with dry toluene to remove the excess perfluorodecyltrichlorosilane and dried again.

### **5.2.3 Probe liquids with different surface tensions**

Probe liquids with different surface tensions for contact angle measurements were prepared by mixing ethanol and deionized water. The surface tensions of those mixtures were measured with a digital tensiometer K10T (Krüss GmbH, Hamburg) at 20 °C.

### **5.2.4 Contact angle measurements**

Contact angles of ethanol/water mixtures and n-hexadecane were measured with the Dataphysics OCA 30 instrument at room temperature. All the contact angles were determined by averaging values measured at three different points on each sample surface. Dynamic advancing and receding angles were recorded while the probe fluid was added to and withdrawn from the drop, respectively.

Static contact angles of oleic acid and sunflower oil were measured with the same instrument. A liquid droplet was put on the sample surface by a tip of a micro-syringe. The liquid droplet was dropped to the sample surface from the distance of 1 cm by vibrating the syringe. The diameter of the droplet was about 1 mm.

## **5.3 Results and discussion**

As we know from Young's equation, the contact angle of a liquid on a solid surface depends on both the surface tension of the liquid and the surface energy of the solid surface. For example, on the same surface, the contact angle of a droplet of oil is much lower than that of a droplet of water because the latter has a much higher surface tension. In this study, to find out if our superhydrophobic coatings are also lipophobic, we measured the contact angles of liquids with different surface tensions on the superhydrophobic coating surface. Because water and ethanol are completely miscible at

all fractions, we used mixtures of water and ethanol as probe liquids. As shown in Figure 5.1, the surface tension decreases from 73 mN/m to 22.5 mN/m at 20 °C when the ethanol volume concentration in the mixture increases from 0 to 100 %.

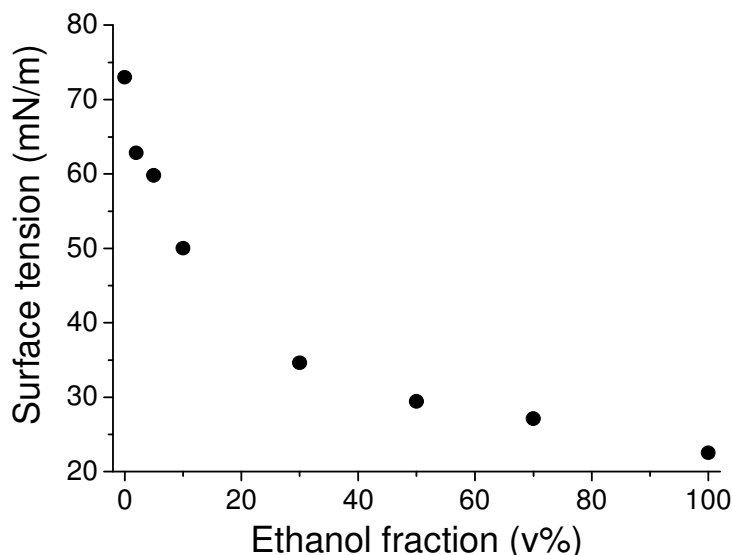


**Figure 5.1.** Surface tension of water/ethanol mixture as a function of ethanol volume fraction at 20 °C.

Contact angles of the water/ethanol mixture on PDMS-based superhydrophobic surfaces were examined first. As shown in Figure 5.2, although the advancing CA is greater than 140° for the interrogating liquids with a surface tension larger than 35 mN/m, a small contact angle hysteresis (< 5°) was only observed for those interrogating liquids with a surface tension larger than 60 mN/m. Most lipophilic liquids have a surface tension less than 40 mN/m, thus the PDMS-based superhydrophobic surfaces are not really lipophobic, as judged from the standpoint of contact angle hysteresis.

Next, contact angles of the water/ethanol mixture on perfluoroalkyl-modified superhydrophobic surfaces were examined. The advancing CA for water on this film is 168° with a CA hysteresis as low as 2° (Figure 5.3). For the water/ethanol mixture with a surface tension greater than 35 mN/m, the CA is above 160° and CA hysteresis is less than 10°, as demonstrated in Figure 5.3, indicating that the surface-fluorinated superhydrophobic surfaces may also be superlipophobic.

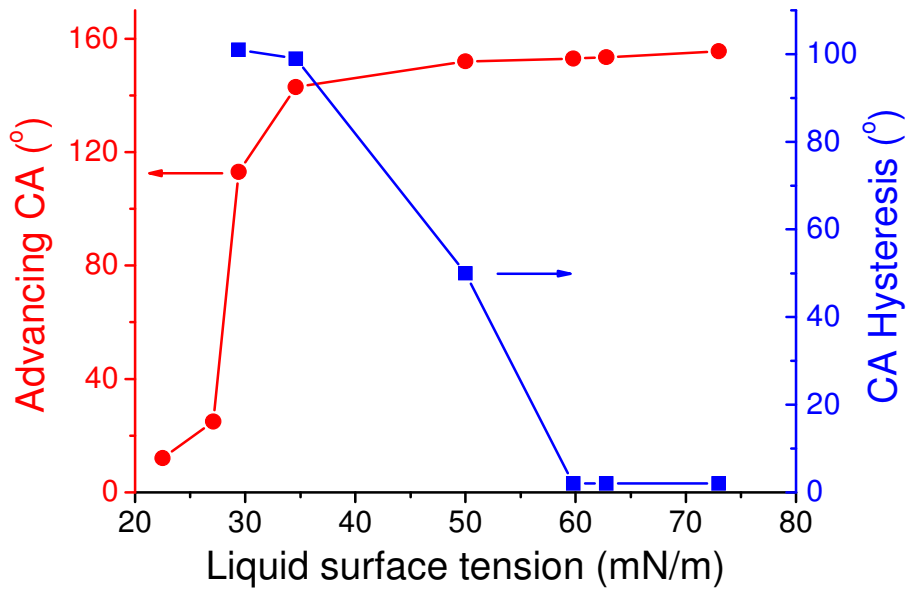


**Figure 5.2.** Contact angles and CAHs of water/ethanol mixture on a PDMS-based superhydrophobic surfaces.

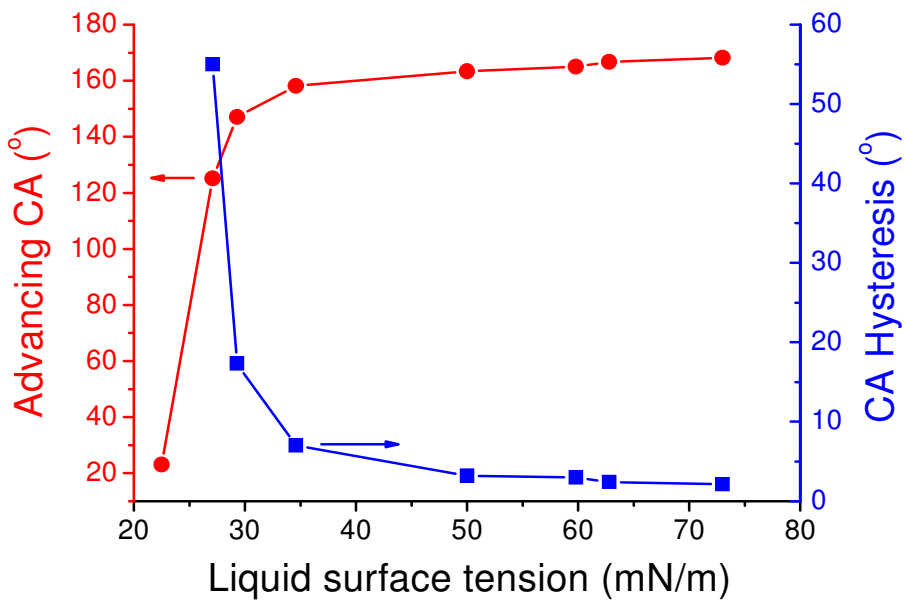


**Figure 5.3.** Contact angles and CAHs of water/ethanol mixture on a perfluoroalkyl-based superhydrophobic surface.

The film was then subjected to the interrogation with a series of hydrophobic liquids, namely hexadecane, sunflower oil and oleic acid. Figure 5.4 shows the droplets (5  $\mu\text{L}$ ) of those liquids on the surface-fluorinated superhydrophobic surface and contact angles of these liquids together with their surface tension values are listed in Table 5.1. All the contact angles are above  $125^\circ$ , indicating that the surface is lipophobic. However, the roll-off angles of all these hydrophobic liquids on the superhydrophobic surface appeared to be very high ( $> 60^\circ$ ). Therefore, we can only deem the surface lipophobic, not yet superlipophobic.

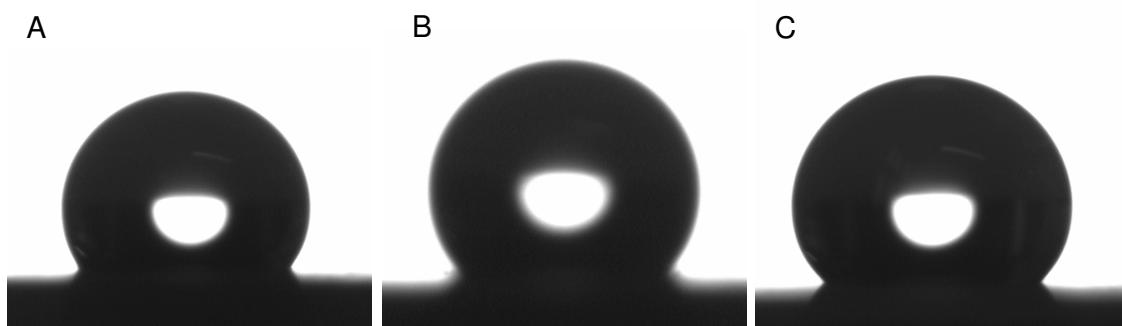


**Figure 5.4.** Images of 5  $\mu\text{L}$ -droplets of hexadecane (A), sunflower oil (B) and oleic acid (C) on the surface-fluorinated superhydrophobic surface, respectively.

**Table 5.1.** Static contact angles of various kinds of hydrophobic liquids (5  $\mu\text{L}$ ) on the surface-fluorinated superhydrophobic surface.

Probe liquid	Surface tension (mN/m, 20°C)	Contact angle ( $^\circ$ )
Hexadecane	27.5	125
Sunflower oil	33.0	132
Oleic acid	32.5	135



## 5.4 A Modeling approach toward superlipophobicity

In Chapter 3, we mentioned a free energy description of water droplets on a dual-size structure. From that description, the apparent CAs on the dual-size structured film containing raspberry-like particles can be calculated as a function of intrinsic CAs, as shown in Figure 5.5.

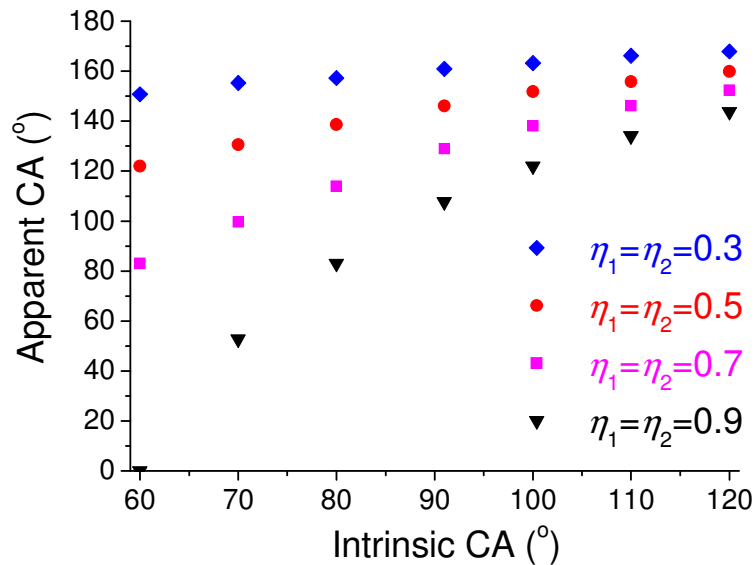


**Figure 5.5.** Apparent CA as a function of intrinsic CA on dual-size, raspberry-like surfaces; the packing factors for primary ( $\eta_1$ ) and secondary ( $\eta_2$ ) particles are indicated.

The first conclusion we can draw from Figure 5.5 is that for a probe liquid whose intrinsic CA (on a smooth surface) is larger than  $90^\circ$  (so-called “lyophobic”), it is easy to make a super liquid-repellent (superlyophobic) surface by employing a dual-size surface structure based on raspberry-like particles. Second, a looser packing for both primary and secondary particles facilitates the superlyophobicity (by comparing the effects on the apparent CA with different packing factors,  $\eta_1$  and  $\eta_2$ ), since a larger air/liquid interfacial area is generated (this corresponds well to the low density of the protrusions on the lotus leaf). Of course, the packing factor cannot be too low; otherwise the gravity of the liquid would lead to the collapse of the droplet. Third, for a probe liquid whose intrinsic CA (on the smooth surface) is lower than  $90^\circ$  (so-called “lyophilic”), it is still possible to obtain superlyophobicity for the films with a dual-size surface structure. For hydrophobic (or,

lipophilic) probe liquids like hexadecane, lipophobicity or even superlipophobicity may be obtained. A preliminary example is shown in Figure 5.3 and Figure 5.5.

## 5.5 Conclusions

In this chapter, we have demonstrated that it is possible to achieve lipophobicity on the fluorinated surface with a dual-size structure. The lipophobicity was obtained by treating the surface with 1*H*,1*H*,2*H*,2*H*-perfluorodecyltrichlorosilane through a self-assembling process. Probe liquids with the surface tension ranging from 22.5 mN/m to 73 mN/m were prepared by mixing water and ethanol, and the contact angles of these probe liquids on the superhydrophobic surface were examined. The contact angle results on such a surface are in a good agreement with a free-energy modeling study. The surface-fluorinated superhydrophobic surface appears to be also lipophobic. However, this oil-repellent surface is still far from ideal due to the high oil roll-off angle on it.

## References:

1. Tsujii, K.; Yamamoto, T.; Onda, T.; Shibuichi, S. *Angew. Chem. Int. Ed.* **1997**, *36*, 1011.
2. Shibuichi, S.; Yamamoto, T.; Onda, T.; Tsujii, K. *J. Colloid Interface Sci.* **1998**, *208*, 287.
3. Yabu, H.; Takebayashi, M.; Tanaka, M.; Shimomura, M. *Langmuir* **2005**, *21*, 3235.
4. Nicolas, M.; Guittard, F.; Geribaldi, S. *Angew. Chem. Int. Ed.* **2006**, *45*, 2251.
5. Tian, Y.; Liu, H.; Deng, Z. *Chem. Mater.* **2006**, *18*, 5820.
6. Abraham, U. *Chem. Rev.* **1996**, *96*, 1533.
7. Wasserman, S.R.; Tao, Y.-T.; Whitesides, G.M. *Langmuir* **1989**, *5*, 1074.
8. Le Grange, J.D; Markham, J.K; Kurjian, C.R. *Langmuir* **1993**, *9*, 1749.
9. Brandriss, S.; Margel, S. *Langmuir* **1993**, *9*, 1232.



## Chapter 6

### Superhydrophobic and superlipophobic textiles<sup>\*</sup>

**Abstract:** We report a biomimetic procedure to prepare superhydrophobic cotton textiles. By in-situ introducing silica particles to cotton fibers to generate a dual-size surface roughness, followed by hydrophobization with polydimethylsiloxane (PDMS), normally hydrophilic cotton has been easily turned superhydrophobic, which exhibits a water advancing contact angle of  $155^\circ$  for a  $10\text{-}\mu\text{L}$  droplet. The roll-off angle of water droplets depends on the droplet volume, ranging from  $7^\circ$  for a droplet of  $50\ \mu\text{L}$  to  $20^\circ$  for a  $7\text{-}\mu\text{L}$  droplet. We also prepared superlipophobic textile by modifying the particle-covered cotton textile with *1H,1H,2H,2H*-perfluorodecyltrichlorosilane. The lipophobicity was examined with sunflower oil and hexadecane. For sunflower oil, the highest measured static contact angle is  $141^\circ$  and the roll-off angle is  $24^\circ$  for a  $15\text{-}\mu\text{L}$  droplet.

---

<sup>\*</sup> Part of this Chapter has been submitted for publication: Hoefnagels, H.F.; Wu, D.; de With, G.; Ming, W. Biomimetic superhydrophobic and ultraoleophobic cotton textiles, submitted to *Langmuir*, 2007.

## 6.1 Introduction

Attracted by its water and soil repellent property, superhydrophobic textile has been one of the major targets for textile scientists and manufactures for decades. There are many approaches to develop superhydrophobic textile, such as the use of simple silicone coating procedures<sup>1</sup>, silica nanoparticles and perfluorooctylated quaternary ammonium silane coupling agents<sup>2</sup>, gold micro- and nanostructures<sup>3</sup> and surface confined grafting of glycidyl methacrylate<sup>4</sup>. For instance, Gao and McCarthy, according to a 1945 patent,<sup>5</sup> grafted a silicone coating to a microfiber polyester fabric to render the fabric superhydrophobic<sup>1</sup>, but the microfiber fabric (with a single fiber as small as 2-5  $\mu\text{m}$ ) needs to be tightly woven and this approach may not be suited to cotton textiles. Gold particles have been incorporated to cotton fabrics to induce a dual-size surface topology by Dong, *et al.*<sup>3</sup> but obviously there is no chemical bond between the gold particles and cotton fiber. Similarly, particles have been introduced to various substrates to obtain water repellency by sol-gel methods<sup>2,6</sup>.

Inspired by the lotus leaf structure, we have prepared epoxy-based, polydimethylsiloxane (PDMS)-surface-modified, superhydrophobic films with dual-size hierarchical structure originating from well-defined raspberry-like particles<sup>7</sup> in Chapter 3 and Chapter 4. In this Chapter, we apply this particle approach to cotton textiles, aiming at transforming highly hydrophilic cotton textiles into both superhydrophobic and superlipophobic textiles that are completely non-wettable by water and oil.

Cotton consists of almost pure cellulose so the chemical structure of cotton is the same as the chemical structure of cellulose as shown in Figure 6.1. The cellulose structure contains a high concentration of hydroxyl-groups which can be used for further reactions.

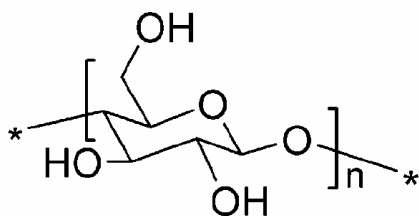
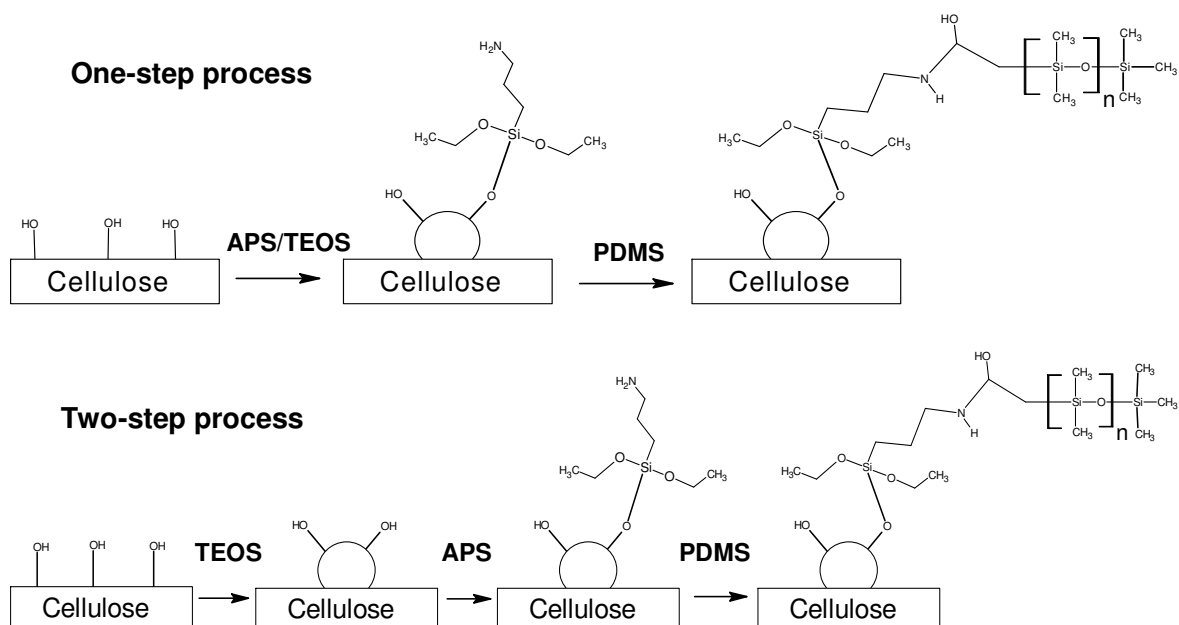


**Figure 6.1.** *The chemical structure of cellulose.*

In our approach, silica particle with amine groups at the surface was first covalently bonded to the cotton fibers by either a 1-step or 2-step reaction (Scheme 6.1). In the 1-step reaction, different TEOS/APS ratio was used to get surfaces with different surface topology. The amine groups were then used to hydrophobize the surface via the reaction with mono-epoxy-functionalized PDMS. The simplicity of the procedure may allow large-scale production of superhydrophobic cotton textiles.



**Scheme 6.1.** 1-step reaction (above) and 2-step reaction (below) to prepare superhydrophobic textile.

## 6.2 Experimental

### 6.2.1 Materials

A cotton textile was purchased from a local fabric store. Before chemical modification, a 16-cm<sup>2</sup> square piece of cotton textile was cleaned with water and ethanol before it was extracted with toluene to remove possible impurities. Hexadecane and 3-aminopropyl-triethoxysiloxane (APS) were purchased from Merck. Tetraethylorthosilicate (TEOS) was purchased from Fluka. Monoglycidyl ether terminated PDMS (MGE-PDMS, average MW = 5000), and 1H,1H,2H,2H-

perfluorodecyltrichlorosilane and sunflower oil was obtained from Aldrich. Other chemicals were purchased from Merck and used without further purification.

### **6.2.2 *In-situ* 1-step formation of amine-functional silica particles on cotton fibers**

The cleaned cotton textile was added to a solution of 25 mL of methanol, 75 mL of 2-propanol, 21 mL of ammonia solution and a mixture of APS and TEOS in different molar ratios with a combined volume of 10 mL. The three APS/TEOS ratios used were 1/19, 1/9 and 1/4. The synthesis followed the traditional Stöber method<sup>8</sup>. The reaction mixture containing the cotton textile was mechanically stirred at 300 rpm for 6 h at room temperature. After the modification, the cotton textile was extensively cleaned with toluene to remove possibly physically absorbed reactants. To check if there are free amine groups on the surface, the ninhydrin test<sup>9</sup> is performed. The occurrence of a blue/purple color indicates the presence of amine groups in the cotton sample.

### **6.2.3 Two-step formation of amine-functional silica particles**

The above-described reaction was also performed in two steps: (1) silica particles were first formed on the cotton fibers in the absence of APS, thus the particle surface contained hydroxyl functionality; (2) the particle-containing cotton textile was added to an APS solution in toluene (5 mL APS in 100 mL toluene), and the mixture was mechanically stirred for 6 h at 60 °C. A similar cleaning procedure as above was performed afterwards.

### **6.2.4 Surface modification by PDMS**

The particle-containing cotton textile was further modified with the mono-functional MGE-PDMS by dipping the particle-containing textile in a MGE-PDMS solution in toluene (concentration: 5 vol%), and cured for 1 h at 80 °C. MGE-PDMS can also be incorporated into the textile without prior dissolution in toluene. After the reaction, the excess PDMS was rinsed away with toluene.

### **6.2.5 Surface modification by 1H,1H,2H,2H-perfluorodecyltrichlorosilane**

First, toluene was dried via a distillation in the presence of active molecular sieves. In a glove box, a solution of 0.1 mL of 1H,1H,2H,2H-perfluorodecyltrichlorosilane in 25 mL of dry toluene was prepared. The particle-containing cotton textile was dried and added to the solution and left for 1 h. Subsequently, the samples were rinsed with dry toluene to remove the excess perfluorodecyltrichlorosilane and dried again.

### **6.2.6 Characterization**

#### **Thermogravimetric analysis (TGA)**

TGA analyses were performed on a TA instruments Q500 TGA. The analysis was performed using the Hi-Res<sup>TM</sup> procedure available in the TGA software of TA instruments. High resolution TGA involves a dynamic variation of the heating rate as a function of weight change in the sample, thus improving the resolution of the individual of weight loss events. The samples were heated from 30 to 500 °C with a heating rate of 20 °C/min under nitrogen or oxygen flow.

#### **X-ray photoelectron spectroscopy (XPS)**

X-ray photoelectron spectroscopy (XPS) measurements were performed with a VG- Escalab 200 spectrometer using an aluminum anode (Al K $\alpha$  = 1486.3 eV) operating at 510 W with a background pressure of  $2 \times 10^{-9}$  mbar. Spectra were recorded using the VGX900 data system. All carbon 1s (C1s) peaks corresponding to hydrocarbon were calibrated at a binding energy of 285 eV to correct for the energy shift caused by charging. Spectra were acquired at a take-off angle of 90° relative to the sample surface, corresponding to the probe depths of ~10 nm<sup>10</sup>.

The descriptions of scanning electron microscopy (SEM), and contact angle measurement are given in previous chapters.

## **6.3 Results and discussion**

### **6.3.1 Chemical modification of cotton textiles**

The cotton textile was modified to incorporate chemically bonded silica particles as well as surface amine groups to the cotton fibers for further hydrophobization. It is,



therefore, crucial to identify the presence of amine groups in the modified cotton textiles, which can be conveniently examined by the ninhydrin test. For both the 1-step or 2-step reactions in our procedure, when a ninhydrin solution was added to the modified cotton, the cotton color turned immediately blue or purple, indicating the presence of primary amine groups in the modified cotton.

We used XPS to characterize the cotton samples modified with only APS. Although XPS cannot give a full account of the chemical composition for cotton samples due to their rough surface, it does provide qualitative information on the chemical changes before and after the modification<sup>11</sup>. For the unmodified cotton, only peaks corresponding to C and O were observed (Figure 6.2a). After being modified by APS, three more peaks appeared (Figure 6.2b) at 400.5, 153.2, and 102.4 eV, which are attributed to N1s, Si2s, and Si2p signals, respectively, indicating the successful grafting of APS to the cotton fiber. The free amine group will be available for further modification. A preliminary quantitative analysis reveals that the Si content is about 10 mol%, which is significantly greater than the value assuming that a monolayer is formed during the APS modification. This is likely due to the formation of a 3D network layer from self-condensed APS in the presence of moisture<sup>12</sup>, resulting in a much higher Si content. After the further surface modification with MGE-PDMS, only signals due to Si, C, and O were observed (Figure 6.2c), and in the meantime, the N1s peak in Figure 1b almost disappeared completely, suggesting that a layer of PDMS has covered the surface of the cotton fibers.

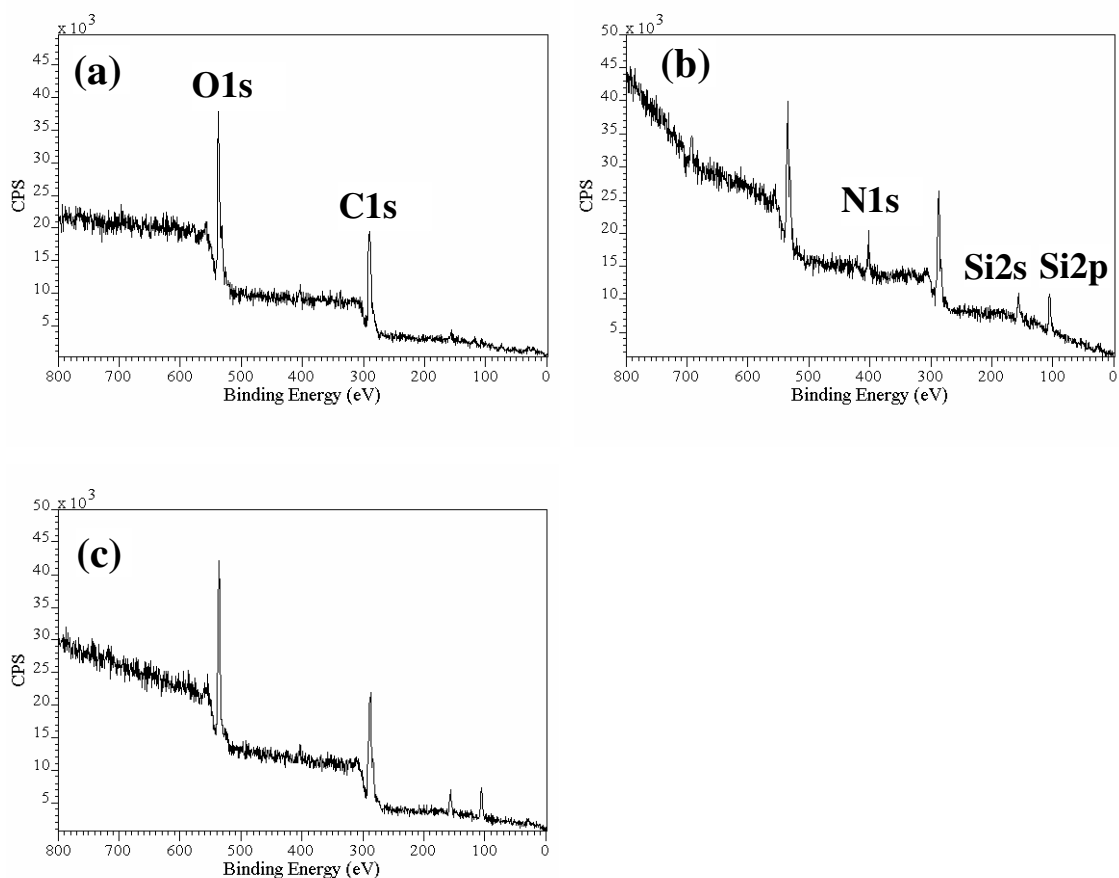


**Figure 6.2.** XPS spectra for (a) a cotton textile before modification, and the cotton sample after the APS modification (b) and after the further modification with MGE-PDMS (c).

TGA was used to determine the remaining weights for the cotton sample after each step of the 2-step modification procedure (Figure 6.3). For the pure cotton prior to the modification, the remaining weight percentage was 1.5% after being heated to 700 °C in an oxygen atmosphere (the cotton fabric may not be pure cellulose). After silica particles were chemically grafted to the cotton fiber, this percentage increased to 4.0%. When APS was incorporated to the surface of the particles and, possibly, the remaining hydroxyl groups from the cotton fiber, the remaining weight percentage increased to 8.9% (the burning of the APS moiety would lead to  $\text{SiO}_2$ ). This large increase, in comparison to the sample with only particles, implies that the APS modification leads to more than a monolayer grafting of APS on the silica surface; instead, a 3D-network layer comprising

self-condensed APS is formed (similar to the XPS results for the APS-modified sample without particles, as discussed above). A further increase of the remaining weight percentage to 10.4% was observed for the sample modified with PDMS, indicating the successful grafting of PDMS onto the particle surface.

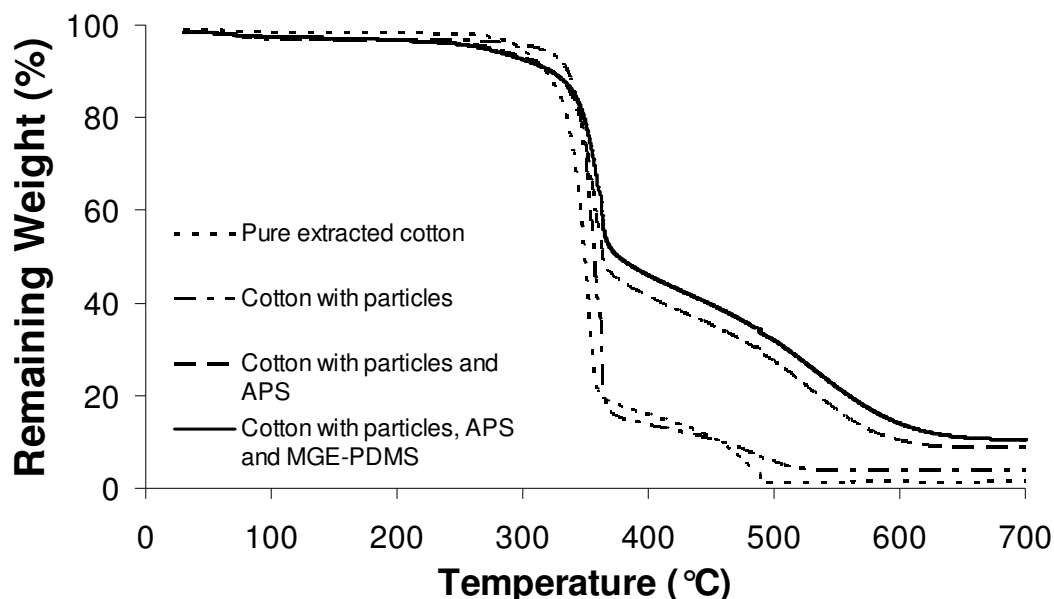


**Figure 6.3.** Weight loss for the cotton textile modified by the 2-step procedure before and after each step of the modification by TGA.

### 6.3.2 Surface wettability and topology of PDMS-modified textiles

The surface wettability was examined by contact angle (CA) measurements. The pure cotton sample can be completely wetted by water, which is common and well known for cotton textiles. The sample modified by APS and, subsequently, PDMS (i.e., without particles) was turned highly hydrophobic, with a static CA of 142° and a roll-off angle of 36° (both for a 10- $\mu$ L droplet). The hydrophobicity was further enhanced by incorporating silica particles to the modified textile samples (Table 6.1), as especially judged from the roll-off angle standpoint. The water static CAs range from 142° to 155° for a 10- $\mu$ L droplet; even though these values are not super high, the modified cotton samples are completely water non-wettable. It should be noted that, due to the stick-out of fibers from the cotton sample (as depicted in Figure 6.5), the measurement of contact

angles is often not straightforward, in terms of the difficulty of determining the baseline of the water droplet, which may in turn lead to possible underestimation of the contact angle data. Also because the protruding fibers have some elasticity and can thus exhibit forces on the water droplet<sup>7</sup>, it is also difficult to yield accurate values for advancing and receding water contact angles, so only static CAs for 10- $\mu$ L water droplets are reported here.

**Table 6.1. Water contact angles on PDMS modified cotton textiles.**

<b>Sample ID</b>	<b>Sample preparation<sup>†</sup></b>	<b>Static CA [°] (10-<math>\mu</math>L droplet)</b>	<b>Roll-off angle [°] (10-<math>\mu</math>L droplet)</b>
6A	APS (No particles)	141.9 $\pm$ 3.4	36.0 $\pm$ 4.4
6B	1-step: APS/TEOS = 1/19	141.9 $\pm$ 1.7	29.9 $\pm$ 4.9
6C	1-step: APS/TEOS = 1/9	144.0 $\pm$ 0.9	22.2 $\pm$ 1.6
6D	1-step: APS/TEOS = 1/4	148.9 $\pm$ 2.4	15.9 $\pm$ 0.9
6E	Particles from 2-step reaction	154.7 $\pm$ 0.6	14.7 $\pm$ 0.7

<sup>†</sup>All samples were hydrophobized by MGE-PDMS.

On the other hand, roll-off angles can be measured in a relatively accurate way. For a 10- $\mu$ L water droplet, the roll-off angle decreases from 30° to 15° for Samples 6B to 6E (all with silica particles; Table 6.1). For Samples 6D and 6E, the roll-off angle for a 50- $\mu$ L was about 7°; in contrast, on a recently reported superhydrophobic woven structure<sup>13</sup>, the roll-off angle for a 500- $\mu$ L droplet was 5°. When we used 500- $\mu$ L water droplets, the roll-off angle on Samples 6D and 6E was less than 2°. We also made a video clip, showing roll-off of a water droplet on a tilted superhydrophobic cotton textile, bringing away pencil graphite powder pre-deposited on the surface and leaving a clean path. For the one-step modification procedure, it is obvious from Table 6.1 that the higher the amount of APS in the reaction mixture, the higher the water CA and the lower the roll-off angle. Sample 6E from the 2-step procedure appears to have the best superhydrophobicity. We also checked the dependence of water roll-off angles on the droplet volume. As shown in Figure 6.4, for all the hydrophobic cotton textiles, the roll-off angle decreases as

the water droplet size increases. This is as expected since, as the water droplet exceeds a certain size, its gravity would overcome the adhesion force between the cotton fibers and the water droplet. It is interesting to notice that, for Sample 6E, we were unable to deposit a 7- $\mu\text{L}$  water droplet on the textile surface, and the water droplet always stuck to the needle, indicating that the adhesion force between the droplet and the textile surface is even lower than that between the droplet and the needle.

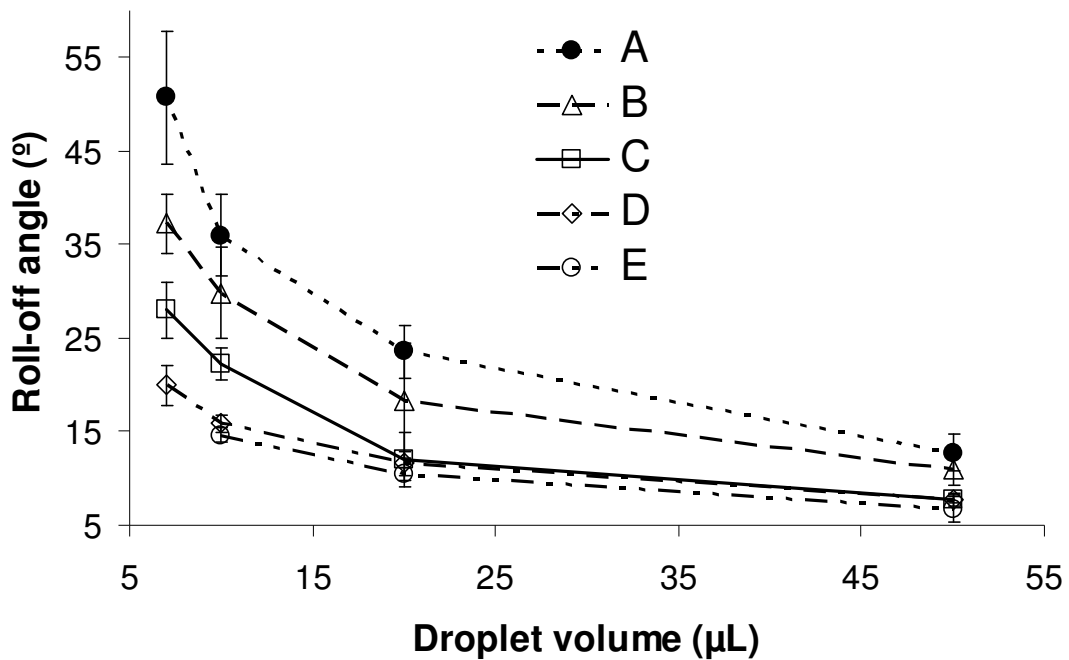


**Figure 6.4.** Roll-off angles of water droplets on modified cotton textiles as a function of the droplet volume. Symbols A-E correspond to the films 6A-6E listed in Table 6.1.

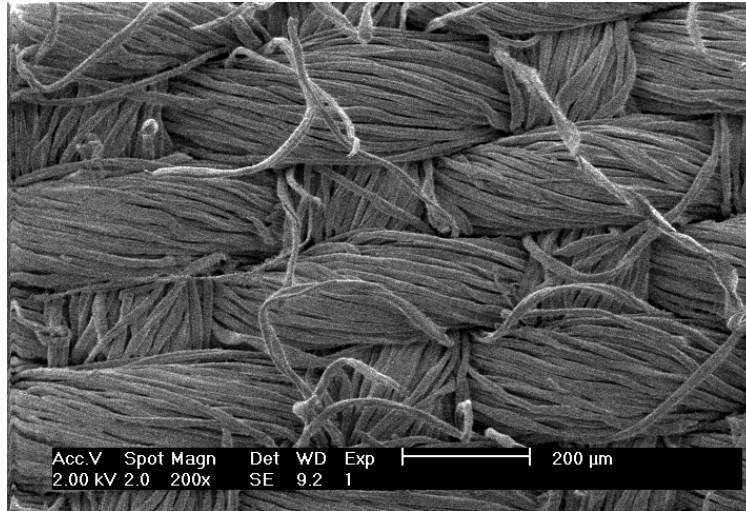


**Figure 6.5.** A SEM image of the pure cotton textile used in this study.

We used SEM to determine the topology of the cotton samples. The pure cotton sample has a tightly woven, fibrous structure, as shown in Figure 6.5. When the cotton was only modified by APS and followed by the PDMS grafting, no significant change was observed by SEM (Figure 6.6A). On the other hand, when particles were incorporated into the cotton fibers, particles of sizes ranging from 500 nm to 2  $\mu\text{m}$  are clearly visible (Figure 6.6B-E). By the chemical incorporation of silica particles to the cotton fibers, a dual-size surface structure has been conveniently generated. For the 1-step modification procedure, the size of the particles does not change much (Figure 6.6B-D), but the particle population and distribution differ significantly. It appears that, as the APS/TEOS ratio increases, the silica particles become more numerous, and even non-spherical particles are formed, possibly due to the aggregation of smaller particles. For Samples 6B and 6C, although the TEOS content was higher than Sample 6D, the area density of particles is lower, possibly due to the formation of free particles (instead of being chemically connected to the cotton fiber). For the 2-step procedure, the particle area density is the highest (Figure 6.6E) among the samples we have investigated, and the cotton fiber is almost completely covered by particles. The difference in the roll-off angles in Table 6.1 can be attributed to the different dual-size surface structure of the modified cotton samples. The area density of particle needs to be high enough to reduce the contact area between a water droplet and the cotton surface, which is we believe why

the cotton sample made by the 2-step procedure demonstrates the lowest roll-off angles in the current investigation.

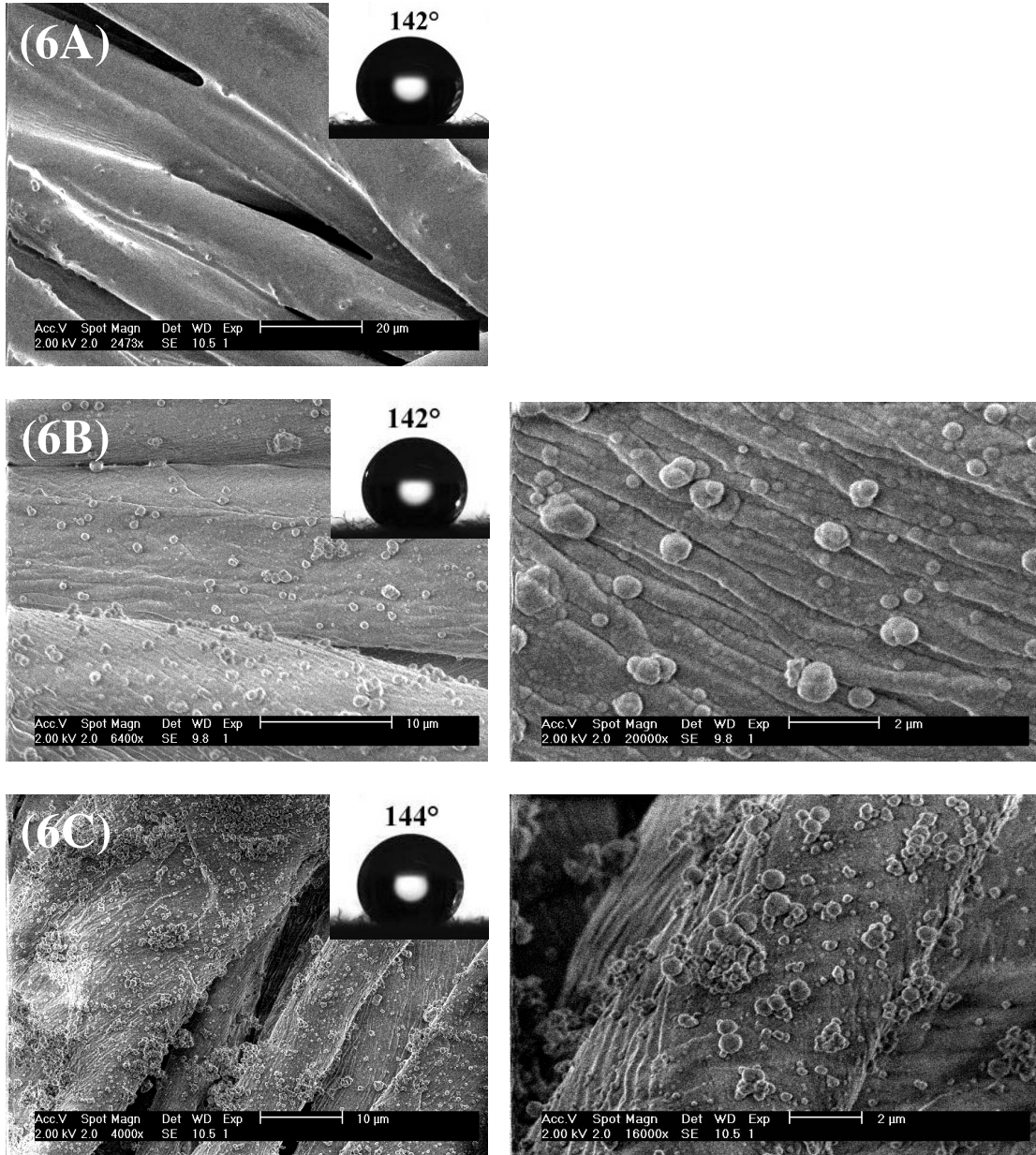


(Figure 6.6. to continue on the next page)

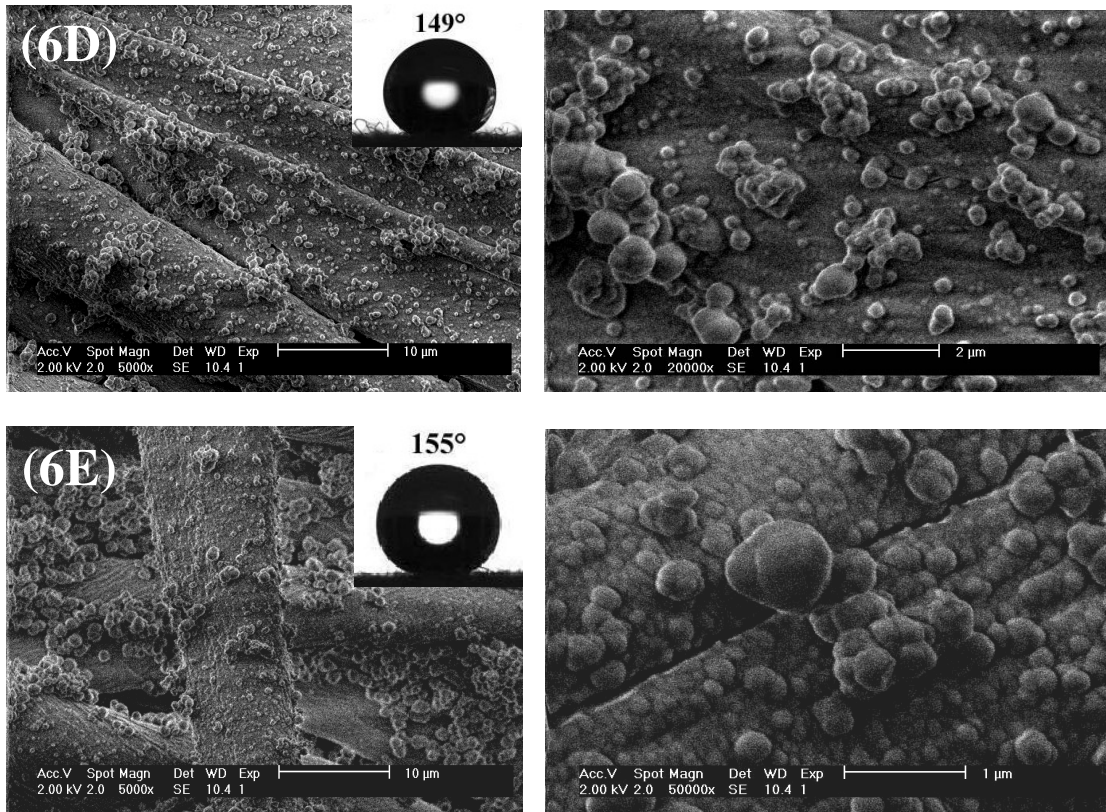


**Figure 6.6.** SEM images for modified cotton textiles (without PDMS). The images on the right are higher-magnification ones for those on the left. Shown in insets are the images of static water droplets (10  $\mu$ L) on the respective PDMS-modified textiles.

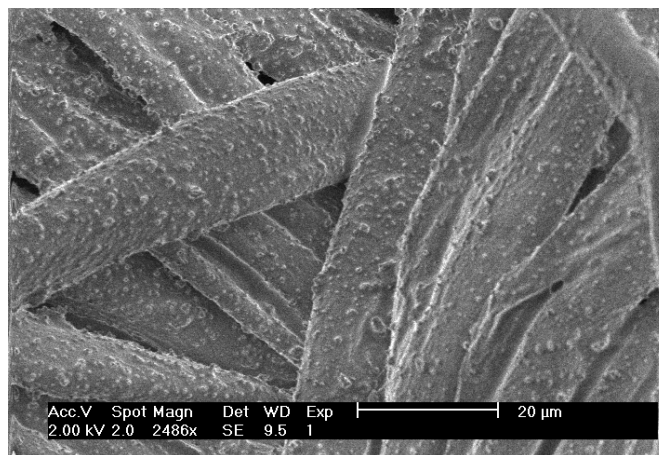


**Figure 6.7.** SEM images for a modified cotton textile with PDMS (Sample 6C in Table 6.1).



The surface of the textile after the further modification by MGE-PDMS was also examined by SEM, as shown in Figure 6.7. It appears that both the silica particles and the cotton fibers are covered by a thin layer of PDMS, but the surface feature due to the incorporation of silica particles is preserved despite the PDMS surface grafting.

We recently extended this modification strategy to synthetic textiles, such as polyester fabrics. To render the polyester fabric surface reactive, a UV/ozone treatment was performed for 30 min to generate surface hydroxyl groups for the polyester before the incorporation of silica particles and PDMS. The polyester fabric was also turned superhydrophobic: the static and roll-off angles for a 10- $\mu$ L water droplet were  $140 \pm 3^\circ$  and  $12 \pm 1^\circ$ , respectively.

### 6.3.3 Lipophobicity of fluorinated, particle-coated textiles

The lipophobicity of the perfluoroalkyl modified textile was examined with sunflower oil and hexadecane. The static contact angle of a 15- $\mu$ L sunflower oil droplet is  $140 \pm 1.6^\circ$ , and the static contact angle for a 10- $\mu$ L hexadecane droplet is about  $135^\circ$ . The roll-off angle of a droplet of 15- $\mu$ L sunflower oil is about  $24^\circ$ . Figure 6.8 shows the images of droplets of sunflower oil and hexadecane on the perfluoroalkyl modified textile. The contact angle and roll-off angle results indicate that we have successfully turned a normal cotton textile into a superlipophobic textile by using surface fluorination. More details have been described in the Master thesis of Hoefnagels<sup>14</sup>.

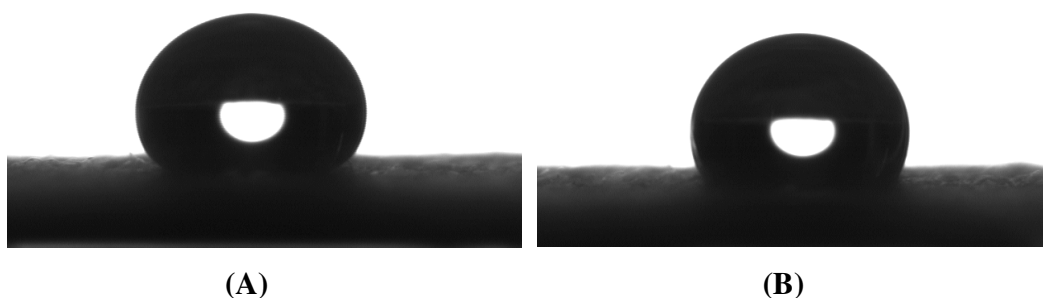


**Figure 6.8.** Droplets of sunflower oil (A) and hexadecane (B) on a perfluoroalkyl-modified textile.

## 6.4 Conclusions

In summary, by in-situ growing silica microparticles to hydrophilic cotton textiles and using a hydrophobization step, we have generated a dual-size surface structure for the textiles and successfully turned them superhydrophobic. For a 10- $\mu$ L water droplet, the static contact angle and roll-off angle are 155° and 15°, respectively. The area density of the silica particles needs to be high enough to achieve a low water roll-off angle. A superlipophobic textile was obtained by modifying the microparticles-covered cotton textiles with perfluoroalkylsilane.

## References:

1. Gao, L.; McCarthy, T. *Langmuir*, **2006**, *22*, 5998.
2. Yu, M.; Gu, G.; Meng, W.; Qing, F. *Appl. Sur. Sci.* **2007**, *253*, 3669.
3. Wang, T.; Hu, X.; Dong, S. *Chem. Commun.*, **2007**, 1849.
4. Nyström, D.; Lindqvist, J.; Östmark, E.; Hult, A.; Malmström, E. *Chem. Comm.*, **2006**, 3594.
5. Norton, F. J. U.S. Patent 2386259, **1945**.
6. Daoud, W. A.; Xin, J. H.; Tao, X. *J. Am. Ceram. Soc.* **2004**, *87*, 1782.
7. Ming, W.; Wu, D.; van Benthem, R.; de With, G. *Nano Lett.* **2005**, *5*, 2298.
8. Stöber, W.; Fink, A.; Bonn, E. *J. Colloid Interface Sci.* **1968**, *26*, 62.
9. (a) Moore, S.; Stein, W. H. *J. Biol. Chem.* **1954**, *211*, 907. (b) Eiselt, P.; Lee, K. Y.; Mooney, D. J. *Macromolecules* **1999**, *32*, 5561.
10. Tanuma, S.; Powell, C. J.; Penn, D. R. *Surf. Interface Anal.* **1994**, *21*, 165.
11. Kontturi, E.; Thüne, P. C.; Niemantsverdriet, J. W. *Langmuir* **2003**, *19*, 5735.
12. Vandenberg, E. T.; Bertilsson, L.; Liedberg B.; Uvdal, K.; Erlandsson, R.; Elwing, H.; Lundström, I. *J. Colloid Interface Sci.* **1991**, *147*, 103.
13. Michielsen, S.; Lee, H. J. *Langmuir* **2007**, *23*, 6004.
14. Hoefnagels, H.F. Biomimetic superhydrophobic and superlipophobic textiles, Master thesis, Eindhoven University of Technology, July **2007**.



## Chapter 7

### Conclusions and recommendations

#### 7.1 Conclusions

The aim of this work was to develop robust superhydrophobic (both superhydrophobic and superlipophobic) coatings. To realize this aim, the water repellent and oil repellent behaviors on solid surfaces have been studied and several methods to develop superhydrophobic surfaces have been investigated.

First, a rough polyurethane film enriched with fluorinated species at surface was prepared through self-stratification process. The advancing water contact angle on this surface was above  $150^\circ$  with a CA hysteresis of about  $68^\circ$ . The PU film was a cross-linked film with a  $T_g$  of about  $15^\circ\text{C}$ , so the network and the perfluoroalkyl side chains have some degree of mobility. On the unwetted surface, the perfluoroalkyl side chains were oriented preferentially towards the coating-air interface, resulting in a low surface energy and high advancing water contact angle. However, for the surface already wetted by water, water may penetrate into deeper layers and “drag out” some polar groups (e.g., urethane), leading to a relatively low water receding contact angle. Thus, we come to the conclusion that a superhydrophobic surface may not be easily developed from a surface which can reorganize upon contact with water.

Next, by employing raspberry-like particles, we developed superhydrophobic films based on conventional silica particles and epoxy films in an effort to mimic the two-level surface structure of lotus leaves. On our superhydrophobic films, the advancing water contact angle is about  $165^\circ$ , and the roll-off angle of a  $10\text{-}\mu\text{L}$  water droplet is about  $2^\circ$ .

By investigating the relation between the topology of the superhydrophobic surface and the corresponding water contact angles and roll-off angles, we indicate that it is the dual-size surface topology originating from the raspberry-like particles that allows air pockets to exist between the water droplet and the solid surface and turns the film superhydrophobic. By comparing our preliminary modeling study results and our experimental data, we get the conclusion that the size ratio between large and small particles of raspberry particles does not have a significant effect on the wettability of film when it is larger than 10.

In order to improve the mechanical robustness of the superhydrophobic coating with dual-size surface structure, we developed a layer-by-layer approach in Chapter 4. SEM results proved that the microparticles were partially imbedded into polymer matrix in our superhydrophobic coating which increased the mechanical robustness of the film. After treating the film with  $\text{SiCl}_4$  as a cross-linker, the robustness of the film was further increased due to increasing adhesion strength between nano- and microparticles as demonstrated by pull-off and tissue rubbing tests.

The lipophobicity on superhydrophobic surface was discussed in Chapter 5. By measuring the contact angles and contact angle hysteresis of liquid with different surface tension on superhydrophobic surface with dual-size surface structure, we demonstrated that it was possible to achieve lipophobicity on the fluorinated surface with dual-size structure. The contact angle results on such surface were in a good agreement with the results of a free-energy modeling study.

In Chapter 6, we also demonstrated that common cotton textiles can be successfully transferred into superhydrophobic textiles by introducing silica particles on the surface of cotton fiber. By in-situ introducing silica particles to cotton fibers to generate a dual-size surface roughness, followed by hydrophobization with polydimethylsiloxane (PDMS), normally hydrophilic cotton has been easily turned superhydrophobic, which exhibits a water advancing contact angle of  $155^\circ$  for a 10- $\mu\text{L}$  droplet. Moreover, A superlipophobic textile was prepared by modifying the microparticle-covered cotton textiles with perfluoroalkylsilane.

## 7.2 Recommendations

In this research, superhydrophobic surfaces have been developed by mimicking the lotus leaf and the mechanical robustness of the film has been improved. Of course there are still many challenges ahead for optimization of these superhydrophobic coatings.

A very important issue of a superhydrophobic coating is its transparency. Due to the large particle size, our superhydrophobic coating with dual-size structure is not optically transparent yet. If much smaller raspberry-like particles (less than 200 nm in diameter) can be synthesized and homogeneously deposited on the surface of a transparent polymer coating, a transparent superhydrophobic surface may be created.

We have developed a lipophobic coating by grafting fluorinated molecules on a surface with a dual-size structure. From our modeling study, we know it is possible to obtain superlipophobicity on the film with dual-size surface structure. So if a perfect self-assembled monolayer of perfluoroalkyl chains can be applied on the surface with dual-size structure by carefully controlling the reaction condition, a superlipophobic surface may be achieved.



## Summary

For many years, people have been attracted by the self-cleaning property of the lotus leaf, and dream to develop man-made superhydrophobic surfaces. Many methods have been developed to produce a surface with a water contact angle higher than  $150^\circ$  and a low roll-off angle. In general, a superhydrophobic surface is prepared by combining high surface roughness and low surface energy. The challenge here is to develop a robust superhydrophobic surface with a simple process, so that it can be manufactured in an industrial scale and can be applied in our daily life. The aim of this PhD research is to develop a simple method to prepare a robust superhydrophobic surface. On the other hand, besides superhydrophobicity, oil repellency is also an attractive property which is essential to maintain self-cleaning property of a surface and has many potential applications. So another goal of this study is to investigate lipophobicity for superhydrophobic surfaces.

In Chapter 2, we developed a polymeric film with very low surface energy through a self-stratification process. In this Chapter, we stressed that a low contact angle hysteresis is the most important factor for a superhydrophobic surface, and the low contact angle hysteresis only exists when the water droplet is in the Cassie state. The surface reorganization may be one of the reasons for the high water contact angle hysteresis on the polyurethane films with surface rich in perfluoroalkyl side chains.

By mimicking the lotus leaf structure, we developed a raspberry-approach to synthesize superhydrophobic coatings with a dual-size surface structure in Chapter 3. The film was prepared by depositing well-defined silica-based raspberry-like particles on an epoxy-based polymer matrix, followed by the surface modification with PDMS. On this superhydrophobic film, advancing water contact angle is about  $165^\circ$ , and the roll-off angle of a  $10\text{-}\mu\text{L}$  water droplet is about  $2^\circ$ . In addition, the size ratio between large and



small particles of raspberry particles does not have a significant effect on the film wettability when it is larger than 10. The effect of the dual-size roughness on the surface wettability has also been studied by a free-energy modeling.

In Chapter 4, a layer-by-layer (LbL) approach was developed to prepare a superhydrophobic surface, with the aim of improving the mechanical robustness of the film. Epoxy-based films were partially cured to a proper extent, followed by deposition of silica microparticles. After that, the films were completely cured. Subsequently, silica nanoparticles were grafted on the microparticle surface through amine-epoxy reactions. Finally, the surfaces were modified with a layer of PDMS to obtain their superhydrophobicity. To further increase the mechanical robustness of the films, the films were treated with  $\text{SiCl}_4$ , which cross-linked the nano- and microparticles, and among nanoparticles. The films were then modified with a perfluoroalkylsilane to obtain superhydrophobicity. The partial embedment of the large silica particles in the polymer matrix and the cross-linking between large and small particles by  $\text{SiCl}_4$  have proven to be sufficient to obtain mechanically robust superhydrophobic surfaces.

Lipophobicity on superhydrophobic surfaces was studied in Chapter 5. In this Chapter, we examine the lipophobicity on the superhydrophobic films with dual-size surface roughness. A surface with a dual-size roughness structure was modified with *1H,1H,2H,2H*-perfluorodecyltrichlorosilane. Probe liquids with surface tensions ranging from 22.5 to 73 mN/m were prepared by mixing water and ethanol, and the contact angles of these probe liquids on the superhydrophobic surface were examined. The contact angle results on such a surface are in a good agreement with the free-energy modeling study. On this surface, the contact angles of hexadecane, sunflower and oleic acid were  $125^\circ$ ,  $132^\circ$  and  $135^\circ$ , respectively, indicating that the superhydrophobic surface is also lipophobic. However, this oil-repellent surface is still far from ideal due to the high oil roll-off angle.

As an example of practical applications, a process of developing superhydrophobic textiles is described in Chapter 6. By in-situ growing silica microparticles to hydrophilic cotton textiles and using a hydrophobization (PDMS) step, the cotton textiles have been turned completely water non-wettable. Moreover, a superlipophobic textile was prepared

by modifying the microparticle-covered cotton textiles with a perfluoroalkylsilane; the textile was then effectively turned superlipophobic.



## Summary

Al vele jaren zijn mensen geïnteresseerd in de zelfreinigende eigenschappen van de bladeren van de lotus plant en dromen van een kunstmatig gecreëerd superhydrofoob oppervlak. Vele methoden zijn ontwikkeld om oppervlakken te creëren met water contacthoeken die groter zijn dan  $150^\circ$  en een lage afrolhoek. Over het algemeen wordt een superhydrofoob oppervlak bereid door een hoge oppervlakte ruwheid en een lage oppervlakte-energie te combineren. De uitdaging is om een robuust superhydrofoob oppervlak te ontwikkelen in een simpel proces, zodat het op een industriële schaal geproduceerd kan worden en toegepast kan worden in alledaagse toepassingen. Het doel van dit promotieonderzoek is om een eenvoudige, goedkope manier te ontwikkelen om robuust superhydrofoob oppervlak te produceren. Daarnaast is, naast superhydrofobiciteit, olie-afstotendheid ook een aantrekkelijke eigenschap die essentieel is voor zelfreinigende eigenschappen van een oppervlak en heeft ook vele mogelijke toepassingen. Dus een ander doel in dit onderzoek is het onderzoeken van de mogelijkheid om oppervlakken naast superhydrofoob ook lipofob te maken.

In Hoofdstuk 2 hebben we een polymere film ontwikkeld die een zeer lage oppervlakte-energie heeft door middel van zelfstratificatie. In dit Hoofdstuk hebben we benadrukt dat contacthoek hysteresis de belangrijkste factor is voor een superhydrofoob oppervlak en de contacthoek hysteresis is alleen laag als de waterdruppel zich in de Cassie-toestand bevindt. Het oppervlakte-reorganisatie is de belangrijkste reden voor de hoge contacthoek hysteresis op de polyurethaan films met een oppervlak dat rijk is aan perfluoroalkyl zijketens.

Door het nabootsen van de structuur van het blad van de lotusbloem hebben we een framboos-aanpak ontwikkeld om superhydrofobe coatings met een tweevoudige oppervlaktestructuur in Hoofdstuk 3. De film was bereid door goed gedefinieerde, op

silica gebaseerde, framboosachtige deeltjes op een op epoxy gebaseerde polymere matrix te plaatsen, gevolgd door de oppervlaktemodificatie met PDMS. Op deze superhydrofobe film is de advancing contacthoek ongeveer  $165^\circ$  en de afrolhoek voor een  $10\text{-}\mu\text{L}$  waterdruppel is ongeveer  $2^\circ$ . Daarnaast heeft de grootte-ratio tussen de grote en kleine deeltjes geen effect op de benatting als deze ratio groter is dan 10. Het effect van de tweevoudige oppervlaktestructuur op de benatting van het oppervlak is bestudeerd met vrije-energie modellering.

In Hoofdstuk 4 is een laag-bij-laag aanpak ontwikkeld om een superhydrofoob oppervlak te creëren, met als doel de mechanische sterkte van de film te verbeteren. Films, gebaseerd op epoxy, waren gedeeltelijk gecured tot een bepaalde graad, gevolgd door de plaatsing van silica microdeeltjes. Daarna werden de films compleet gecured. Na deze stap zijn de nanodeeltjes aan de microdeeltjes verbonden door middel van amine-epoxy reacties. In de laatste stap is het oppervlak gemodificeerd met een laag PDMS om het oppervlak superhydrofoob te maken. Om de mechanische sterkte nog verder te verbeteren, werd de film behandeld met  $\text{SiCl}_4$ , die de nano- en microdeeltjes met elkaar verbond. Hierna werd de film met perfluoroalkylsilaan om het oppervlak superhydrofoob te maken. De gedeeltelijke verankering van de grote silica deeltjes in de polymere matrix en het verbinden van de kleine en grote deeltjes door middel van  $\text{SiCl}_4$  is bewezen om voldoende te zijn om een mechanisch robuust oppervlak te genereren.

De lipofobiciteit op superhydrofobe oppervlakken is bestudeerd in Hoofdstuk 5. In dit Hoofdstuk is de lipofobiciteit op superhydrofobe films met een tweevoudige oppervlaktestructuur onderzocht. Een oppervlak met een tweevoudige oppervlaktestructuur was gemodificeerd met *1H,1H,2H,2H*-perfluorodecyltrichlorosilane. Onderzoeksvloestoffen met oppervlaktespanning variërend van  $22.5$  tot  $73$  mN/m zijn geproduceerd door water en ethanol te mengen en de contacthoeken van deze vloeistoffen op de superhydrofobe oppervlakken zijn onderzocht. De contacthoeken op dit oppervlak zijn in goede overeenstemming met de vrije-energie modellering studie. Op dit oppervlak zijn de contacthoeken van hexadecaan, zonnebloemolie en oliezuur waren respectievelijk  $125^\circ$ ,  $132^\circ$  en  $135^\circ$ . Dit geeft aan dat het superhydrofobe oppervlak ook lipofob is. Echter, dit olieafstotende oppervlak is verre van ideaal, want de afrolhoeken van de oliën zijn hoog.

Als een voorbeeld voor een praktische toepassing, een proces op superhydrofoob textiel te ontwikkelen is bescheven in Hoofdstuk 6. Door het in-situ groeien van silica microdeeltjes op hydrofiel katoen en het gebruiken van stap om het oppervlak hydrofoob te maken (PDMS), is katoen textiel compleet onbevochtigbaar. Bovendien is er ook een superlipofob textiel bereid door het katoen textiel, dat bedekt is met microdeeltjes, te modificeren met perfluoroalkylsilaan. Het katoen textiel was na deze stap effectief zowel superhydrofoob als superlipofob.



## Acknowledgements

Four years ago, I knocked out the door of prof. Bert de With's office with an invitation letter of interview. At that moment, I didn't know that I also knocked out a door of a new life that I'll never forget. During this four years study, I have been accompanied and supported by many people. It is a pleasant aspect that I have now the opportunity to express my gratitude for all of them.

I give my special thanks to Marshall Ming for his daily supervision. Marshall, thank you for all those meeting and discussion, thank you for all those valuable suggestions and innovative ideas and thank you for reading and correcting my thesis. Dear Marshall, thank you for your continuous support and invaluable guidance.

I would like to thank prof. Bert de With for giving me a chance to start my PhD research in his laboratory. Bert, thank you for your understanding and encouragement throughout the course of my research.

I also would like to give my thanks to prof. dr. R. A. T. M. van Benthem. This thesis could have never been completed without his help.

For all these wonderful pictures in this thesis, my sincere thanks go to Wei Han, for his instructions on how to use ESEM. Thanks to Mingwen Tian for those AFM measurements he performed and Xiaoni Yang for TEM observations. I have to thank Rik, who did most practical work to developing superhydrophobic textiles and wrote my Dutch summary of my thesis. I would like to thank R. Vrancken and Bart van Loenen for their contribution on the modeling study in my thesis. I would like thank Srdjan and Olavio for helping me on the pull-off test.

I also express my gratitude to all the SMG group members. Tamara, thank you for all the discussion we had. Thanks to Francesca for her help in performing the ATR-FTIR. Thanks to my officemate Amir and Kangbo. Your presence makes our office a warm place to stay. I am grateful to Imanda for all the help and office supplies I got from her. I would like to thank Anneke, Sacha, Huub, Baris, Francesca, Daniela, Przemyslaw, Willem-Jan, Nick, Marco, Laura, Ming and the other SMG members for their friendships.



I would like to thank my Chinese friends Zhili, Kangbo, Ming, Lijing, Mingwen, Marshall, Zongquan, Wei, Shaoxian and Buo. Dear friends, your friendship and help make my life easier and happier in The Netherlands. Buo, it's wonderful to talk and practice martial art with you.

I would like to thank dr. Edwin Currie and dr. Jens Thies for all those wonderful discussions. And I would like thank DSM for the financial support of this project.

Finally, I would like to thank my wife ChunLing for her love and patience during the PhD period. I would like to thank my parents and my brothers for their love and supports.

## **Curriculum Vitae**

Di Wu was born on the 29<sup>th</sup> of March 1969 in TianJin, P.R. China. After finishing his bachelor degree in Department of Chemistry at the NanKai University in 1991, he started working in the Institute of Biomedical Engineering, Chinese Academy of Medical Science as a research assistant. In 1998, he joined the Global Card Company in Tianjin. Three years later, he went to Germany, and work as a research assistant in the Physical Institute of University of Muenster. In 2002, he move to Netherlands and start his master program in the Chemical Department at the University of Twente. After graduation, he joined the group of Materials and Interface Chemistry within the Department of Chemical Engineering and Chemistry at Eindhoven University as a Ph.D. student under the supervision of dr. Marshall Ming and prof. dr. G. de With. The most important results of his Ph.D. research are described in this thesis.